3-2-2021

Development of an Electronic Stability Control for Improved Vehicle Handling using Co-Simulation

Wonjo Jung
University of Windsor

Development of an Electronic Stability Control for Improved Vehicle Handling using Co-Simulation

By

Wonjo Jung

A Thesis
Submitted to the Faculty of Graduates Studies
Through the Department of Mechanical, Automotive & Materials Engineering
in Partial Fulfillment of the Requirements for
the Degree of Master of Applied Science
at the University of Windsor

Windsor, Ontario, Canada

2020

Development of an Electronic Stability Control for Improved Vehicle Handling using Co-Simulation

by

Wonjo Jung

APPROVED BY

N. Kar
Department of Electrical and Computer Engineering

J. Johrendt
Department of Mechanical, Automotive & Materials Engineering

B. Minaker, Advisor
Department of Mechanical, Automotive & Materials Engineering

December 14, 2020

Declaration of Originality

I hereby certify that I am the sole author of this thesis and that no part of this thesis has been published or submitted for publication.

I certify that, to the best of my knowledge, my thesis does not infringe upon anyone's copyright nor violate any proprietary rights and that any ideas, techniques, quotations, or any other material from the work of other people included in my thesis, published or otherwise, are fully acknowledged in accordance with the standard referencing practices. Furthermore, to the extent that I have included copyrighted material that surpasses the bounds of fair dealing within the meaning of the Canada Copyright Act, I certify that I have obtained a written permission from the copyright owner(s) to include such material(s) in my thesis and have included copies of such copyright clearances to my appendix.

I declare that this is a true copy of my thesis, including any final revisions, as approved by my thesis committee and the Graduate Studies office, and that this thesis has not been submitted for a higher degree to any other University or Institution.

Abstract

The research project focuses on integrating the algorithms of recent automotive Electronic Stability Control (ESC) technologies into a commercial multi-body dynamics (MBD) software for full vehicle simulations. Among various control strategies for ESC, the sliding mode control (SMC) method is proposed to develop these algorithms, as it is proven to be excellent at overcoming the effect of uncertainties and disturbances. The ESC model integrates active front steering (AFS) system and direct yaw moment control (DYC) system, using differential braking system, therefore the type of the ESC model is called as integrated vehicle dynamic control (IVDC) system. The IVDC virtual model will be designed using a specialized control system software, called Simulink. The controller model will be used to perform full vehicle simulations, such as sine with dwell (SwD) and double lane change (DLC) tests on Simulink to observe its functionality in stabilizing vehicles. The virtual nonlinear full vehicle model in CarSim will be equipped with the IVDC virtual model to ensure that the proposed IVDC virtual model passes the regulations that describes the ESC homologation process for North America and European countries, each defined by National Highway Traffic Safety Administration (NHTSA) and United Nations (UN). The proposed research project will enable automotive engineers and researchers to perform full vehicle virtual simulations with ESC capabilities.

To my loving wife, family, and friends.

Acknowledgements

To my supervisor and role model, Dr. Bruce P. Minaker: I truly appreciate all your support and guidance since I started working on your Outstanding Scholars research project. Your encouragement and immense knowledge greatly contributed to the formation of this work. I greatly appreciate the opportunity to advance my education and your guidance throughout my bachelor and master degree programs has truly shaped me into the researcher I am today.

In addition, I would like to thank my committee members, Drs. Johrendt and Kar for reviewing this thesis. I greatly appreciate your respected feedback and suggestions.

Thank you to all the FCA engineers from whom I gained valuable knowledge, skills, and tips. Thank you to Guanmin Feng, Reza Atashrazm, Marie Mills, and Mohammed Malik.

Thank you to my financial supporters without whom this thesis would not be possible. I am grateful to the University of Windsor and the Faculty of Engineering for endless opportunities and financial support. In addition, thank you to the Korean Canadian Scholarship Foundation (KCSF), Ontario Graduate Scholarship (OGS), and MITACS.

Finally, I would like to thank my loving family members who have always supported me throughout my academic endeavours. Thank you to my mom and dad, Ki Suk Kim and Jae Hoon Jung, for their continuous love and support. Thank you to my grandparents, Seyul Oh, Daejun Kim, Junglim Won, and Cheol Jung, who have supported my decision to study abroad in Canada. Thank you to my lovely wife, Christina Joy Jung, for her constant love and encouragement. Unfortunately, I lost my father, Jae Hoon Jung, my grandmother, Seyul Oh, and my grandfather, Cheol Jung, who always wanted to witness me graduating and starting a career, during my stay in Canada. A great part of my work is dedicated to their love and support.

Contents

Declaration of Originality iii

Abstract iv

Dedication v

Acknowledgements vi

List of Figures x

List of Tables xv

List of Abbreviations xvi

List of Symbols xviii

1 Introduction 1

1.1 Background . . . 1
1.2 Objectives . . . 3
1.3 Limitations . . . 4
1.4 Methodology . . . 5

2 Literature Review 7

2.1 Vehicle Dynamics . . . 7
2.1.1 Longitudinal Vehicle Dynamics . . . 8
2.1.2 Lateral Vehicle Dynamics . . . 10
2.2 Active Safety Systems of the Vehicles . . . 12
2.2.1 Antilock Braking System (ABS) . . . 13
2.2.2 Traction Control System (TCS) . . . 15
2.2.3 Electronic Stability Control (ESC) . . . 16
2.3 Vehicle Parameters Estimation . . . 18
2.4 Control Strategies for VDC . . . 19
2.5 Co-Simulation . . . 20

3 Vehicle Model 22

3.1 Bicycle Model . . . 22
3.1.1 Model Properties & Geometry . . . 23
3.2 Nonlinear Full Vehicle Model (CarSim) . . . 23
3.2.1 Model Properties & Geometry . . . 24

4 IVDC Controller Design & Implementation 38
4.1 Estimated Vehicle Parameters . . . 40
4.1.1 Side Slip Angle . . . 40
4.1.2 Desired Yaw Rate & Desired Side Slip Angle . . . 40
4.2 Vehicle Stability Region . . . 42
4.3 Active Front Steering (AFS) Control System . . . 43
4.3.1 Side Slip Angle Control . . . 44
4.3.2 Yaw Rate Control . . . 45
4.4 Direct Yaw Moment Control (DYC) System . . . 46
4.4.1 Side Slip Angle Control . . . 46
4.4.2 Differential Braking System . . . 46
4.5 Integration of AFS and DYC . . . 48
4.6 Block Diagram . . . 50
4.7 Controller Tuning . . . 51
4.7.1 Sign function and Chattering Issues . . . 51
4.7.2 Control Parameters . . . 53
4.7.3 AFS Tuning . . . 57

5 Simulation Results and Discussion 59
5.1 ESC Homologation Process . . . 59
5.1.1 Slowly Increasing Steer (SIS) Maneuver . . . 60
5.1.2 Sine with Dwell (SwD) Test . . . 60
5.2 Target Vehicle Side Slip Angle for Vehicle Stability Controller Design . . . 68
5.2.1 Case 1: DLC test with a $\beta_{\text{desired}} = \beta_{\text{steady state}}$ . . . 73
5.2.2 Case 2: DLC test with a $\beta_{\text{desired}} = 0$ . . . 77
5.3 Variable Control Effort distribution vs Fixed Control Effort Distribution of the AFS Controller . . . 79
5.3.1 Case 1: DLC test with a fixed linear setting . . . 80
5.3.2 Case 2: DLC test with a variable setting . . . 84
5.4 Comparison of Standalone Controllers Performance . . . 89
5.4.1 Case 1: DLC test with a vehicle equipped with the AFS controller . . . 93
5.4.2 Case 2: DLC test with a vehicle equipped with the DYC controller . . . 97
5.4.3 Case 3: DLC test with a vehicle equipped with the IVDC controller (AFS+DYC) 101

6 Conclusions and Recommendations 106

6.1 Summary 106
6.2 Conclusions 106
6.3 Recommendations 108
6.4 Contributions (Engineering Significance) 109

References **110**

Appendix A MATLAB File for the IVDC Controller **115**

Appendix B Block Diagrams **116**

Appendix C MATLAB Function for the Differential Braking System **120**

Vita Auctoris **121**

List of Figures

2.1 Longitudinal vehicle motion is affected by traction, aero resistance, rolling resistance and gravitational forces. Figure reproduced from Rajamani[21]. 8
2.2 Longitudinal traction force between tire and road surfaces as a function of slip ratio. Reproduced from Rajamani[21]. 9
2.3 A 2-DOF bicycle model, often used for modeling lateral vehicle dynamics. The width of the vehicle is ignored simplify the model. Reproduced from[18]. 12
2.4 Kinematics of one wheel on the road. Reproduced from Eriksson[17]. 14
2.5 Types of Traction Control Systems (TCS). 15
2.6 Trajectories of vehicles with and without ESC. Bottom line can be considered as the reference path. Reproduced from Rajamani[21]. 16
2.7 Schematic of signals for ESC to stabilize the vehicle. 17

3.1 Sprung mass of a nonlinear full vehicle in CarSim. The vehicle parameters that were introduced from the 8-DOF vehicle model are shown, while the parameters that were not introduced from Table 3.1 are from the CarSim template model. . . . 26
3.2 Powertrain model of a nonlinear full vehicle in CarSim. 27
3.3 Brake model of a nonlinear full vehicle in CarSim. 28
3.4 Driver's input to the steering wheel is multiplied by the steering ratio. The ESC controller takes the calculated road wheel angle to generate the corrective road wheel angle for vehicle stabilization. 29
3.5 Steering model of a nonlinear full vehicle in CarSim. 29
3.6 Steering ratio results from the second test. Steady state steering ratio is 18.33. . . 30
3.7 Front suspension configuration of a nonlinear full vehicle model in CarSim. . . . 31
3.8 Rear suspension configuration of a nonlienar full vehicle model in CarSim. 32
3.9 Front spring setting of a nonlienar full vehicle model in CarSim. 32
3.10 Rear spring setting of a nonlienar full vehicle model in CarSim. 33
3.11 Tire model of a nonlienar full vehicle model in CarSim. 34
3.12 Tire look up table of a nonlienar full vehicle model in CarSim. The lateral force is based on the given normal force and the slip angle. 34
3.13 Undesired huge spikes are observed when the cornering stiffness is calculated directly from the lateral force and the slip angle. 35

3.14 Cornering stiffness from static event is used. Transient behaviour tracking is poor. Values of C_f = 54030 N/rad, C_r = 38411 N/rad are used. Measured values are the simulated values from the virtual vehicle. 36
3.15 Cornering stiffness from the literature is used. Transient behaviour tracking is much improved, compared to the other test sets. Values of C_f = 40000 N/rad, C_r = 40000 N/rad are used. 36
3.16 Mean cornering stiffness from the time history is used. Transient behaviour tracking is good, compared to other test sets. Values of C_f = 30697 N/rad, C_r = 30436 N/rad are used. 37

4.1 Structure of the IVDC. AFS and differential braking system are used as actuators to control VSA and yaw rate. 39
4.2 Simulated VSA and estimated VSA during the simulation. Vehicle velocity: 120km/h. Constant steering input: 120deg. 41
4.3 Reference stable region in the vehicle side slip phase plane for the controller design. Reproduced from He[49]. 42
4.4 Individual differential braking system. Reproduced from Anwar[24]. 47
4.5 Adaptation gain ρ is used to achieve smooth transition between AFS and DYC for improving handling performance and improving the stability. Reproduced from Mousavinejad[18]. 49
4.6 Co-simulation setup between the modified IVDC controller and CarSim S-function. 50
4.7 Structure of the modified IVDC controller. 50
4.8 Comparison among three alternative options for the sign function generated from the input pulse in three magnitudes of 1, 2 and 10. 52
4.9 Yaw rate difference between the actual and the desired values of the vehicle when the controller design employs three different options for the sign function in the original design. 53
4.10 Magnitude of each term in Equation 4.17 before any control parameters are multiplied. SwD test at 120 km/h. 54
4.11 Magnitude of each term in Equation 4.17 after controller tuning parameters are multiplied. SwD test at 120 km/h. 55

5.1 Result of the SIS maneuver test at V_x = 80 km/h. The target lateral acceleration a_y = 0.3 g is reached at A = 30.18°. 60
5.2 Steering wheel angle input and yaw rate to be simulated during the SwD test. Reproduced from Lutz[66]. 61
5.3 SwD Test: Run 1 with steering amplitude of 1.5A = 45.27°. The vehicle model is not equipped with the IVDC controller. 63
5.4 SwD Test: Run 2 with steering amplitude of 1.5A = 45.27°. The vehicle model is equipped with the IVDC controller. 64

5.5 SwD Test: Run 3 with steering amplitude of 270°. The vehicle model is not equipped with the IVDC controller. 65
5.6 SwD Test: Run 4 with steering amplitude of 270°. The vehicle model is equipped with the IVDC controller. 66
5.7 Steering input of DLC test with steering amplitude of 200°. 69
5.8 DLC simulation result of a reference vehicle model without the IVDC controller. Vehicle spun out. A significant amount of the wheel corrective angle is calculated, but AFS is deactivated. Measured values are the simulated values from the virtual vehicle. 70
5.9 DLC simulation result of a reference vehicle model without the IVDC controller. The DYC controller calculated the required corrective moment but it is not applied to the vehicle since the DYC is deactivated. 71
5.10 DLC simulation result of a reference vehicle model without the IVDC controller. A vehicle shows a great lateral slip, and it did not come back near the initial axis of y=0. 72
5.11 Case 1: DLC simulation results (1 of 2). Yaw rate:1 = simulated yaw rate. Yaw rate:2 = desired yaw rate. Measured values are the simulated values from the virtual vehicle. 74
5.12 Case 1: DLC simulation results (2 of 2). 75
5.13 Case 1: Vehicle travel coordinates over time. The controller vehicle in this case came back to near the starting line of $y = 0$. 76
5.14 Case 2: DLC simulation results (1 of 2). Measured values are the simulated values from the virtual vehicle. 77
5.15 Case 2: DLC simulation results (2 of 2). 78
5.16 Case 2: Vehicle travel coordinates over time 79
5.17 Case 1: DLC simulation results (1 of 2). Measured values are the simulated values from the virtual vehicle. 81
5.18 Case 1: DLC simulation results (2 of 2) Sliding surface for the standalone yaw rate controller stays near zero for most of the simulation time. 82
5.19 Case 1: Vehicle travel coordinates over time. 83
5.20 Case 2: DLC simulation results (1 of 2) Yaw rate tracking is still very good, but greater deviations are observed in case 2, compared to case 1. Measured values are the simulated values from the virtual vehicle. 85
5.21 Case 2: DLC simulation results (2 of 2). The corrective braking torque appeared here did not affect the vehicle motion, but it is shown in the figure to imply that the corrective yaw moment would have been generated by the DYC system due to the vehicle stability index exceeding 0.8 and yaw rate error being greater than 5°/s. 86
5.22 Case 2: Vehicle travel coordinates over time. 87

5.23 Steering input data during the DLC test with an amplitude of 600°. Zero steering input is maintained for about 3.8 seconds after the COS to observe any residual vehicle motion from steering and braking actuation. 89
5.24 DLC simulation results (1 of 2) of reference vehicle model. The vehicle model spun out causing peaks in yaw rate. Corrective steering angle shown here did not affect the vehicle motion, but it is calculated in the AFS controller in the background. Measured values are the simulated values from the virtual vehicle. 90
5.25 DLC simulation results (2 of 2) of reference vehicle model. 91
5.26 Reference vehicle travel coordinates over time Sliding surface for the VSA controller, VSA error between simulated and desired VSA values, grows over the simulation. 92
5.27 Phase plane of the reference vehicle during the DLC test. VSA and side slip velocity increased significantly as the vehicle spun out. 92
5.28 Case 1: DLC simulation results (1 of 2). Yaw rate is matched to the desired yaw rate. Corrective wheel steering angles are generated when the steering angle changes direction to counter the inertia. Measured values are the simulated values from the virtual vehicle. 94
5.29 Case 1: DLC simulation results (2 of 2) Corrective moments and braking torques shown here are only calculated values inside the DYC controller, but the DYC did not affect the vehicle motion. 95
5.30 Case 1: Vehicle travel coordinates over time. The vehicle is heading slightly towards the right at the end of the simulation. 96
5.31 Case 1: Phase plane. Red lines are stable region boundaries. The DYC would have been activated once the vehicle state left the stable region, but only AFS generated the corrective steering wheel angle to bring the vehicle motion state back into the stable region. 96
5.32 Case 2: DLC simulation results (1 of 2). The corrective wheel angle, δ_{desired} presented here do not affect the vehicle motion since the AFS controller is deactivated. Measured values are the simulated values from the virtual vehicle. 98
5.33 Case 2: DLC simulation results (2 of 2). 99
5.34 Case 2: Vehicle travel coordinates over time. The DYC controller did not provide good path following performance, but its primary goal is to keep the vehicle stable. 100
5.35 Case 2: Phase plane. Red lines are stable region boundaries. The DYC was activated when the state was outside the stable region. 100
5.36 Case 3: DLC simulation results (1 of 2). Measured values are the simulated values from the virtual vehicle. 101

5.37 Case 3: DLC simulation results (2 of 2). Individual braking torques were generated shortly. The second corrective yaw moment peak from the M^*_{DYC} did not generate the braking torque at the same time since the yaw rate threshold of $5^\circ/s$ was not reached. 102
5.38 Case 3: Vehicle travel coordinates over time. 103
5.39 Case 3: Phase plane. 103

A.1 IVDC controller setup file in MATLAB. This .m file must be run prior to the co-simulation so that all blocks of the IVDC controller in Simulink can use the corresponding values 115

B.1 Structure of the VSA and side slip velocity estimator. 116
B.2 Structure of the phase plane where the stable region and the adaptation gain is calculated 116
B.3 Structure of the desired yaw rate and desired VSA generator. 117
B.4 Structure of the AFS controller. 117
B.5 Structure of the yaw rate controller part of the AFS controller using NFTSM control strategy. Adaptation gain is used to replace the M_{AFS}. 118
B.6 Structure of the VSA controller part of the AFS controller using ITSM control strategy. 118
B.7 Structure of the DYC controller. 118
B.8 Structure of the VSA controller using NFTSM control strategy. Adaptation gain is used to replace the M_{DYC}. 119
B.9 Structure of the differential braking system. Positive steering wheel angle means counter clockwise turning in CarSim. If the yaw rate difference between the actual and the desired values is less than 5°/s, DYC is not activated. 119

C.1 Differential braking system function in MATLAB. This .m file determines how much braking torques are required and which wheel must be activated for braking, based on oversteer/understeer state and the travel direction 120

List of Tables

2.1 All known acronyms for active safety features. Reproduced from SAE[31]. 13

3.1 Vehicle parameters of the 8-DOF validated vehicle model[26]. The bicycle model in the controller design use these values to represent the CarSim vehicle model. . 25
3.2 Transmission gear ratio of the nonlinear full vehicle model in CarSim. 27
3.3 Simulation setting and results in order to find the steering ratio of the modified vehicle model in CarSim. 30
3.4 Simulation setting and results in order to find the steering ratio of the modified vehicle model in CarSim. 36

4.1 Modified IVDC controller tuning parameters. 56
4.2 Various combinations of the AFS weighting coefficients are compared during the SwD simulation. 58

5.1 SwD Test Results. 67
5.2 DLC Test Results: Case 1 uses a linear combination and case 2 uses a variable AFS coefficient of stability index, χ. 88
5.3 DLC test results comparison among different controller settings: only AFS activated, only DYC activated, both of AFS and DYC activated. 105

List of Abbreviations

All abbreviations used in this work are described in this section.

Abbreviation	Meaning
4WAS	4 Wheel Active Steering
ABS	Anti-Lock Braking System
ADAS	Advanced Driver Assistance System
AFS	Active Front Steering
ARS	Active Rear Steering
AS	Active Steering
BTCS	Brake only Traction Control Systems
CDC	Continuous Damping Control
COS	Completion Of Steer
DLC	Double Lane Change
DOF	Degrees Of Freedom
DSC	Dynamic Stability Control
DYC	Direct Yaw moment Control
EBTCS	Engine and Brake Traction Control Systems
ECU	Electronic Control Unit
EKF	Extended Kalman Filter
ESC	Electronic Stability Control
ESP	Electronic Stability Program
ETS	Engine only Traction Systems
FCA	Fiat Chrysler Automobiles
FE	Finite Element
FMVSS	Federal Motor Vehicle Safety Standards
HiL	Hardware in-the Loop
ITSM	Integral Terminal Sliding Mode
IVDC	Integrated Vehicle Dynamic Control
LQR	Linear Quadratic Regulator
MBD	Multi Body Dynamics
MPC	Model Predictive Control

NFTSM	Non-singular Fast Terminal Sliding Mode
NHTSA	North america Highway Traffic Safety Administration
OEM	Original Equipment Manufacturers
RMSE	Root Mean Square Error
SAE	Society of Automotive Engineers
SiL	Software in-the Loop
SIS	Slowly Increasing Steer test
SMC	Sliding Mode Control
SUV	Sports Utility Vehicle
SwD	Sine with Dwell
TCS	Traction Control System
UCC	Unified Chassis Control
UN	United Nations
VDC	Vehicle Dynamics Control
VSA	Vehicle Side slip Angle
SbW	Steer by Wire
YCS	Yaw Control Systems

List of Symbols

m	mass	kg
F_{xf}	traction force on front tires	N
F_{xr}	traction force on rear tires	N
F_{aero}	aerodynamic resistance force on rear tires	N
g	gravitational accleration	$\mathrm{m\,s^{-2}}$
x	longitudinal displacement	m
V_x	longitudinal velocity	$\mathrm{m\,s^{-1}}$
$\ddot{x}$	longitudinal acceleration	$\mathrm{m\,s^{-2}}$
R_{xf}	rolling resistance force at front tire	N
R_{xr}	rolling resistance force at rear tire	N
R_e	effective rolling radius of tire	m
C_d	aerodynamic drag coefficient	-
A_f	frontal area of the vehicle	$\mathrm{m^2}$
V_{wind}	wind velocity	$\mathrm{m\,s^{-1}}$
F_{rolling}	rolling resistance force	N
F_{zf}	vertical force on front tire	N
F_{zr}	vertical force on rear tire	N
f	rolling resistance coefficient	-
l_f	distance from centre of gravity to front wheel centre	m
l_r	distance from centre of gravity to rear wheel centre	m
L	wheel base of the vehicle	m
F_y	vehicle lateral force	N
I_{zz}	yaw moment of inertia	$\mathrm{kg\,m^2}$
M_z	yaw moment	N m
V_y	lateral velocity	$\mathrm{m\,s^{-1}}$
a_y	lateral acceleration	$\mathrm{m\,s^{-2}}$
C_f	cornering stiffness of each front tire	$\mathrm{N\,rad^{-1}}$
C_r	cornering stiffness of each rear tire	$\mathrm{N\,rad^{-1}}$
m_s	sprung mass of the vehicle	kg
h_s	distance between the centre of sprung mass and the roll centre	m
I_w	rotational moment of inertia of the wheel	$\mathrm{kg\,m^2}$
T	driving torque	N m

T_b	braking torque on the wheel	N m
T_r	rolling resistance torque on the wheel	N m
k_u	understeer coefficient	-
s	sliding mode surface	-
d	track width of the vehicle	m
θ	inclination angle of the road	$^\circ$
σ_x	slip ratio	%
ω	angular velocity	rad s^{-1}
ρ	adaptation gain	-
ψ	yaw angle	$^\circ$
γ	yaw rate	$^\circ$ s^{-1}
β	vehicle side slip angle	$^\circ$
$\dot{\beta}$	vehicle side slip velocity	$^\circ$ s^{-1}
δ_w	road wheel steering angle	$^\circ$
α_f	front tire slip angle	$^\circ$
α_r	rear tire slip angle	$^\circ$
ϕ	roll angle	rad
δ_{driver}	steering wheel angle from the vehicle cabin	$^\circ$
μ	road-tire friction coefficient	-
χ	stability index	-

Chapter 1

Introduction

1.1 Background

The following thesis focuses on the development of a virtual controller model of automotive electronic stability control, for application to a full vehicle simulation. It further explores the procedure of co-simulation using different simulation platforms.

Performance and design improvements of automobiles have been accelerated along by technological advancements in the automotive industry. During the early stage of the vehicle design era, without computers, the vehicle design process had to rely on manual mathematical modeling and intensive experimental testing of prototypes. This is no longer desirable due to the significant amount of time and cost involved in the prototype development and physical testing. Thus, vehicle simulation and dynamic modeling using software tools, capable of computing solutions to complex equations describing vehicle motions and of considering physical characteristics of many components, must be used during the development process, simultaneously with the overall design of the vehicle[1].

Modern commercial multi-body dynamics (MBD) software tools, such as ADAMS or CarSim, are now widely used in the automotive industry. Mechanical components and their physical characteristics are modeled and can be connected with one another using linear or non-linear approaches in the software. In some cases, simpler elements representing the actual components are used to reduce the computational effort in the software. Some of these tools can import finite element (FE) models that represent the physical components more accurately, even though it increases the computational efforts significantly[2], [3]. In the automotive industry, MBD software tools are used to model full vehicles to allow accurate prediction of their motion. These software tools incorporate the vehicle subsystems, such as the powertrain, steering, and suspension systems, to improve the model fidelity. Most automotive companies around the world increasingly rely on vehicle dynamics simulations, since they significantly reduce the time and cost of vehicle optimization when building prototypes, which in turn leads to improvements in both the vehicles' durability and stability[4].

In 2017, the Society of Automotive Engineers (SAE) published their SAE J2564 standard describing currently known automotive active stability enhancement systems, such as anti-lock braking system (ABS), traction control system (TCS) and electronic stability control (ESC)[5]. The ABS prevents the wheel slippage by controlling braking pressure during braking. Similarly, TCS prevents wheel slippage by controlling engine torque or braking pressure during acceleration[5]–[7]. The ESC assists drivers in keeping the vehicle on their intended path. For instance, numerous vehicle state parameters are dynamically measured or estimated to generate a corrective yaw moment to stabilize the vehicle when it does not travel as the driver intends[5], [8]. Therefore, ABS and TCS share similar objectives in that they both prevent wheel slip, but ESC focuses on the lateral dynamics of the vehicle. A significant number of studies have been conducted with a focus on the applications of various control strategies, such as sliding mode control, H-infinity control, or fuzzy control methods to improve existing automotive active stability enhancement systems[9]–[12]. Physically, the active stability enhancement systems are embedded in the electronic control unit (ECU), which collects the vehicle state information from various sensors and controls the various vehicle subsystems, such as braking and engine output, based on the measured data.

This thesis focuses on the development of the ESC for a full vehicle simulation. Implementation of ESC on vehicles has significantly reduced the rate of vehicle accidents due to improved vehicle lateral stability. Studies show that in some situations, single-vehicle accidents have been reduced by up to 49%[13]. Lie et al[14] estimated that 20% of the total vehicle related fatalities in Sweden could be saved annually if all vehicles are equipped with ESC. International standards and regulations are established to encourage the inclusion of of these active safety technologies on passenger vehicles as standard equipment. Since September 2011, the Federal Motor Vehicle Safety Standard (FMVSS) has required that all passenger vehicles sold in the United States must be equipped with ESC[15].

The MBD software tools developed for automotive industry specifically, such as CarSim and ADAMS Car, have convenient features for automotive engineers. Various templates for suspension subsystems or powertrain subsystem configurations are available, and may be easily modified to represent the target vehicle model. However, the default approach to general full vehicle simulation on MBD software has a challenge to overcome for accurate simulation. Vehicle models built on MBD software predict accurate load transfers between components and subsystems; therefore, it is very useful in many aspects of design, like durability and clearance checking. However, the mechanical vehicle model still does not account for how the active stability enhancement systems (ABS, TCS, ESC), which are now equipped to the vehicles by law, affect the vehicle dynamics. Therefore, the prediction of vehicle behaviour with the active safety technologies is not possible unless the virtual controllers that represent ABS, ESC and TCS features, were modeled and integrated with the virtual full vehicle model. Therefore, more realistic vehicle dynamics behaviour with the active safety control systems can be observed either from the physical testing on a track or a virtual simulation where these control systems are considered. However, the physical testing takes a significant amount of time to set up, and it is costly. Therefore, it will be very beneficial for

automotive engineers to be able to predict the vehicle behaviour, including the effects of the active safety features, by combining the virtual vehicle model and a model of the active safety systems.

There are two main methods to integrate active stability enhancement systems into a virtual vehicle model. The hardware-in-the-loop (HiL) method uses an actual ECU from a vehicle, where the ECU is connected to numerous vehicle components that generate the virtual vehicle responses. Its benefit is the high accuracy in vehicle response, since the actual ECU and components are used. However, it requires substantial time and effort to assemble and troubleshoot. The software-in-the-loop (SiL) method gets rid of the need of an actual ECU. This method only uses virtual models that represent both a vehicle model and an ECU. For instance, a full vehicle model in an MBD software, such as ADAMS, can be exported as a self-contained system model file, so that it can be used in a different simulation environment, such as Simulink. This block represents the virtual vehicle model that contains input and output ports. This can be combined with a controller that represents the active safety enhancement system to observe the vehicle behaviour with the active stability enhancement features. A controller model for the vehicle stability control system, e.g., as obtained from the ECU supplier, is sometimes described as a *black-box* model, since its internal algorithms are usually hidden, due to proprietary knowledge concerns. Nevertheless, accurate vehicle behaviours are generally expected when using a virtual vehicle model and a black-box ECU model, since it is typically the ECU supplier's virtual ECU model that is implemented in the physical ECU.

The combined use of different models from different platforms is called *co-simulation*, and allows the study of global behaviour of complex systems[16]. Similar research on the co-simulation of a full vehicle model and its ABS model in Simulink is available in the literature[17]. However, the main problem of this method is that automotive engineers cannot diagnose the issues when the simulations result in errors or produce unrealistic behaviour, since the algorithm of the black-box model cannot be observed.

Therefore, this thesis will focus on developing a controller model of ESC to stabilize the vehicle during extreme manoeuvres using robust control strategies. The functionality of the designed controller will be verified by using a FMVSS 126 standard, which defines the ESC homologation process.

1.2 Objectives

The long-term goal of the proposed research project is to develop a virtual controller that represents active vehicle safety enhancement systems and to implement it in a full vehicle virtual simulation during the design stage. It is expected to improve the quality of the full vehicles simulation results using MBD software, since the effects of the ECU will be included in the results. This will save significant amount of simulation process time, compared to the HiL method since all models are virtual. The full vehicle simulation with active stability enhancement features will

contribute to passengers' safety improvement early in the design cycle by being able to observe the vehicle's actual response with ABS, TCS and ESC. The primary objective of the research project can be broken down into three sub-objectives as follows:

The first sub-objective is to develop an ESC controller model in Simulink using a robust control strategies and to verify its functionality with a full vehicle model. CarSim is chosen for the co-simulation for its convenient user interface and faster computational speed due to the reduced vehicle model complexity, compared to the virtual vehicle model in ADAMS Car. The virtual full vehicle model from CarSim will be imported into Simulink as an S-function model, then it will be connected with a virtual ESC controller for a full vehicle simulation.

The second sub-objective is to ensure that the ESC controller passes the FMVSS 126 ESC homologation standards. Making a correlation between the developed ESC controller to an actual ESC blackbox model from the ECU supplier ensures the same behaviour with the actual ECU. However, the blackbox model could not be obtained from the supplier, therefore the design goal of the ESC controller is that it qualifies for a road-approved level, which can be confirmed by FMVSS 126 standards.

The third sub-objective is to study various properties of the ESC controller design and implementation process for co-simulation. The ESC controller will be tuned to ensure its functionality and to improve its performance. During the controller tuning and implementation process, undesired phenomena either from control output calculations or implementation process between two different software platforms may be observed. Any observed undesired phenomena and how to solve them will be explored. In addition, selection of desired vehicle side slip angle (VSA) and new method of achieving multiple control objectives in a single standalone controller will be explored.

1.3 Limitations

The following limitations of the research are realized at the beginning of the research project.

The lack of a blackbox model that represents the actual ECU is a significant limitation. The blackbox model could have been significantly helpful during the controller tuning process so that the correlation is made between the designed ESC controller model to an actual ECU model. Therefore, the design goal of the ESC controller is not necessarily to correlate with the actual ECU, but its design goal is to be robust and sufficiently good enough to pass the FMVSS 126 standards.

In addition, this research focuses on developing a robust ESC controller; therefore, sophisticated control strategies are used to implement the ESC. In real life, suppliers of the ECU tend to not share the specific details of the algorithms implemented in their ECU, in order to protect their intellectual property. Therefore, simple logic maybe used in actual ECUs in the market.

Active front steering (AFS) is utilized to stabilize the vehicle's yaw motion and VSA deviation, and the control logic was based on the assumption that a steer-by-wire (SbW) system is available

in the vehicle. Active front steering systems typically replace the pinion in a rack and pinion style steering system with a planetary style gear drive, so that both the driver and the electronic control system can directly affect the steering angle; for example, the driver may control the sun gear with the steering wheel, while the SbW system controls the planet gears, and the ring gear drives the steering rack. Steer-by-Wire is popular in the vehicle dynamics research community for its numerous applications in a field of vehicle dynamics control (VDC); however, most automotive companies in the industry still use a more traditional design in the steering system. Therefore, the actual vehicle may not control the front wheel steering angles to stabilize the lateral behaviour, while the designed ESC controller in this paper uses the front road wheel steering angles to stabilize the vehicle motions.

The simulation results with the controller can be validated by comparison to proprietary physical test data from experiments. This validation of the simulation results means that the actual behaviour on the road, with the active stability enhancement systems in operation, can be accurately predicted on the virtual simulation platform. However, this is not within the timeline of this thesis, therefore can be done in the future.

Therefore, the proposed research project does not focus on developing a virtual controller that represents the actual ECU. However, the focus of the paper is to design a sophisticated virtual ECU controller that can be used for a full vehicle simulation.

1.4 Methodology

First, recent and robust algorithms for ESC will be studied during the literature review. Among various control strategies for ESC, the non-singular fast terminal sliding mode (NFTSM) control method and integral terminal sliding mode (ITSM) control method are proposed to develop these algorithms at a current level of the research, as it is proven to be excellent at overcoming the effect of uncertainties and disturbances[12]. The proposed strategies are also applicable to non-linear systems, which is suitable for complex vehicle dynamics systems.

The controller model of the ESC will be implemented in Simulink by modifying the approach to integrated control of ground vehicle stability described in Mousavinejad et al[18]. The controller will explore various variables that specify the dynamic states of the vehicle model, such as yaw rate, VSA, brake pressures on different wheels and road-tyre friction force. The VSA and side slip angular velocity phase plane (β-$\dot{\beta}$) will be used to define the reference region. This reference region will be used by a controller to determine the vehicle's preferred dynamic state. A full vehicle simulation, such as sine with dwell (SwD), will be run. The results of the full vehicle simulation with and without the controller will be compared to verify the functionality of the controller. It is expected the controller will correct front steering wheel angles and individual braking pressures so that it minimizes slipping and keeps the vehicle as close as possible to the intended path.

The full vehicle simulation will be set up according to the simulation criteria specified in FMVSS 126 regulation released by the National Highway Traffic Safety Administration (NHTSA). This regulation is used in North America for the ESC homologation process. After a functionality is confirmed in an earlier stage, the controller will be further tuned so that the virtual vehicle model equipped with the designed ESC controller will pass the FMVSS 126 ESC homologation test.

Improved capability of the full vehicle simulation with the controller will play a significant role to improve the vehicle stability, ultimately leading to better passenger safety.

Chapter 2

Literature Review

2.1 Vehicle Dynamics

Vehicle dynamics is a very broad range of study to be defined in one sentence, but it is the study of the motion of passenger vehicles, with a purpose of improving the safety, comfort and dynamic performance of the vehicle by realizing the effects of many vehicle parameters. Based on the Cartesian coordinate planes, the subject of vehicle dynamics is often divided into the three subjects: longitudinal, lateral and vertical dynamics.

Longitudinal dynamics applies laws of physics to explore the vehicle motion in a longitudinal axis. The subject of longitudinal dynamics studies all factors that affect the longitudinal motion of the passenger vehicles. For instance, the tire-road interactions, longitudinal load transfer during acceleration and braking, and pitching motions are included. In summary, the subject of longitudinal dynamics deals with the acceleration and braking performance.

Similarly, lateral dynamics apply laws of physics, but to study the vehicle motion in a lateral axis. The lateral motion of a passenger vehicle is crucial in changing the vehicle travel direction; following the intended path or avoiding obstacles on the road abruptly. Controlling the yaw motion is important for vehicle stability and passenger safety.

Vertical motions of the vehicle are explored in the field of vertical dynamics. Vertical dynamics are required since the roads are not perfectly smooth; therefore, there are elevation changes from the irregularities. In addition, passenger vehicles do not always travel on paved roads but they operate off-road, where the elevation changes are larger and even more irregular. Passenger comfort is heavily influenced by the vertical motion of the vehicle. The vertical dynamics affect the design of the suspension, especially in regards to the range of vertical travel.

In addition, the study of tire behaviour is often characterized as a separate branch in vehicle dynamics, even though it is heavily involved in the other branches. Tires are one of many flexible components of the vehicle. The flexibility characteristics of tires cause non-linear behaviour. This makes the tires one of the most difficult components to model. Tires can be considered simultaneously as a pressure vessel with complex geometry, under effects of centrifugal force, large

deflections, and friction[19]. Pacejka is widely recognized as a pioneer in a field of tire behaviour, and published an extensive text entirely dedicated to the subject[20].

In this thesis, the focus will be primarily on longitudinal and lateral dynamics, since anti-lock braking system (ABS), traction control system (TCS) and electronic stability control (ESC), which will be introduced in the main body of the paper, are primarily designed to control the longitudinal and lateral motions of the passenger vehicles.

2.1.1 Longitudinal Vehicle Dynamics

Longitudinal vehicle dynamics or longitudinal dynamics deal with vehicle's longitudinal motion, which are directly related to acceleration and braking performance of vehicles. Consider a vehicle moving on a flat surface as shown in Figure 2.1. The resultant longitudinal force acting on the vehicle can be predicted by considering longitudinal tire traction forces, aerodynamic resistance forces, and tire rolling resistance forces. Gravitational force is also a factor if the vehicle travels on an inclined road, but it becomes irrelevant on a flat road[21]. One of the most commonly

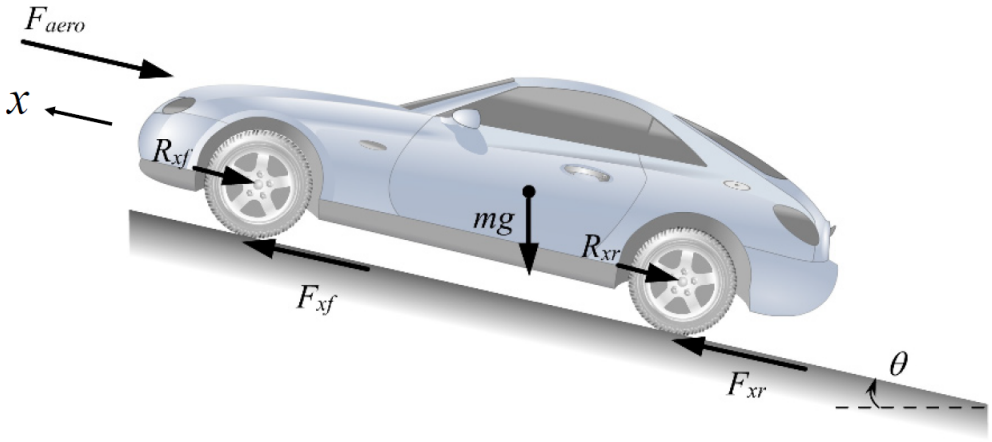

FIGURE 2.1: Longitudinal vehicle motion is affected by traction, aero resistance, rolling resistance and gravitational forces. Figure reproduced from Rajamani[21].

used equations for longitudinal motion of the vehicle is Newton's law, expressed as:

$$m\ddot{x} = F_{xf} + F_{xr} - F_{\text{aero}} - R_{xf} - R_{xr} - mg\sin(\theta) \tag{2.1}$$

where m is the mass of a vehicle, x is the longitudinal displacement (travel distance) of the vehicle motion, and F_{xf}, F_{xr} are the traction forces on front and rear tires, developed by the front and rear axles, respectively. The aerodynamic resistance force is F_{aero}, and R_{xf}, and R_{xr} are the rolling resistance forces at front and rear tires, respectively. The portion of the vehicle weight affecting the vehicle's longitudinal force is $mg\sin(\theta)$, where θ represents the inclination angle of the road.

The traction forces F_{xf}, F_{xr} are the forces between the tire and road surfaces. Therefore, they depend on the road-tire friction coefficient, vertical loads, and longitudinal slip ratio. The vertical

loads (normal loads) consist of the vehicle weight distributed by four wheels and the longitudinal and lateral weight transfer if the vehicle is not in an equilibrium state (no acceleration).

The longitudinal slip refers to the magnitude of how much the tire slips on the road. This can be expressed as the difference between the longitudinal velocity of the vehicle and the calculated longitudinal velocity based on the tire's effective rolling radius R_e and the rotational speed of wheels ω. Therefore, the slip ratio can be defined as:

$$\sigma_x = \frac{\omega R_e - V_x}{V_x} \tag{2.2}$$

or:

$$\sigma_x = \frac{\omega R_e - V_x}{\omega R_e} \tag{2.3}$$

where Equation 2.2 is the slip ratio used during braking and Equation 2.3 is the slip ratio during acceleration. Equation 2.3 is used to prevent the result where Equation 2.2 goes to infinity in a case of the stationary vehicle ($V_x = 0$) with rotating wheels ($\omega \neq 0$), as is the case immediately after pulling away from a stop.

Both Equation 2.2 and Equation 2.3 show that the longitudinal slip ratio is zero ($\sigma = 0$) if the tire behaves like a rigid body; therefore, there is no slip occurring as it rolls where $V_x = \omega R_e$. The effective rolling radius R_e is generally very close to the physical radius, but not exactly. It depends on the normal load, and it can be obtained as the value that satisfies $V_x = \omega R_e$ when the wheel rolls freely without braking or accelerating.

Figure 2.2 shows the typical relationship between the longitudinal traction force at the tire-road surface as a function of a slip ratio. It is observed that the traction force of the tire is highly

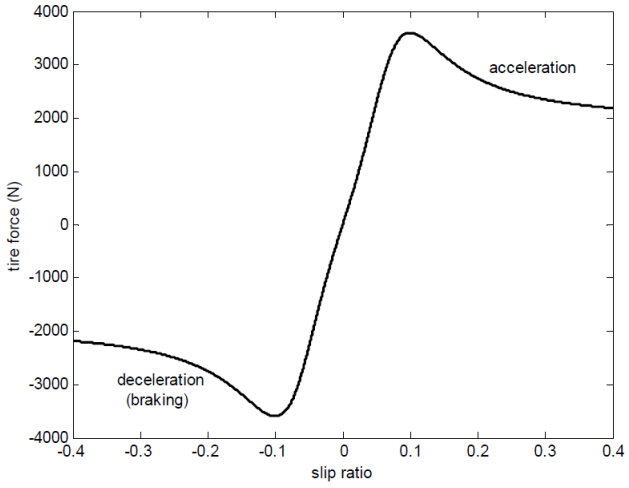

FIGURE 2.2: Longitudinal traction force between tire and road surfaces as a function of slip ratio. Reproduced from Rajamani[21].

dependent on the slip ratio, and the maximum traction forces are achieved at around 10% slip

ratio. Linear behaviour is observed when the slip ratio is small $0 < \sigma < 0.1(10\%)$. Therefore, the linear region in the traction force and the slip ratio graph can be utilized for active stability enhancement systems, such as ABS and TCS, due to its convenience in numerical expression and the maximum traction forces near 10% slip ratio. If the longitudinal slip ratio is not small $0.1 < \sigma$ where the nonlinear relationship between the traction force and the slip ratio exists, a nonlinear tire model must be used to calculate the longitudinal traction force; (e.g., the 'magic' formula tire model developed by Pacejka[20], or the FTire model developed by Cosin[22]). These nonlinear tire models are capable of generating the nonlinear traction forces at the higher slip ratios, based on an experimental validation process, or a sophisticated finite element (FE) model.

The equation for aerodynamic drag force is:

$$F_{aero} = \frac{1}{2}\rho C_d A_f (V_x + V_{\text{wind}})^2 \tag{2.4}$$

where ρ is the density of air, C_d is the aerodynamic drag coefficient, A_f is the frontal area of the vehicle, V_x is the longitudinal velocity of the vehicle and V_{wind} is the wind velocity, where the positive value refers to a wind blowing towards the front of the vehicle. It can be observed that the aerodynamic drag force is not linearly proportional to the vehicle and the wind speeds.

The equation for rolling resistance force is:

$$F_{rolling} = R_{xf} + R_{xr} = f(F_{zf} + F_{zr}) \tag{2.5}$$

where f is the rolling resistance coefficient and F_{zf}, F_{zr} are the vertical loads on the front and rear tires. As the vehicle changes speed, longitudinal load transfer will occur, which will change the vertical load distribution between the front and the rear axles. This load transfer affect the rolling resistance as seen in Equation 2.5.

Equation 2.1 contains non-linearities in its terms, caused by tire behaviour, aerodynamic and rolling resistance forces. These non-linear characteristics makes solving the equation of motion very challenging. [19] suggest a numerical solution as the most accurate approach for solving the longitudinal acceleration problem while considering existing non-linearity in the calculation.

Numerous studies are done in an effort to control the longitudinal vehicle motion for improved performance of propulsion and braking of passenger vehicles, contributing to the developments of ABS, TCS, cruise control and other control systems. The ABS and TCS will be described in more detail in Section 2.2.

2.1.2 Lateral Vehicle Dynamics

Where longitudinal vehicle dynamics deal with the acceleration and braking performance of the vehicle, it can be said that the lateral vehicle dynamics govern the steer-ability and stability of the vehicle. As the longitudinal vehicle dynamics are difficult to be modeled mathematically while

accounting for its non-linearity from different sources, such as tire forces, aerodynamic drag force and so on, the lateral vehicle dynamics also pose the same challenge, perhaps in a bigger scale. Understanding the lateral vehicle dynamics is crucial in stabilizing the vehicle motions, which further contribute to the passengers' safety. The National Highway Transportation Safety Administration (NHTSA) in the United States reported that about $1,575,000$ vehicle accidents occur by distracted drivers, where the majority are attributed to unintended lane departure. The NHTSA also considers lane departures as one of the major causes of rollover accidents[23].

The most commonly used vehicle model to explain the lateral vehicle dynamics is the so-called 'bicycle' model, or yaw plane model. The width of the vehicle is ignored in the bicycle model, therefore, the effects of lateral weight transfer that affect the tire dynamics and suspension motions are omitted. Due to its simplicity, numerous papers exploring vehicle dynamics control systems use a bicycle model, or other similar vehicle models with more degrees of freedom (DOF) to account for more broad range of vehicle motions, such as roll motion[24]–[26].

As shown in Figure 2.3, the two left and right wheels are represented by one single wheel at the front and rear. The given bicycle model does not account for rear wheel steering, but it can be easily included if needed. The front wheel steering angle is represented by δ_w. The centre of gravity is used as a reference point to measure yaw rate $\dot{\psi} = \gamma$ and vehicle side slip angle (VSA) β, which are significant in designing the ESC. The yaw rate or yaw velocity refer to the rate of rotation about the vertical axis of the vehicle. The distance from centre of gravity to front and rear wheel centres are l_f and l_r respectively, although the notations a and b are also frequently used in the vehicle dynamics literature. The wheelbase of the bicycle model is $L = l_f + l_r = a + b$. The tire slip angles, α_f and α_r, refer to the difference between the the tire's actual travel direction and the physical heading direction for both the front and rear wheels, respectively. Similarly, the VSA β refers to the angle between the vehicle's longitudinal axis and the direction of its motion, taking the centre of gravity as the reference. This is also sometimes referred to as the 'drift angle'. Note that both the tire and body slip angles are typically very small, often only a few degrees, and may not be immediately visible to the naked eye.

Assumptions must be made for the bicycle model's equations of motion to be valid. The forward speed is assumed to be constant so that it is considered as a parameter. Wheel slip angles are assumed to be small so that linear behaviour of the tire lateral forces are expected from the simple mathematical equations[27]. The basic equations of motion for the 2-DOF bicycle model are

$$mV_x(\dot{\beta} + \gamma) = F_y \tag{2.6}$$

$$I_{zz}\dot{\gamma} = M_z \tag{2.7}$$

Here, M_z and F_y are body yaw moment around the vertical axis, and the lateral force, respectively. This model will be used in the ESC controller design in Chapter 4.

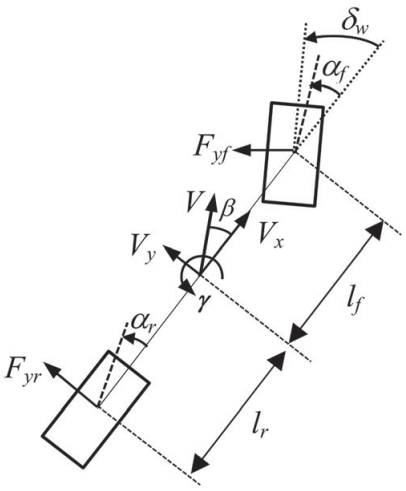

FIGURE 2.3: A 2-DOF bicycle model, often used for modeling lateral vehicle dynamics. The width of the vehicle is ignored simplify the model. Reproduced from[18].

There are many types of the vehicle safety features that are based on the longitudinal and lateral dynamics of the vehicle, some of them are often called as 'advanced driver-assistance system (ADAS)'. Recent ADAS technologies and its development history are further explored in Section 2.2.

2.2 Active Safety Systems of the Vehicles

Traffic injuries account for one of many fatal public health issues. Therefore, safety enhancement systems on automobiles are considered as valuable tools to save lives of the occupants during vehicle accidents. Håland[28] shows a 54% reduction in the probability of death and injury from vehicle accidents by using a three point seat belt. These safety systems are active before and during an accident, which explains why these safety features are categorized by passive and active types.

Passive safety features remain deactivated under normal driving conditions, but are activated when the start of the crash event is detected to reduce the level of injury during the impact[29]. Occupant restraint systems, such as airbags and seat-belts, are typical passive safety systems. Unlike passive safety systems, active safety systems are always active, even during normal driving situations. Therefore, its purpose is to prevent the accident before it occurs. The active safety features are mostly computer-controlled since the systems must monitor the vehicle states at all time using numerous sensors on board. The ABS, TCS, and ESC are typical examples of the active safety systems for automobiles.

It is obvious that greater benefits can be achieved in terms of the passenger's safety when the passive and active safety systems are developed considering their integration[30]. This chapter will explore three types of active safety enhancement systems: ABS, TCS, and ESC since these

are the most relevant active safety features to the focus of the study; the development of the ESC. Names of those active safety systems can be confusing since these systems are called by different names depending on many factors; different developers, companies, and countries. In 2017, the Society of Automotive Engineers (SAE) published a report listing all currently known acronyms for these active safety control systems, as shown in the Table 2.1 below.

Table 2.1: All known acronyms for active safety features. Reproduced from SAE[31].

Anti-lock Braking System	Traction Control System	Electronic Stability Control System
ABS (Antilock Brake System)	ASC (Automotive Stability Control)	ABC (Active Brake Control)
RWAL (Rear Wheel Antilock)	ASR (Automatic Stability Regulation)	AH (Active Handling System)
SCS (Stop Control System)	Brake Only Traction	Active Safety
RABS (Rear Antilock Brake System)	ETS (Enhanced Traction System)	AdvanceTrac
	TCS (Traction Control System)	ASMS (Automotive Stability Management System)
	TCB (Traction with Brake Intervention)	ASTC (Active Skid and Traction Control)
	TRAC (Traction Control System)	CBC (Cornering Brake Control)
	EDS (Electronic Differential-lock System)	DSC (Dynamic Stability Control)
		DSTC (Dynamic Stability and Traction Control)
		ESC (Electronic Stability Control)
		ESP (Electronic Stability Program)
		ICCS (Integrated Chassis Control System)
		IVD (Integrated Vehicle Dynamics)
		PCS (Precision Control System)
		PSM (Porsche Stability Management)
		SCS (Stability Control System)
		Stabilitrak
		STC (Stability and Traction Control System)
		Traxxar
		VDC (Vehicle Dynamics Control)
		VSA (Vehicle Stability Assist)
		VSES (Vehicle Stability Enhancement System)
		YCS (Yaw Control Stability)

2.2.1 Antilock Braking System (ABS)

Originally, ABS was developed in an attempt to only prevent wheels from locking up during braking. The very first attempt to develop ABS dates back to the 1920s, and the system described in the patent was purely mechanical due to the limitation of available sensors at the time. The reliability of the purely mechanical ABS could not provide a satisfactory level of reliability. In the 1960s, Bosch developed the first electronically controlled ABS; however, it still did not provide reliable functionality due to the technological limitations[32].

The kinematics for one wheel to help understand the development of the ABS is presented in the Figure 2.4. Here, ω is the rotational velocity of the wheel, V_x is the longitudinal velocity at the center of the wheel, R_e is the effective rolling radius of the wheel, and V_r is the velocity of the wheel measured at the contact patch. The definition of slip set by the SAE is shown in Equations 2.2 and 2.3. If the wheel rolls freely, there will be no slip ($\sigma_x = 0$), i.e. $V_x = \omega R_e$. If the wheel is locked up, the rotational speed will be zero $\omega = 0$ therefore $\sigma_x = -1$. Along the advancements of the sensors, it was possible to monitor the wheel speed ω and the vehicle's longitudinal speed directly V_x using sensors. Therefore, Equations 2.2 and 2.3 can be used as

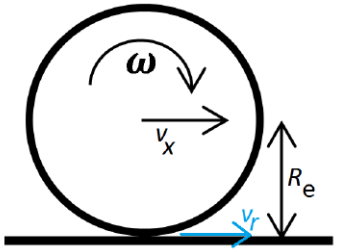

FIGURE 2.4: Kinematics of one wheel on the road. Reproduced from Eriksson[17].

a basis for the development of modern ABS. In 2017, the definition of the ABS is described by SAE[31] according to the available ABS technologies in the industry. The ABS in the SAE report is defined as a system that is controlled by a computer, can detect if any wheel is about to lock, and can control the brake torque at individual wheels or as a pair (front & rear) to limit wheel locking. It detects the wheel slippage or locking by monitoring individual wheel speed sensors.

Tire longitudinal force is approximately linearly proportional to the slip ratio until it reaches the maximum values at the slip ratio values of approximately 0.1 – 0.15. As the slip ratio exceeds these values, the generated longitudinal force between the road and the tire contact patch decreases. This explains why locked wheels are not desired for better braking performance. The relationship between the longitudinal tire force and the slip ratio can be seen in Figure 2.2. Due to this reason, modern ABS attempts to maximize the braking force by controlling the slip ratio to the desired values, in addition to preventing the wheels from just locking up. In addition to providing the vehicle the maximum braking force to avoid obstacles on the road, ABS can improve the vehicle stability significantly in this particular situation. Using ABS, steer-ability of the vehicle will be maintained by controlling the wheel slip, which provides the driver with more controllability of the vehicle.

Owing to its great benefits in vehicle stability, equipping ABS in automobiles has been mandated by many countries. The European Union mandated ABS equipment on all passenger vehicles since 2004, and the USA soon after followed and mandated ABS equipment on all passenger vehicles in conjunction with ESC under the Federal Motor Vehicle Safety Standard (FMVSS) 126 in 2013[15]. Numerous studies have been conducted in an effort to improve the performance and efficiency of ABS by using different control strategies. Schinkel[33] adopted the sliding mode control strategy to achieve the maximum braking force during the ABS logic development. Kueon[34] combined the sliding mode control and fuzzy logic control strategies to develop algorithms that are effective in rejecting parameter uncertainties, called fuzzy-neural-sliding model control. With advanced sensors and control strategies, there have been studies that can estimate uncertain parameters that have been considered unable to be measured. In 2019, Rajendran[35] developed a novel friction estimation technique using a sliding mode control. Velardocchia[36] performed ABS hardware-in-the-loop (HiL) tests and analyzed the control algorithms of different ABS units to evaluate the performance of active braking systems.

2.2.2 Traction Control System (TCS)

As discussed previously, two major objectives of ABS are to prevent wheels from locking up and to generate the maximum braking force during braking. Similarly, TCS was developed to prevent wheels from slipping, caused by providing an excessive amount of drive torque, and to generate the maximum traction force by controlling the wheel slip ratios. The TCS uses wheel speed sensors, similar to ABS, to compare measured acceleration and deceleration of individual wheels. Wheel spin on a specific wheel can be detected by comparing the measured wheel speed data. Once the wheel spin is detected, TCS can apply braking torques to wheels experiencing the wheel slipping, or control the engine torque transferred through the differential to the appropriate wheels. Based on which actuator is used, TCS can be categorized into three types; one that controls the engine torque, another that controls the braking pressures, and the one that combines both[31]. This can be seen in Figure 2.5: The BTCS is used when only one of the driven wheels is slipping

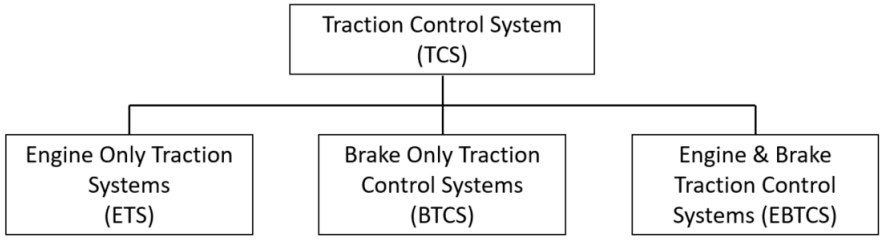

FIGURE 2.5: Types of Traction Control Systems (TCS).

on a split-μ road. The ETS is preferred for its better efficiency in the situation where both driven wheels are spinning, even though BTCS still can be used[37]. A combination of the two methods (EBTCS) requires more sophisticated control algorithms to integrate both braking and power-train subsystems to operate simultaneously without interference; however, the vehicle's motion can be stabilized more effectively by utilizing them together. In an attempt to improve acceleration, stability and steer-ability of the vehicle from the maximum traction force by adapting TCS in vehicle systems, many original equipment manufacturers (OEM) and tier 1 suppliers developed their own TCS algorithms, such as BMW, GM, Toyota, Bosch, etc[38]–[41].

However, there still are challenges in adapting this theoretical control techniques in real-life applications. Road-tire friction coefficients are not known and very hard to measure in passenger vehicles. In addition, integrating braking and power-train subsystems require sophisticated control strategies. Some approaches use sliding mode control strategies to estimate the road-tire friction force as explained previously[35] and use the slope of the μ–slip look-up curve, which was popular in the past for its simplicity[42]. Popular control techniques used for TCS algorithms development are the fuzzy control strategy[43]–[45] and sliding mode control[46], [47].

2.2.3 Electronic Stability Control (ESC)

Both ABS and TCS are developed primarily for the longitudinal dynamics of a vehicle. Unlike ABS and TCS, ESC is developed to improve the lateral dynamics of a vehicle. The technical report of the SAE[31] defines ESC as a system that is computer-controlled, where the computer contains a closed-loop algorithm designed to, in some circumstances, decrease vehicle yaw rate during spin and increase vehicle yaw rate during plow. The ESC must have adequate sensors and algorithms that can monitor or estimate vehicle yaw rate (yaw velocity) and VSA, and measure the driver steering input. Then, it must be able to apply brakes independently without brake actuation from the driver, where the magnitude of the brake force must be adjusted by ESC to generate the desired yaw moment to stabilize the yaw motion of the vehicle. Finally, ESC must be active over the entire vehicle speed range above a certain speed threshold. A primary goal of implementing ESC is to assist the vehicle to follow the desired path set by the driver's inputs. Figure 2.6 shows the schematic of different travel paths in three different cases. The bottom line is the path defined by a vehicle travelling on a high friction road. The top line is the path made by a vehicle travelling on a low friction road; therefore, the vehicle slipped significantly as seen with its great VSA β. On the same low friction road, it is observed that the vehicle's yaw rate is improved when the yaw stability control is applied to the vehicle.

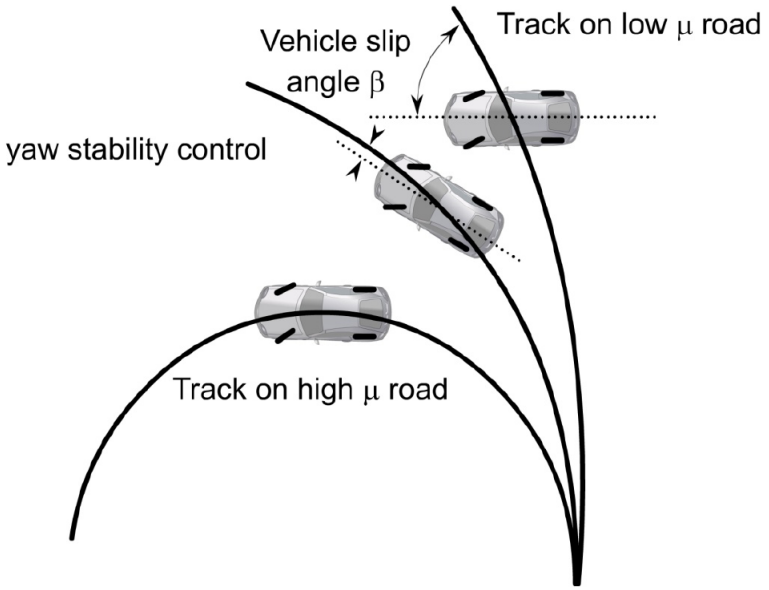

Figure 2.6: Trajectories of vehicles with and without ESC. Bottom line can be considered as the reference path. Reproduced from Rajamani[21].

The types of sensors used for the operation of ESC are wheel speed sensors, a steering wheel angle sensor, a yaw rate sensor and a lateral acceleration sensor. VSA is a vital part in determining the vehicle's directional stability; however, it is most often estimated and this is described in detail in the next section. Figure 2.7 shows how ESC intervenes in the vehicle dynamics to assist the vehicle to follow the desired path. First of all, the driver's inputs, such as throttle input, brake input,

and a steering angle, are received by the on board sensors. Based on the received driver inputs, ESC computes the desired yaw rate and desired VSA, which will be used as control target values. Most commercial ESC systems do not actually predict the desired path and use the predicted path as a control target, but the primary goal of following the desired path is done by controlling the yaw rate of the vehicle. Therefore, regulating the yaw rate closer to the desired yaw rate will eventually help the vehicle to follow the desired path, which explains why ESC is called a yaw control system (YCS) in many studies. However, controlling only the yaw rate of a vehicle is not sufficient for it to follow the desired path. A vehicle will not be able to travel along the desired path if its VSA is too large, even though its yaw rate is controlled so that it satisfies the driver's steering input. For this reason, many studies have been done in an attempt to control both yaw rate and VSA, and eventually controlling yaw rate and VSA together is a part of the definition of ESC in the SAE technical report. Then, the ESC will use the desired yaw rate and VSA values to generate a corrective yaw moment to stabilize the lateral motion of the vehicle. This corrective yaw moment is generated by creating corrective outputs. Examples of corrective outputs can be generated by using different actuators, such as, engine drive torque, braking torque, steering wheel angle, etc.

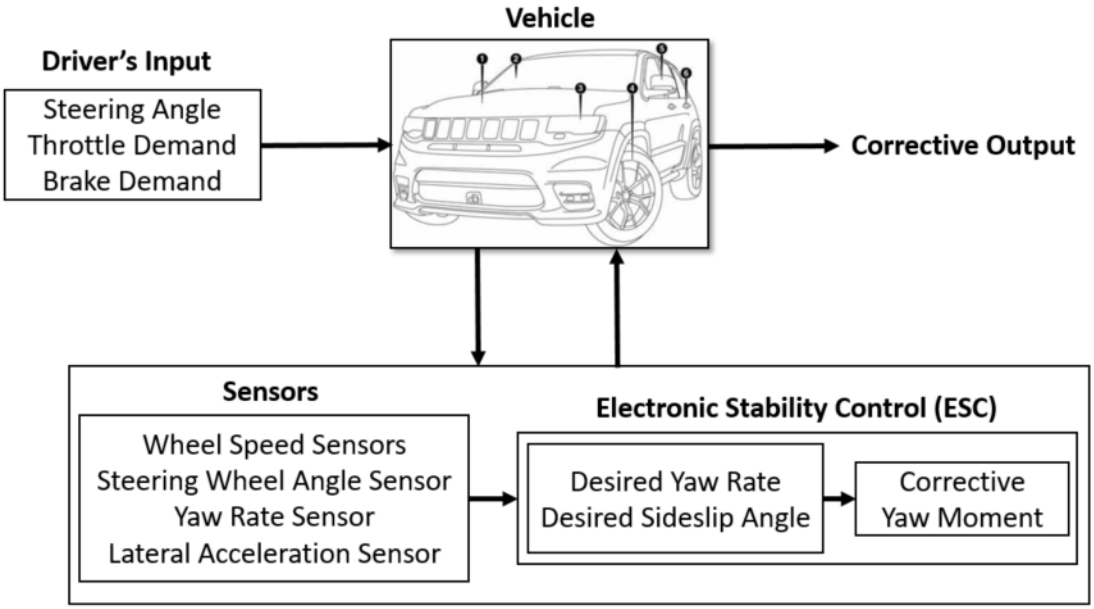

FIGURE 2.7: Schematic of signals for ESC to stabilize the vehicle.

More detailed explanation of how ESC operates to stabilize the vehicle's lateral motion will be discussed in Chapter 4.

The electronic stability control system in the automotive industry was first introduced by Bosch in 1995 as a safety option on the Mercedes-Benz S-Class sedan under the name Electronic Stability Program (ESP)[8]. The ESC improved the vehicle stability significantly, especially in its lateral stability while preventing vehicle skidding[48]. This reduced the number of single-vehicle

accidents significantly; therefore, the FMVSS acknowledged the importance of ESC for the passenger safety and mandated the equipment of ESC on all passenger vehicles since September of 2013[15].

Yaw stability of the vehicle is directly influenced by the steering system and individual wheel braking, which induces a yaw moment about the vertical axis of the vehicle. The active steering system (AS), which can be divided into active front steering (AFS) and active rear steering (ARS) systems depending on steering road wheels, can improve the maneuverability of the vehicle and assist the driver to avoid obstacles in critical handling situations. Such systems have disadvantages that they are only effective in a stable region where the lateral tire forces are approximately linearly proportional to the slip angle. Once the lateral tire force is saturated, it can be in extreme handling situations, the effectiveness of the AS is drastically reduced. The ESC utilizes brake subsystems to induce the corrective yaw moment by generating different longitudinal braking force at each tire, which avoids the limitations of the AFS. Therefore, there have been many studies to improve the effectiveness of the stability control systems by incorporating more than two stability enhancement systems, i.e., AFS+ESC. This is called integrated vehicle dynamics control (IVDC). Crolla et al.[49] proposed an IVDC control scheme with combined AFS and dynamic stability control (DSC) that uses individual braking systems to induce the correct yaw moment, to improve the vehicle handling and stability. Cho et al.[25] proposed a unified chassis control (UCC) strategy to improve the lateral stability of vehicles by integrating ESC, AFS and continuous damping control (CDC). Inclusion of CDC helped in reducing the roll instability in the study. Various control strategies were applied in the development of intelligent vehicle motion control, such as fuzzy, sliding mode, linear quadratic, and etc. These control strategies will be further explored in Section 2.4.

2.3 Vehicle Parameters Estimation

Extensive availability of electronics in the automotive industry, such as electronic control units (ECU), steering angle sensors, yaw rate sensors, etc, have enabled the technological advancements of active safety systems. These electronics communicate with each other to assess the vehicle motion status and to determine if any actuation is needed to stabilize the vehicle motion. Numerous active safety and stability enhancement systems, such as ABS, TCS and ESC, require vehicle state variables to be monitored in real-time, such as yaw rate, lateral acceleration, wheel speeds, VSA and side slip velocity. However, challenges arise when certain vehicle state variables are hard to be measured by commercial sensors. Therefore, the likelihood of the vehicle instability and control failure will be reduced by introducing a robust and accurate estimation methods for certain vehicle state parameters, mandatory for the operation of those active safety enhancement systems.

The VSA indicates the misalignment between the vehicle's orientation and its path trajectory. As discussed in Section 2.4, controlling the VSA is also crucial in addition to controlling the yaw rate. This is because the yaw rate sensitivity to the steering angle is significantly decreased at high VSAs. One direct method to measure the VSA can be done by installing optical transducers

that compare the vehicle's longitudinal axis and the travel direction. However, these are not practical for commercial installation in passenger vehicles due to the high costs and need for extreme precision. Therefore, many approaches to estimate the VSA are studied based on available measurements, such as wheel velocities, lateral acceleration and yaw rate. Gadola et al.[50] proposed a VSA estimation method using an extended Kalman filter (EKF) based on a bicycle model in an attempt to reduce the number of required parameters. In 2018, Chindamo et al.[51] published a paper describing currently known methods for VSA estimation. The paper describes that there are two major methods of estimating the VSA; observer-based and neural network-based. In this paper, an observer-based estimation method will be used for its simplicity and its effectiveness based on a vehicle reference model. The neural network-based methods must replace the artificial neural network (i.e., retrain the network) every time the vehicle parameters change.

Tire cornering stiffness is a crucial variable in tire modeling since it is required to compute the lateral tire forces. The cornering stiffness of a tire can be measured on a test rig; however, it cannot be easily monitored on a passenger vehicle while being driven on a road. Tuononen et al.[52] studied the measurement method of normalized cornering stiffness using vehicle measurements. The study is based on a phenomenon where the sign (+/-) of the vehicle slip angle sensitivity is reversed above a certain velocity, and the proposed method uses the velocity to estimate the normalized cornering stiffness of the tire. Obviously, the controller on passenger vehicles would not have the reference test data for this method; therefore, this method is not a suitable for commercial use. Many studies related to the development of automotive active safety technologies often use a set of fixed cornering stiffness values for their vehicle modeling. This method also does not generate a divergence error which takes place when the cornering stiffness is calculated directly; cornering stiffness measurements can diverge to infinity at near zero tire slip angles. This study will use a set of fixed cornering stiffness values, adapted from Mousavinejad's work[18].

2.4 Control Strategies for VDC

AS and direct yaw moment control (DYC) are two major types of vehicle stability control systems. The AS can control either only front wheels or rear wheels. They are each called AFS and ARS. If all four wheels are controlled for better stability, it is called four wheel active steering (4WAS). The ARS system is effective at low speeds since rear wheels' steering angle are limited. In 2020, Mercedes-Benz released information for the 2021 S-Class sedan. The new S-Class sedan will have the first rear-axle steering system integrated to their vehicle[53]. This should enable the large-sized sedan to park much easier in a limited space due to its improved parking maneuvers. The DYC system induces a desired yaw moment by generating braking or driving torques. The AS, however, has a limitation. Its effectiveness decreases drastically when the tire-behaviours are in the nonlinear ranges or when the tires' lateral forces are saturated. Once the lateral forces are saturated on tire-sides, more steering angles do not help the vehicle's yaw stability. However, the DYC system operates in both linear and nonlinear regions of the tire lateral forces. The drawbacks

of the DYC system are undesirable longitudinal kinetic energy loss from braking and insufficient traction force on a slippery road when a vehicle travels at a high speed. The desired driving torque will not be able to induce an adequate yaw moment in this situation.

Aripin and Abe et al.[54], [55] suggested that integrating both AS and DYC can result in the maximum benefits. This system is called IVDC where the AS and DYC systems operate in combination to minimize the kinetic energy loss and to improve the vehicle stability simultaneously. Shelby et al.[56] conducted a study in 2001 and concluded that AFS is more suitable to coordinate with a DYC system, compared to ARS and 4*WAS* when the goal is improved vehicle stability. In this paper, IVDC strategy is used in an effort to minimize the kinetic energy loss and to improve lateral stability.

Development of vehicle dynamics control systems, such as AS, DYC, and IVDC could be studied and commercialized due to robust and efficient control strategies. Types of control strategies that can be used for vehicle dynamic control systems vary depending on the order of the dynamic systems and other factors. The sliding mode control (SMC) strategy is one type of variable structure control strategy. This has been widely used in the control system industry for its robustness against uncertainties and external disturbances. The development of the various control strategies based on SMC is described in Yang[57]. Khoo et al.[58] adopted the integral terminal sliding mode (ITSM) control strategy for the first order dynamic system and concluded that fast finite time consensus can be reached on the ITSM surface. Iman et al.[59] adopted the nonsingular fast terminal sliding mode control (NFTSM) to the development of the AFS system. The NFTSM was proven to provide a fast transient response without singularity problems that used to be an issue for earlier types of SMC. In 2015, Iman et al.[12] reviewed control strategies for vehicle stability control applications. The paper studied numerous control strategies, such as PD, PID, model predictive control (MPC), SMC-based, H-infinity, linear quadratic regulator (LQR), and so on. The paper also categorized the control strategies based on vehicle stability control types, control objectives, advantages and disadvantages. As a result of the review, the study concluded that the SMC-based control strategies are the most suitable for application to IVDC for its robustness against uncertainties.

2.5 Co-Simulation

Automotive companies analyze numerous aspects of a vehicle during the development stage, ranging from thermal analysis to loads analysis at components. Unfortunately, there are no commercially available software tools that can fulfill the automotive engineers' every design purpose. For the proposed study, it is crucial to perform MBD analysis on a full vehicle model using CarSim. CarSim has built-in vehicle stability controller models that can be used for a full vehicle simulation, such as ABS, TCS and ESC. However, their level of sophistication may not be as great as required by the industry.

Co-simulation refers to the process of simulating a system under a certain environment by using more than one separate simulation platform. This process enables engineers to analyze various aspects of the system simultaneously. The software tools interact during the simulation; therefore, the output from one simulation platform affects the other simulation platform. For instance, Li[60] proposed a co-simulation model based on a yaw fuzzy control strategy using ADAMS Car and MATLAB/Simulink platforms. A study in 2014 also shows that Volvo uses co-simulation for the ABS performance testing purpose[17]. Co-simulation enables engineers to observe variables from different fields of engineering and how they affect each other. More complex and sophisticated controller can be designed in MATLAB/Simulink platform to be co-simulated with a full vehicle model in CarSim.

The proposed work has an ESC control system developed in MATLAB/Simulink. As a result, the designed control system will be co-simulated with a full vehicle MBD model in CarSim's limitations in controller designing feature. This co-simulation set-up will enable to see how the vehicle behaviours are affected and stabilized by the proposed ESC control system during the dynamic events.

Chapter 3

Vehicle Model

The software-in-the-loop (SiL) method is chosen for this research project to simulate the full vehicle with the electronic stability control (ESC) capabilities. This gets rid of the need of an actual vehicle and an actual electric control unit (ECU). As a result, virtual models that represent both a vehicle model and an ECU must be designed. This chapter focuses on the vehicle modeling for the co-simulation.

The co-simulation will be performed by using MATLAB/Simulink, responsible for the ESC controller, and CarSim, responsible for the nonlinear full vehicle model and dynamic events. The ESC controller needs a reference vehicle model integrated in its design so that it can generate corrective outputs to stabilize the vehicle, based on the measurements from the real vehicle (a nonlinear full vehicle model). However, a nonlinear full vehicle model is not preferred as a reference model since the design of the controller will be extremely complicated.

In this chapter, two vehicle models will be introduced; a bicycle model and a nonlinear full vehicle model. The bicycle model in this chapter is used for the design of the ESC controller; it is used for active safety enhancement controller development extensively in the literature. The nonlinear full vehicle model is designed on a commercial multibody dynamics (MBD) software, CarSim. The nonlinear full vehicle model in CarSim represents a real vehicle much closer than a bicycle model, since it has more parameters to describe the vehicle's topology, flexible body parts, and more factors integrated in the software to describe the vehicle in detail.

3.1 Bicycle Model

For the controller design, a 2 degrees of freedom (DOF) bicycle model is utilized. The vehicle parameters, used to describe the bicycle model, are adapted from Mousavinejad[26]. The equations of motion for the 2-DOF bicycle model are described in Equations 2.6 and 2.7 in Chapter 2. The derivation of those two core equations describing the bicycle model is also described in depth by Minaker[19]. The vehicle parameters used in this study are shown in Table 3.1.

3.1.1 Model Properties & Geometry

The bicycle model or the yaw plane model has been widely used for automotive active safety enhancement control system development in the literature. The vehicle width is ignored in the bicycle model, which is the reason behind its naming; it eventually looks like a bicycle when the yaw plane model is seen from the top. The vehicle width affects the lateral weight transfer, which influences the lateral force developed by tires during the cornering. However, this effect is ignored in the bicycle model.

A bicycle model has two DOFs, which are the lateral velocity V_y and the yaw rate γ. Two assumptions are often made for the bicycle model to be valid. First, the forward speed of the vehicle is assumed to be constant, so it can be treated as a parameter of the vehicle rather than a variable. In addition, it is assumed that the front wheel angle is sufficiently small so that the slip angles can be expressed as the ratio between lateral velocity with respect to the pointing direction of the wheel and the rolling velocity, as shown in Equation 3.1 and Equation 3.2, i.e., the small angle assumption $\tan\theta \approx \theta$ is used.

$$\alpha_f = \frac{V_y + l_f\gamma}{V_x} - \delta_w \tag{3.1}$$

$$\alpha_r = \frac{V_y - l_f\gamma}{V_x} \tag{3.2}$$

Additionally, the bicycle model uses a linear tire model that assumes a linear relationship between the tire slip angle and the lateral force. The lateral forces of the tires can be expressed as seen in the following equations.

$$F_y = F_{yf} + F_{yr} = -2(C_f\alpha_f + C_r\alpha_r) \tag{3.3}$$

Each lateral force for the front and rear axle has a coefficient of 2 to combine the effect of left and right side on each front and rear side of the vehicle. Therefore, the cornering stiffness C_f, C_r in the Equation 3.3 is the value of each side of the tire, assuming the cornering stiffness values are equal for the left and right side. Note the minus sign in the equation exists due to the sign convention of the model; a negative resistant lateral tire force is generated from a positive slip angle.

3.2 Nonlinear Full Vehicle Model (CarSim)

While the bicycle model is used as the simplified version of the real vehicle to be controlled in the controller design, a nonlinear full vehicle model in CarSim is the main vehicle model that

travels on the virtual track, representing the real vehicle. This section describes the model properties of the nonlinear full vehicle designed in the MBD software, such as CarSim and ADAMS Car as well as how the nonlinear full vehicle model is designed in the CarSim user interface.

3.2.1 Model Properties & Geometry

Nonlinear full vehicle models contain numerous factors that make them much more complex than the bicycle model. Nonlinear full vehicle models developed in an MBD software, such as (but not limited to) CarSim, have more DOFs, which results from including more vehicle components in the vehicle assembly, such as suspension models. Commercial MBD software tools like CarSim and ADAMS Car enable users to design every part of a vehicle model, ranging from those as small as a control arm in the suspension to the topology of the entire vehicle. The MBD software is also capable of integrating flexible parts in the assembly design to calculate more accurate vehicle simulation results than entirely rigid body-based vehicle simulation, which is unrealistic. This is because the flexibility of certain components, such as an anti-roll bar, is crucial to represent its physical characteristics in vehicle modeling. These factors differentiate an MBD full vehicle model from the bicycle model, regarding the DOFs, non-linearity, and complexity.

It is beneficial to benchmark the pre-validated vehicle model from the automotive control related literature since the design of the nonlinear full vehicle model on CarSim can have so many variations in its design. This section will describe how the pre-designed full vehicle model template in CarSim is modified to represent the 8-DOF vehicle model that is described and validated in the literature for the active steering control design[26]. The 8-DOF vehicle model describes three vehicular planar motions (longitudinal motion, lateral motion and yaw motion), body roll motion and individual rotational dynamics of four wheels. As a result, this model contains more considerations in calculating the lateral velocity V_y and the yaw rate γ, which were the 2-DOF in the bicycle model; the lateral weight transfer causing roll motions is considered in the 8-DOF vehicle model as seen in Equations 3.4 and 3.5.

Lateral motion:

$$\Sigma F_y = m(\dot{V}_y + V_x\gamma) - m_s h_s \ddot{\phi} \tag{3.4}$$

Yaw motion:

$$\Sigma M_z = I_{zz}\dot{\gamma} - I_{xz}\ddot{\phi} \tag{3.5}$$

where m_s is the sprung mass, ϕ is the roll angle measured between a vertical axis passing through the roll centre and the line passing through the roll centre and the centre of the sprung mass and h_s is the distance between the centre of sprung mass and the roll centre. The rest of equations of motions of the 8-DOF vehicle models are shown below:

Longitudinal motion:

$$\Sigma F_x = m(\dot{V}_x - V_y\gamma) + m_s h_s \gamma \dot{\phi} \tag{3.6}$$

Roll motion:

$$\Sigma M_x = I_{xx}\ddot{\phi} + m_s h_s(\dot{V}_y + V_x\gamma) - I_{xz}\dot{\gamma} \tag{3.7}$$

Wheel rotational motion:

$$I_{wi}\dot{\omega}_{wi} = -R_w F_{xi} + T - T_{bri} - T_{ri} \tag{3.8}$$

where I_{wi} is the i-th wheel's rotational moment of inertia, ω_{wi} is the i-th wheel's rotational velocity, R_w is the effective rolling radius, T is the driving torque, T_{bri} is the braking torque applied on the i-th wheel and T_{ri} is the rolling resistance torque acting on the i-th wheel. This 8-DOF vehicle model with the parameters shown in Table 3.1 is validated with the road vehicle test results of SAE J266[26]. Lateral weight transfer, roll motion and wheel rotational dynamics makes the 8-DOF vehicle model more accurate to the real vehicle, compared to the bicycle model. As a result, this 8-DOF vehicle model becomes a good reference model for nonlinear full vehicle design in CarSim. The same vehicle model parameters are used in the 2-DOF bicycle model for the controller design.

Table 3.1: Vehicle parameters of the 8-DOF validated vehicle model[26]. The bicycle model in the controller design use these values to represent the CarSim vehicle model.

Parameter Type	Notation	Value
Sprung mass of the vehicle	m	1300 kg
Distance from the CG to the front axle	l_f	1.2247 m
Distance from the CG to the rear axle	l_r	1.4373 m
Wheel track width	D	1.437 m
Distance from the ground to the CG (sprung mass)	h	0.445 m
Roll moment of inertia	I_{xx}	346.7 kg.m^2
Yaw moment of inertia	I_{zz}	1808.8 kg.m^2
Effective rolling radius of a wheel	R_w	0.285 m
Cornering stiffness of each front tire	C_f	40000 N/rad
Cornering stiffness of each rear tire	C_r	40000 N/rad

Full vehicle models in CarSim are defined with more design factors than the 8-DOF vehicle model in the literature. For instance, the literature did not consider the suspension system in the vehicle design. However, CarSim has both front and rear suspensions to describe the vehicle topology and behaviour. Therefore, the available full vehicle model in CarSim, sports utility vehicle (SUV) D-Class model, is modified to represent the validated 8-DOF vehicle model. The reason why the D-Class SUV model is chosen to be modified is because it is used for the CarSim's internal lateral stability analysis simulation sets. The detailed modified vehicle description can be found in Figure 3.1.

Sprung mass information of the vehicle description in CarSim allows the user to modify many parameters, such as wheelbase, moment of inertia, CG heights, and more. There are also parameters that users can change that influence the animation of the resulting motion, but these do not

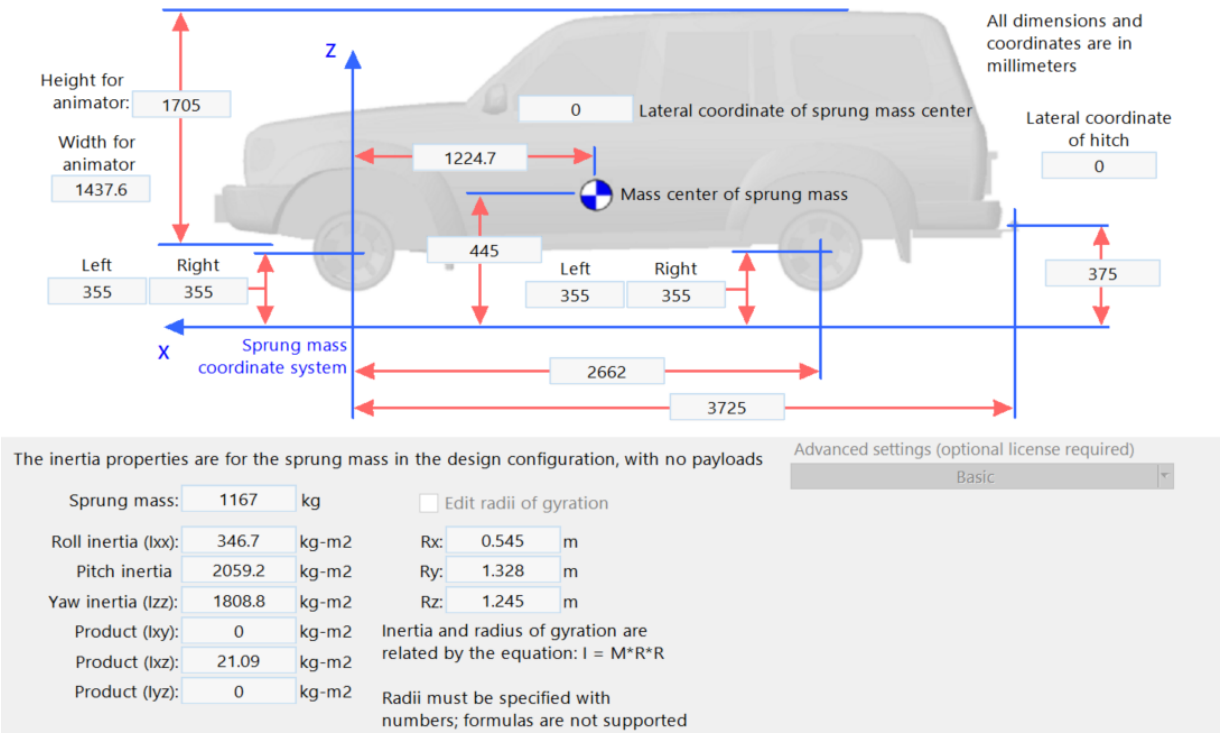

FIGURE 3.1: Sprung mass of a nonlinear full vehicle in CarSim. The vehicle parameters that were introduced from the 8-DOF vehicle model are shown, while the parameters that were not introduced from Table 3.1 are from the CarSim template model.

affect the vehicle dynamics behaviour. Aerodynamics of the full vehicle model is deactivated to reduce the gap between the 8-DOF model and the CarSim vehicle model. The powertrain model is used as a pre-existing template as shown in Figure 3.2.

The powertrain model includes an 150 kW internal engine model with front and rear differential gear ratios of 4.1, which is input shaft angular velocity divided by the average output spin rate of the two half-shafts. The transmission gear ratio for this powertrain model is shown in Table 3.2. Since the literature showed the dynamics simulations based on a constant speed assumption, this powertrain model is expected to result in more realistic results, with undesired fluctuation in the simulation outputs. Similarly, the brake model is not considered in the 8-DOF model; therefore, the template brake model for D-Class is used as well, which expects to add more realistic vehicle behaviour during the simulation, shown in Figure 3.3.

The steering system in most real vehicles has flexible parts in its assembly, involving rubber and fluids, which introduces non-linearity in the dynamic behaviour between the driver's input and the wheel rotation. A steering controller takes initial road wheel angles as inputs, then calculates the corrective wheel angles to stabilize the vehicle. However, importing and controlling the same variable of a vehicle model during the co-simulation can cause an issue; high frequency chattering can be generated from reading and correcting the same variable, since abrupt change

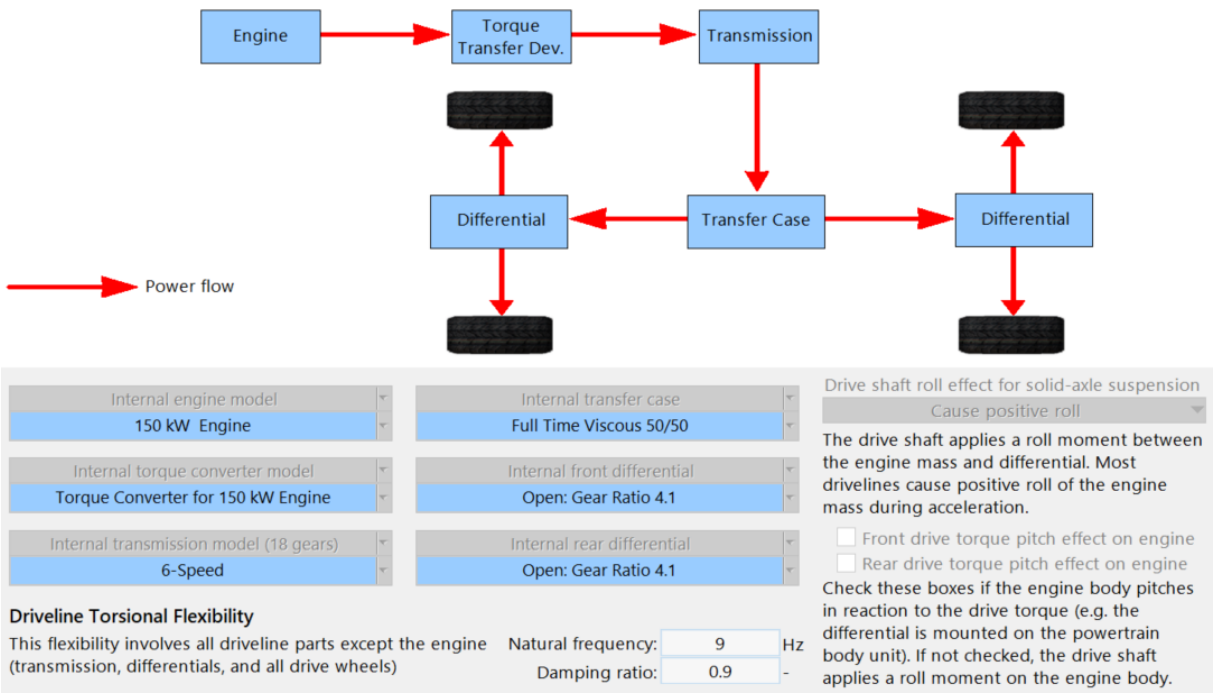

FIGURE 3.2: Powertrain model of a nonlinear full vehicle in CarSim.

in the variable affects the calculation in the controller simultaneously. This issue can be resolved by several methods. One possible solution can be adding a very short time delay function in the controller, so that the vehicle variable that is just updated from the controller does not affect the controller's calculation instantly. However, this method can significantly reduce the efficiency of the controller and it may affect the performance of the other parts of the controller. Therefore, in this work, the controlled vehicle variable and imported vehicle variable (road wheel angle, δ_{wheel}) are separated by using the steering wheel angle that is related to the road wheel angle as seen in Figure 3.4.

The ratio between the steering wheel angle in the cabin and the road wheel angle is called the steering ratio. Most passenger vehicles have a steering ratio ranging from 12 to 20. In the

TABLE 3.2: Transmission gear ratio of the nonlinear full vehicle model in CarSim.

Gear Number	Transmission Gear Ratio
R	−3.168
N	N/A
1	3.538
2	2.06
3	1.404
4	1.00
5	0.713
6	0.582

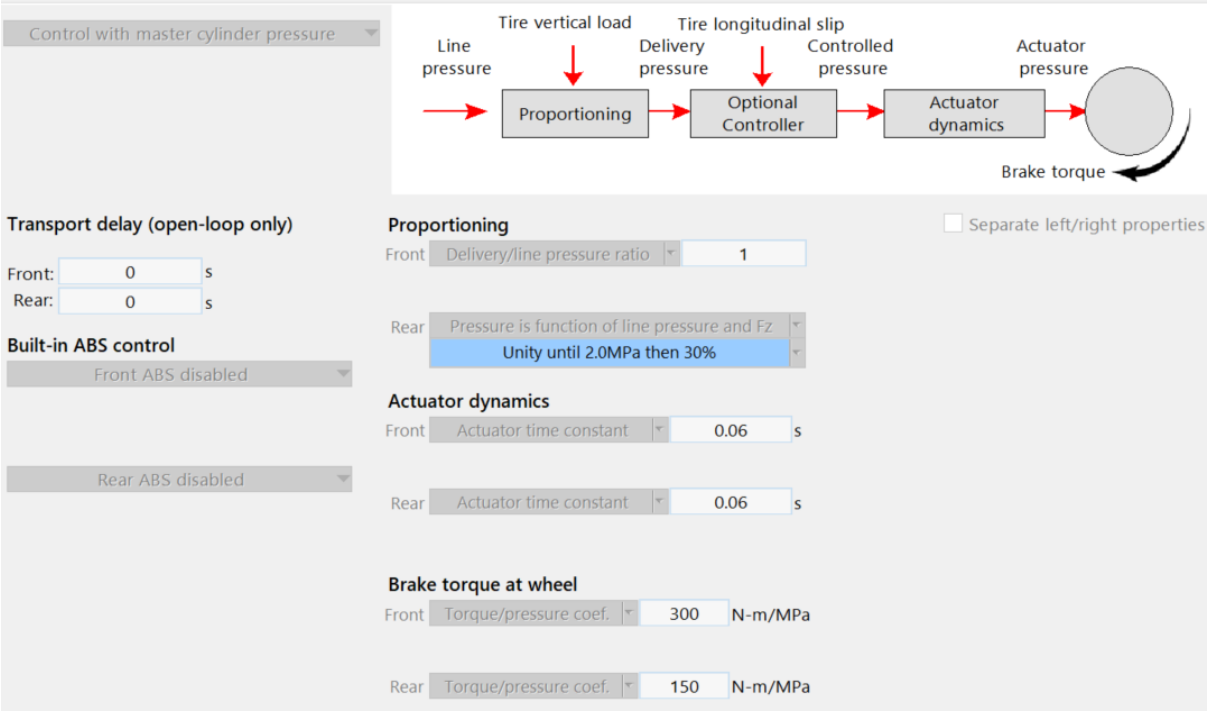

FIGURE 3.3: Brake model of a nonlinear full vehicle in CarSim.

MBD software, the steering system is often not defined by this ratio only. Instead, the connection between the driver's steering wheel angle and the road wheel angle is described by a combination of linear and nonlinear parts of the entire steering system assembly as seen in Figure 3.5. However, the controller prefers simple and linear logic for its design to control the vehicle.

Therefore, an approximate steering ratio is found for the modified vehicle model in this work. This enables the ESC controller to predict the vehicle behaviour by using a bicycle model and linearized steering behaviour between the steering wheel and the road wheel. Both of the simulation types were conducted at constant high speed (120 km/h) and low speed (40 km/h) to observe the steady state steering ratio value. A simulation was performed with a constant steering input from the driver. The steering wheel angle was maintained at 160°. The calculated steering ratio during a second test is shown in Figure 3.6. During this second simulation, the steering wheel angle from the driver slowly increased at a rate of $2^{\circ}/s$ from 0°. The simulation setting and its results are shown in Table 3.3.

The variance of the calculated steering ratios among different simulation runs was not significant even in different speed and different steering input settings. The steady state steering ratio was calculated as shown in the Equation 3.9.

$$SteeringRatio = \frac{\delta_{\text{Driver}}}{\delta_{\text{Road Wheel}}} \tag{3.9}$$

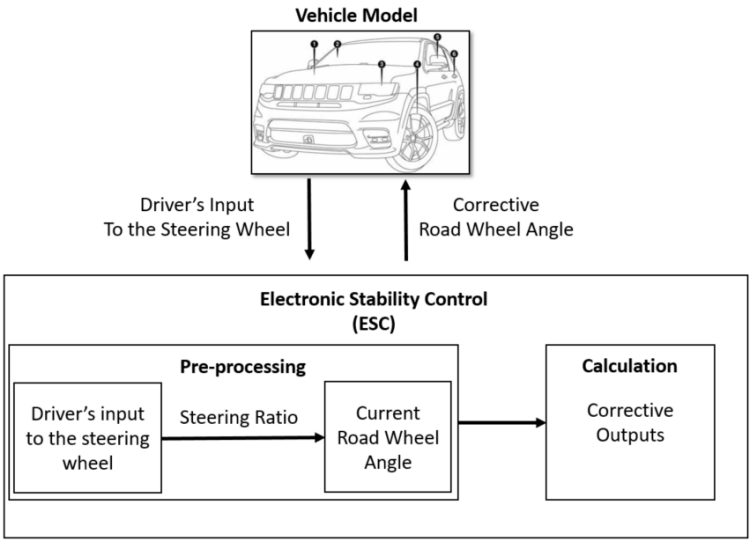

FIGURE 3.4: Driver's input to the steering wheel is multiplied by the steering ratio. The ESC controller takes the calculated road wheel angle to generate the corrective road wheel angle for vehicle stabilization.

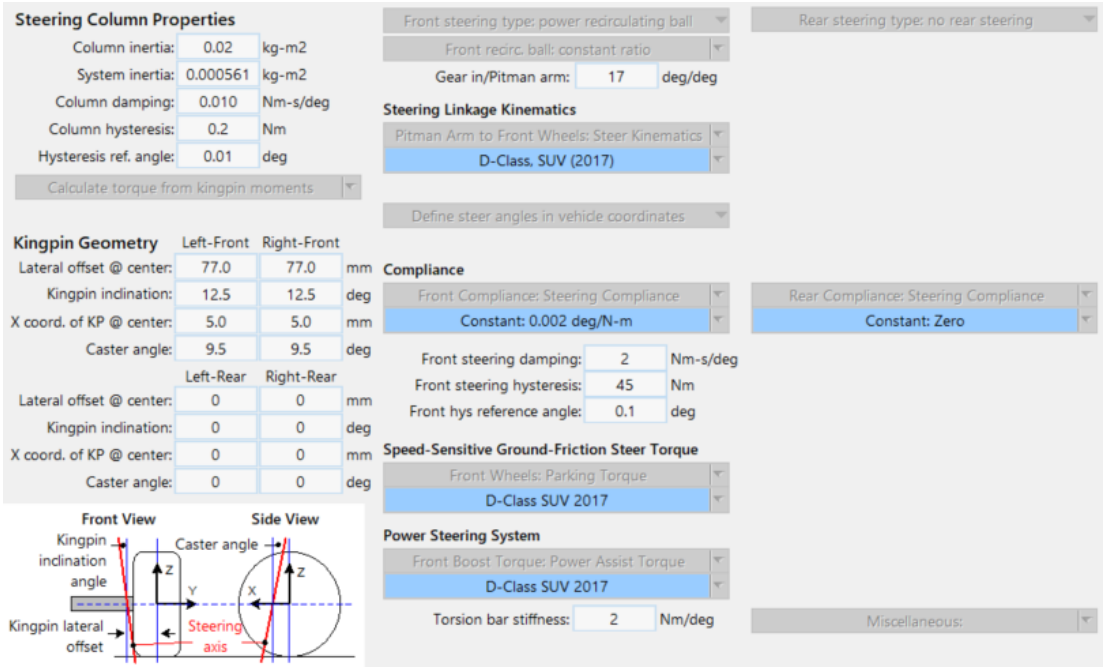

FIGURE 3.5: Steering model of a nonlinear full vehicle in CarSim.

Therefore, the steering ratio of the nonlinear full vehicle model in CarSim is assumed to be 18.4, an average value of the test results in four different simulation runs. This value is multiplied to the simulated driver's steering wheel angle to predict the road wheel angles. Then, the controller uses the predicted road wheel angle to calculate the corrective outputs for the vehicle stabilization. The high frequency noise problem in steering angle, mentioned earlier, was successfully avoided by using this technique. This method can be used for any other steering controller design applications

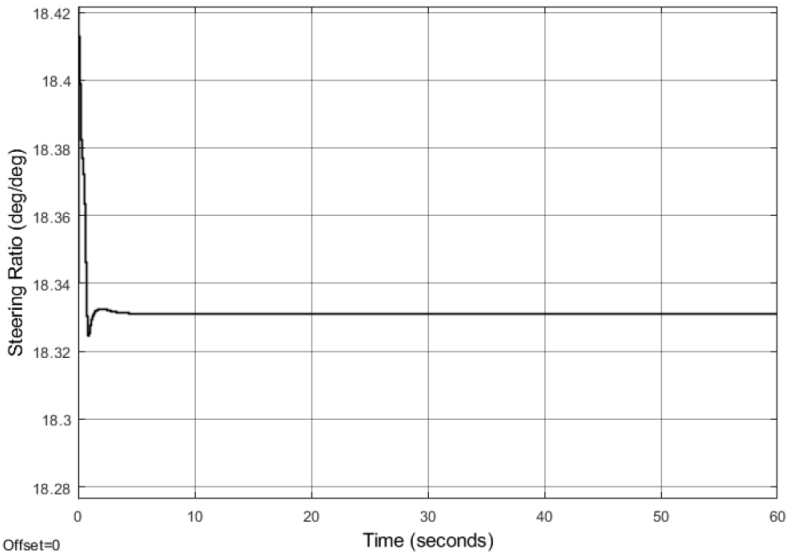

FIGURE 3.6: Steering ratio results from the second test. Steady state steering ratio is 18.33.

using MBD software tools.

The suspension models for the full vehicle are adapted from the CarSim D-Class database for both front and rear, which were used for the CarSim's internal ESC testing simulation sets. The configuration and the parameters of the suspensions can be found in the following figures. The front suspension uses a double wishbone suspension, which is an independent suspension using two wishbone-shaped suspension arms. The rear suspension uses a solid axle.

The vehicle width is modified to 1437.6 mm, in order to match the benchmarked vehicle model from the literature.

Front and rear spring and damper parameters are adapted from the CarSim's D-Class database. Front spring rate is stiffer than the one of the rear spring.

Tire model in full vehicle design is as significant as other major subsystems since the tires are responsible for various limitations of the vehicle dynamics performance. Excellent acceleration

TABLE 3.3: Simulation setting and results in order to find the steering ratio of the modified vehicle model in CarSim.

Simulation Setting				Results
Test Number	Simulation Type	Steering Input	V_x (km/h)	Steady State Steering Ratio
1	Constant Steering Input	160°	120	18.1
2	Constant Steering Input	160°	40	18.3
3	Slowly Increasing Steering	$2°/s$	120	18.6
4	Slowly Increasing Steering	$2°/s$	40	18.7

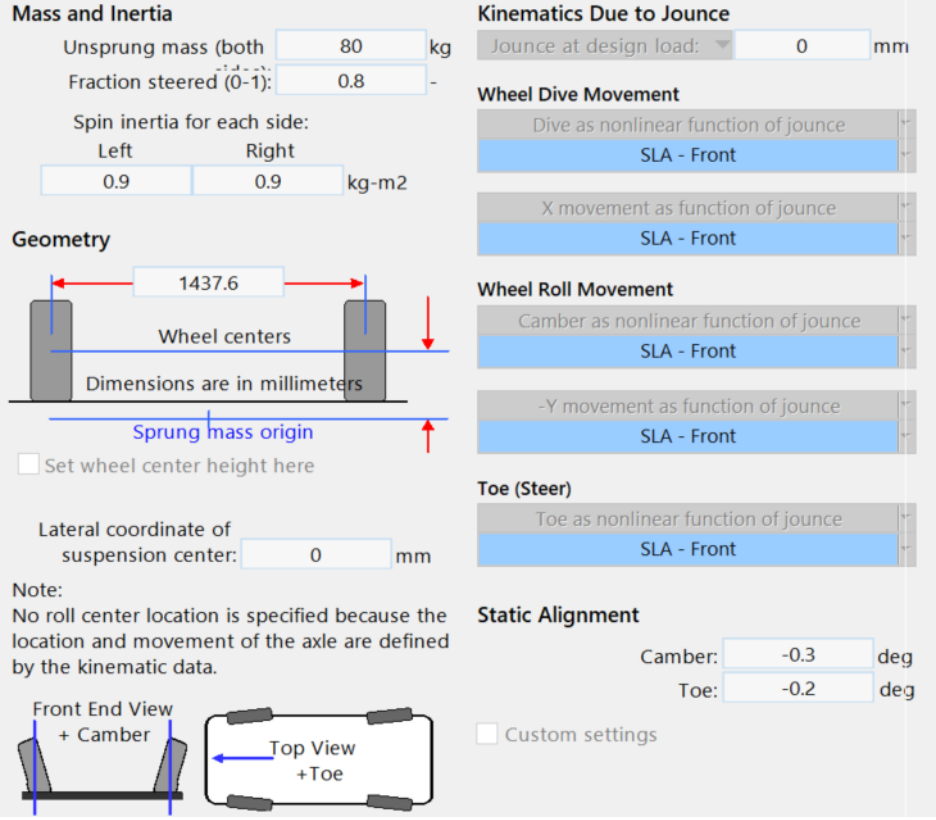

FIGURE 3.7: Front suspension configuration of a nonlinear full vehicle model in CarSim.

and braking can be expected from having a very powerful and efficient powertrain and braking subsystems. However, the expected high performance cannot be achieved if the tire treads are worn out; the tires with the worn out treads cannot deliver the driving torques and braking torques to the road. Also, tires affect the vehicle's lateral dynamics nonlinearly. Tires have its own unique characteristics in how much lateral force it generates at different slip angles. The bicycle model, used in the controller design, assume small slip angles to calculate the lateral force of tires by using the linear relationship between the slip angle and the lateral force. As seen in the Equation 3.3, cornering stiffness is a key parameter to predict the lateral force of the vehicle model in the controller. The parameter for the tire model in CarSim is shown in the Figure 3.11. The effective rolling radius is modified to match the benchmark vehicle model.

CarSim has various tire models available. But, none of that can be simplified as a simple and linear equation. In this paper, tire models, which are used for the Carsim's internal ESC test sets, will be modified to match the benchmark vehicle's tire data. The given tire model in CarSim generates the lateral forces based on the lookup table where the resultant lateral force is calculated from a given normal load and a slip angle to an individual tire, the look up table can be found in the Figure 3.12.

Each line in the Figure 3.12 represents the lateral tire behaviour at different normal loads. The

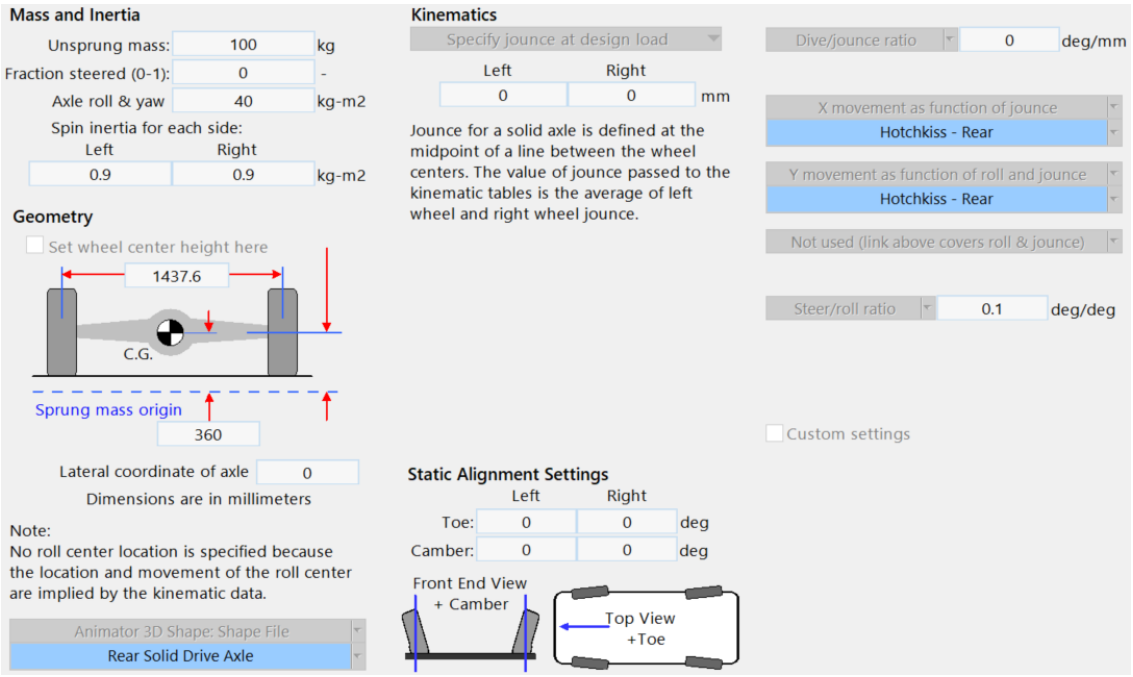

FIGURE 3.8: Rear suspension configuration of a nonlienar full vehicle model in CarSim.

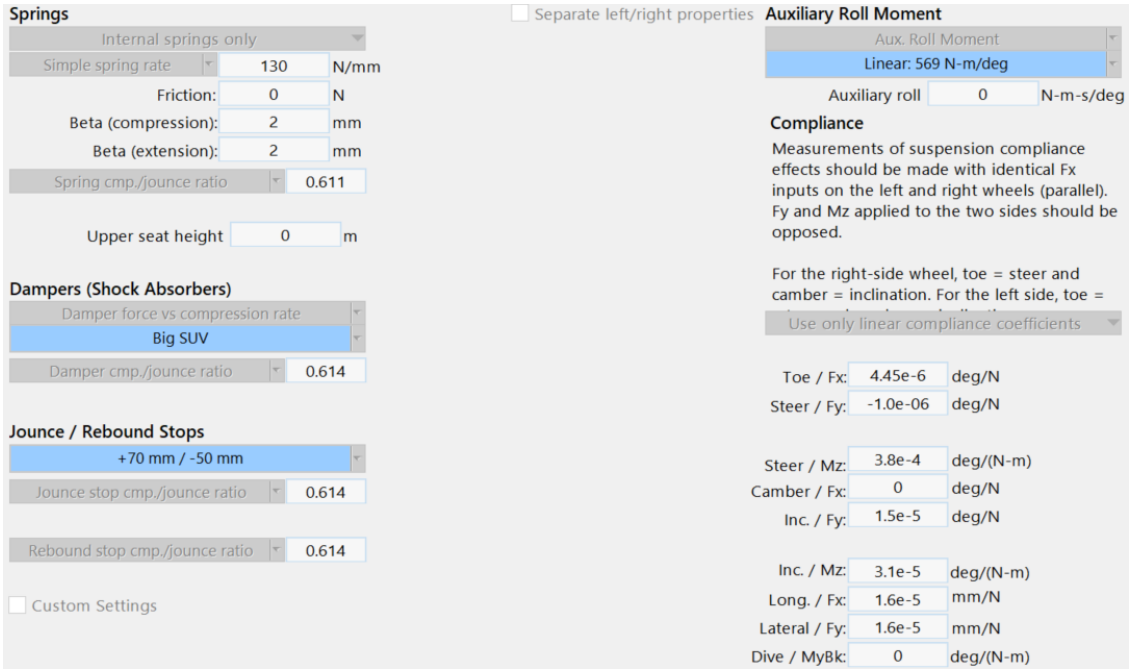

FIGURE 3.9: Front spring setting of a nonlienar full vehicle model in CarSim.

slope in the graph of slip angle and lateral force is cornering stiffness. There are multiple cornering stiffness for a same tire model, which vary depending on the normal loads on the tire. There are multiple methods to decide the fixed value of the cornering stiffness for the controller's design.

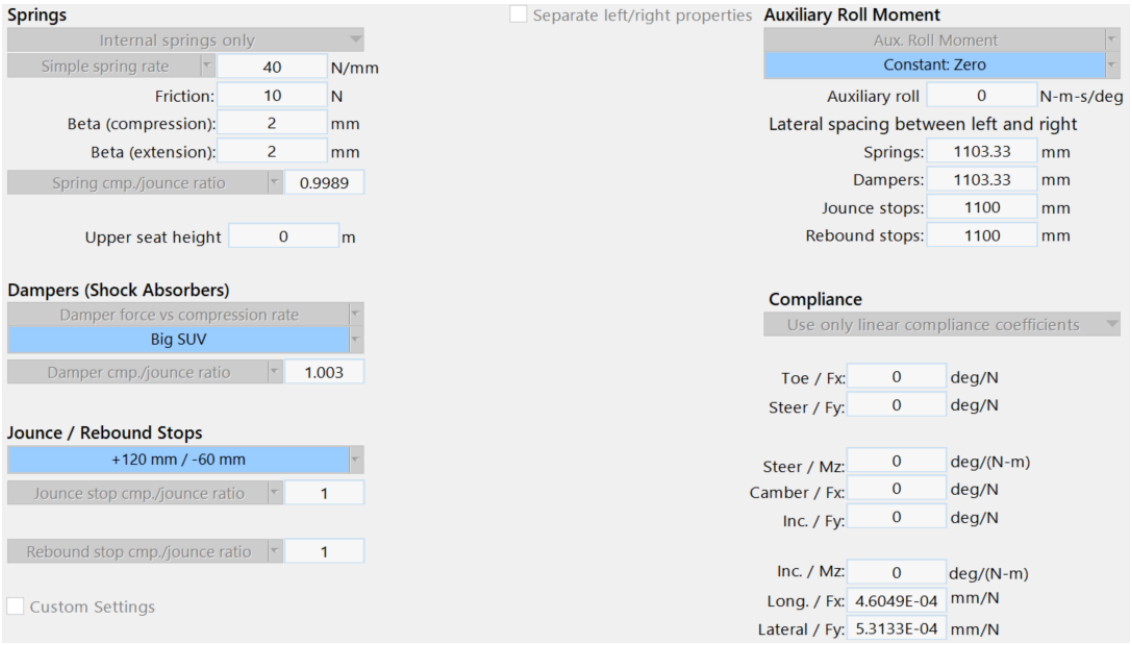

FIGURE 3.10: Rear spring setting of a nonlienar full vehicle model in CarSim.

First method is to take the slopes of the lateral tire force-slip angle graph in a linear region as seen in the Figure 3.12, then to take the average value of them. This method, however, is inaccurate since the look-up table does not contain strictly linear relationship between the lateral tire force and the slip angle. The results can vary depending on the user's choice on the linear region to take the slope from the lateral tire force-slip angle graph.

It is also possible to take the measurement from the individual tire lateral forces and tire slip angles in CarSim. Therefore, it is possible to directly calculate the cornering stiffness; dividing the tire lateral force by the tire slip angle. However, this method often results in huge spikes on the calculated cornering stiffness when the tire slip angle approaches to 0. Therefore, this causes the ESC controller to generate a undesired huge correction yaw moment, which should be avoided. This method was used and this phenomenon was observed, as seen in Figure 3.13.

Another alternative method is to run a simulation with the steering input, which increases slowly, to find the ideal cornering stiffness that tracks the transient response of the vehicle well. In this paper, later method is used to decide approximate value of the cornering stiffness since good transient behaviour tracking of the controller is crucial in controlling the vehicle's transient dynamic behaviour. The simulation is set to increase the steering input by $2^{\circ}/s$ at a constant speed of 120 km/h. The yaw rate of the vehicle is expected to increase almost linearly; transient behaviour, then to saturate at a certain value, which is called steady-state value. The aim is to find the cornering stiffness that shows good tracking on the transient behaviour of the vehicle. Note that the prediction of the tire behaviour by using cornering stiffness is not great prediction method due to the nonlinear behaviour, however, sufficient for the proposed study purpose. In addition, trial and

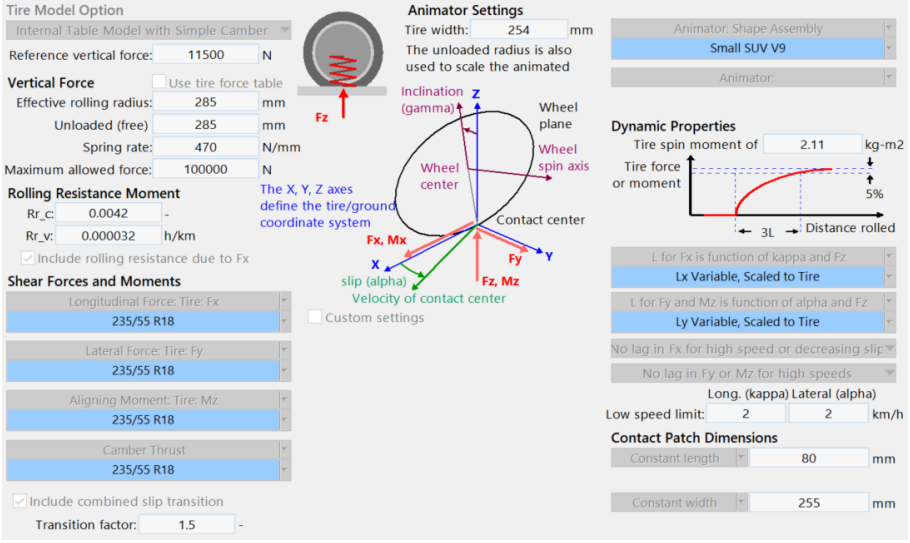

FIGURE 3.11: Tire model of a nonlienar full vehicle model in CarSim.

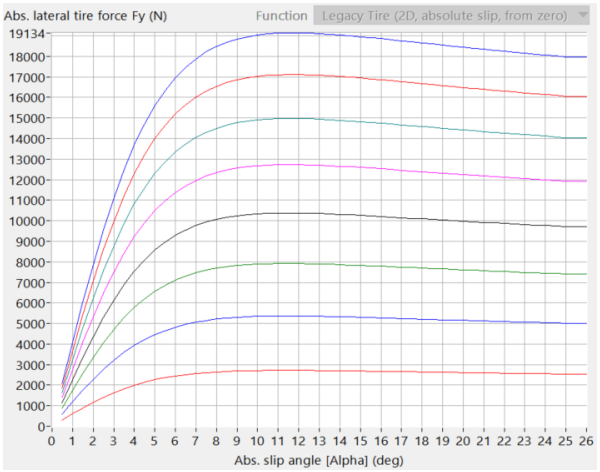

FIGURE 3.12: Tire look up table of a nonlienar full vehicle model in CarSim. The lateral force is based on the given normal force and the slip angle.

error is inevitable to find the suitable cornering stiffness values that predict the full vehicle model tire modelś behaviour sufficiently accurate. Four sets of cornering stiffness values are compared below.

First, the vertical loads at individual wheel hubs are simulated at the static event, where the vehicle does not move, but all sensor signals are simulated on the full vehicle model. Based on the obtained vertical loads at each wheel, corresponding cornering stiffness for each wheel is obtained from Figure 3.12 by taking slopes between the first 2° of the slip angle, in the linear region. Average values of both left and right sides are taken as the C_f and C_r, which are 54030 N/rad and 38411 N/rad, respectively.

Secondly, cornering stiffness values of front and rear are both calculated directly. Tire lateral

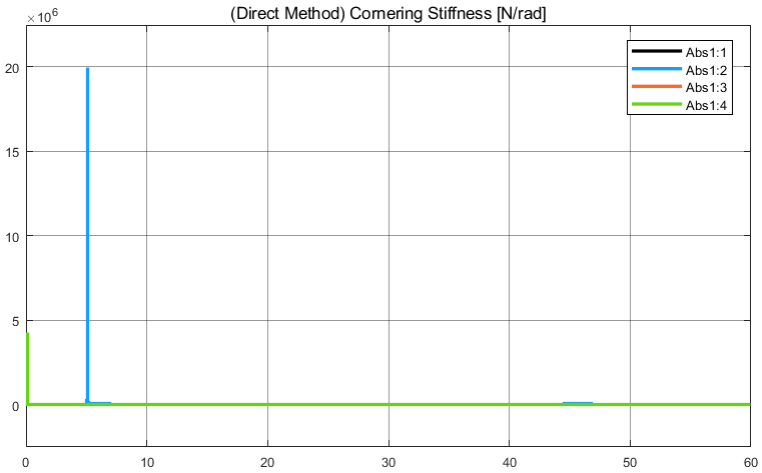

FIGURE 3.13: Undesired huge spikes are observed when the cornering stiffness is calculated directly from the lateral force and the slip angle.

forces during the simulation are divided by the tire slip angles dynamically during the simulation. However, the simulation failed due to the singularity problem. This is why real time calculation of the cornering stiffness is not used in the controller design in the field.

The third set of cornering stiffness is the one that is used by Mousavinejad[18] in the benchmark vehicle. In the literature, it is not explained in depth how this set of cornering stiffness is obtained, but 40000 N/rad for each tire is used.

The last set of the cornering stiffness is obtained from the direct method of calculating the cornering stiffness values during the simulation. The difference between this approach and the second approach is that the second approach tried to use the cornering stiffness that varies throughout the simulation, but this approach looks at the time history of the cornering stiffness calculation, then takes the mean value of the front and rear tires. Note that the undesired peak at the beginning of the simulation is excluded from the calculation.

Four different sets of the cornering stiffness from four different approaches are compared. The best transient response predicting; yaw rate tracking, was achieved by the set from the literature. The yaw rate predicting performance is confirmed visually as seen in Figure 3.14, Figure 3.15 and Figure 3.16. In addition, the results are numerically shown by comparing the root mean square errors (RMSE) between the actual yaw rate and the predicted (desired) yaw rate, as seen in the Table 3.4. Therefore, 40000 N/rad will be used as cornering stiffness for both front and rear in the bicycle model for the controller design, as this showed the minimum error of 0.675°/s in the yaw rate prediction.

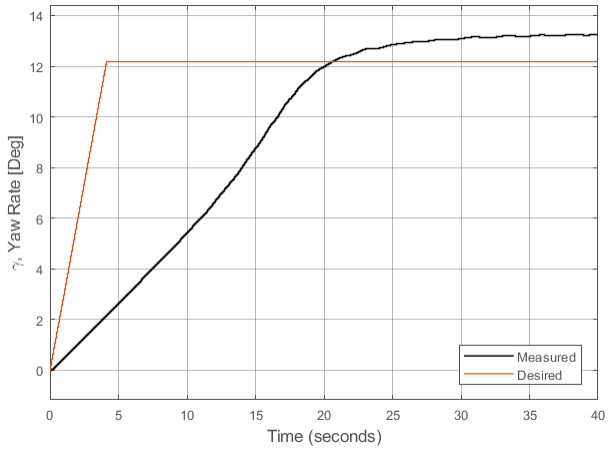

FIGURE 3.14: Cornering stiffness from static event is used. Transient behaviour tracking is poor. Values of C_f = 54030 N/rad, C_r = 38411 N/rad are used. Measured values are the simulated values from the virtual vehicle.

TABLE 3.4: Simulation setting and results in order to find the steering ratio of the modified vehicle model in CarSim.

Simulation Setting				Result
Test Number	Steering Input	V_x (km/h)	C_f, C_r (N/rad)	RMSE-Yaw Rate ($^\circ/s$)
1	$2^\circ/s$	120	54030, 38411	4.2726
2	$2^\circ/s$	120	Directly calculated	Simulation failed
3	$2^\circ/s$	120	40000, 40000	0.675
4	$2^\circ/s$	120	30697, 30436	0.9048

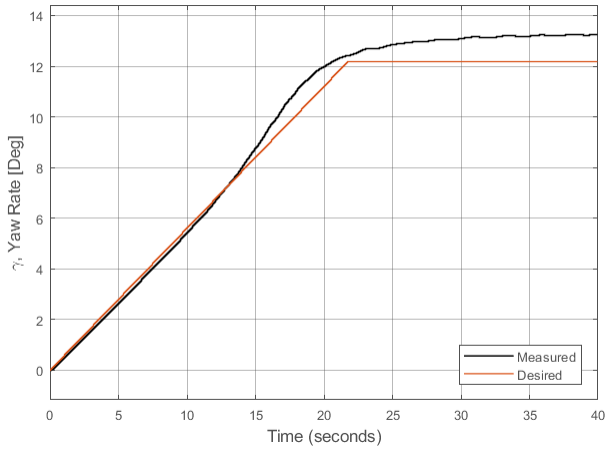

FIGURE 3.15: Cornering stiffness from the literature is used. Transient behaviour tracking is much improved, compared to the other test sets. Values of C_f = 40000 N/rad, C_r = 40000 N/rad are used.

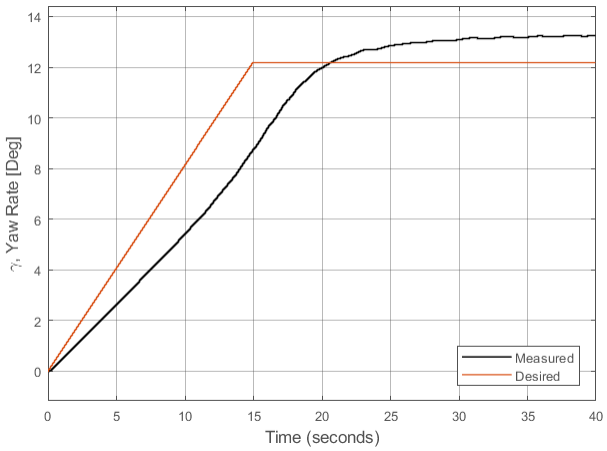

FIGURE 3.16: Mean cornering stiffness from the time history is used. Transient behaviour tracking is good, compared to other test sets. Values of C_f = 30697 N/rad, C_r = 30436 N/rad are used.

Chapter 4

IVDC Controller Design & Implementation

This chapter explores the controller design and challenges in implementing the controller with the full vehicle multi-body dynamics (MBD) software tool. The electronic stability control (ESC) controller, introduced by Mousavinejad[18], was utilized with a 8 degrees of freedom (DOF) non-linear vehicle model that consisted of numerical equations only. Therefore, every vehicle dynamics variables and behaviour can be easily predicted by investigating the numerical equations. However, challenges arise when the controller is implemented using more sophisticated MBD software tools, such as CarSim or ADAMS Car. These software tools use more DOFs to represent the vehicle motion, more subsystems in the vehicle design, and include flexible vehicle components. In addition, minor challenges can occur while using two individual software tools, one for the controller and the other for the full vehicle model, to communicate while simultaneously solving. As a result, in this work the controller is modified to solve the problems that arise during co-simulation.

The main objective of the ESC is to keep the vehicle on the intended path. Therefore, controlling the vehicle yaw rate is crucial in steering the vehicle towards the intended direction. However, this goal cannot be achieved by only controlling the vehicle yaw rate if the vehicle side slip angle (VSA) is too great. This can cause the vehicle to face the correct direction, according to the steering wheel angle, while the vehicle is actually skidding sideways. Therefore, controlling both vehicle yaw rate and vehicle side slip angle is necessary to stabilize the vehicle lateral motion, while keeping the vehicle on the intended path.

Integrated vehicle dynamics control (IVDC) integrates both active steering system (AS) and direct yaw moment control (DYC) to maximize the benefits of both systems while controlling the lateral motion of the vehicle. An active front steering system (AFS) is chosen to be integrated with DYC among different AS types since the AFS is the most suitable type for the IVDC as discussed in He[49]. A reference stable region will be further explained in this chapter. The reference region is used as a mean for the controller to determine how stable the vehicle is, in order to decide which types of control actuation and how much of control effort will be used. Inside the reference region,

the vehicle state is considered as stable since the maneuverability is still effective; however, the maneuverability significantly decreases outside the reference region. This is due to large VSA, which causes the AFS to reach its performance limitation.

Therefore, AFS will be activated mainly in the reference region since the maneuverability is not diminished. The primary goal of the activated AFS is to improve the handling performance, which helps the vehicle to follow the intended path by providing corrective steering wheel angle. The DYC, which uses differential braking systems, will only be activated when the vehicle state is outside the stable (reference) region in the phase plane. Therefore, its primary goal is to stabilize the vehicle state by limiting the VSA to remain inside the boundaries. Figure 4.1 shows types of actuators, control objectives and control strategies used for the controller design.

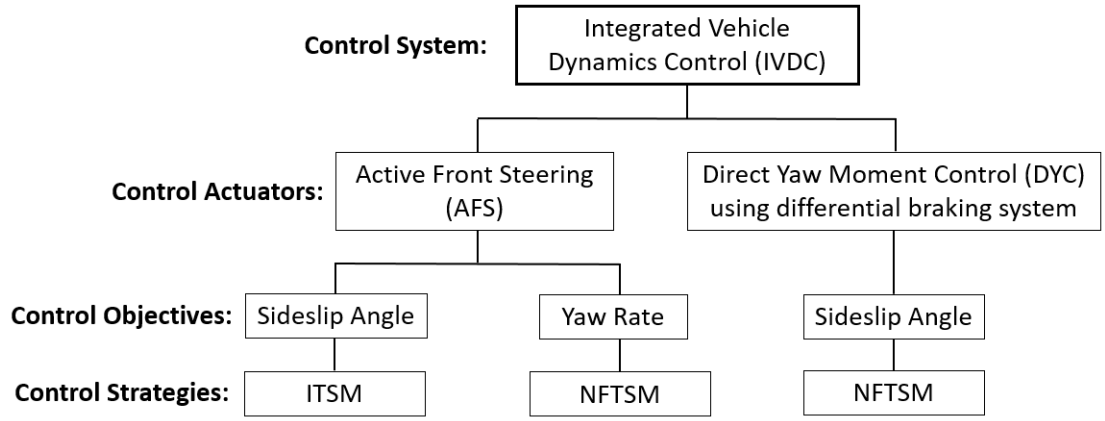

FIGURE 4.1: Structure of the IVDC. AFS and differential braking system are used as actuators to control VSA and yaw rate.

The controller design is adapted from Mousavinejad[18]. Two advanced types of SMC technique are implemented to improve the transient response of the vehicle yaw rate and VSA; integral terminal sliding mode (ITSM) and nonsingular fast terminal sliding mode (NFTSM). The ITSM is utilized to control the first order nonlinear system with uncertainties and external disturbance while providing a fast finite time convergence in the solution. The NFTSM is utilized to control the second or higher order systems while providing a fast finite time convergence in solution without singularity issues. In this research project, the structure of the controller from the literature is modified. New features and filters are implemented in the controller design to prevent undesired intervention of the controller when the vehicle is stable enough. The controller tuning parameter is modified to prevent from generating unrealistic corrective outputs, either corrective yaw moment or steering wheel angles. The AFS subsystem in the controller is tuned in an attempt to find an effective setting to control both yaw rate and VSA. Required vehicle parameter data, such as wheelbase, cornering stiffness and more, is read using MATLAB before the co-simulation is performed on Simulink

4.1 Estimated Vehicle Parameters

CarSim can monitor numerous variables that describe the vehicle dynamics during the simulation. For instance, users of the software can monitor the tire slip angles, normal loads to the wheel hub, VSA, and more. However, while access to this information is convenient during simulation, it is sometimes not practical to use it during the design the controller for the vehicle stabilization, as many of these variables are very hard to monitor in the real vehicle on the road.

4.1.1 Side Slip Angle

The VSA will be estimated based on the data that are available on most commercial vehicles, such as longitudinal velocity, lateral acceleration and yaw rate. VSA can be estimated by calculating the vehicle side slip velocity, then integrating it in the time domain, as seen in Equations 4.1 and 4.2.

$$\dot{\beta}_{\text{estimated}} = \frac{a_y}{V_x} - \gamma \tag{4.1}$$

$$\beta_{\text{estimated}} = \int \dot{\beta}_{\text{estimated}}\, dt \tag{4.2}$$

Similar VSA estimators are also used for Bosch's ESP development and in many other literature. There are sometimes challenges in the implementation of this approach (e.g., integrator windup), and in some cases, more sophisticated methods (e.g., Kalman filter) may be better options. A simple simulation was performed to confirm the accuracy of the estimator during a high speed simulation. The simulation was set for the vehicle to turn at the constant steering input of 160° while traveling at a constant speed of 120 km/h. The simulated VSA and the estimated VSA are compared in Figure 4.2.

It is observed that the estimator predicts the VSA very well, almost identical, when compared to the simulated VSA from CarSim. The root mean square error (RMSE) between the simulated and the estimated VSA was 1.83%.

4.1.2 Desired Yaw Rate & Desired Side Slip Angle

The controller must have a mean to calculate the target values so that it can stabilize/control the vehicle to match its state as close to the target values as possible. Two main target variables for the controller are the yaw rate and the VSA for their significance in the vehicle lateral stability as explained in Chapter 2. Both desired yaw rate and desired VSA are chosen to be the steady state values predicted by the bicycle model, as they are proven to be excellent for the ESC design by Rajamani[21]. The desired yaw rate is obtained from the road wheel steering angle, vehicle longitudinal speed and vehicle parameters as shown in Equation 4.3.

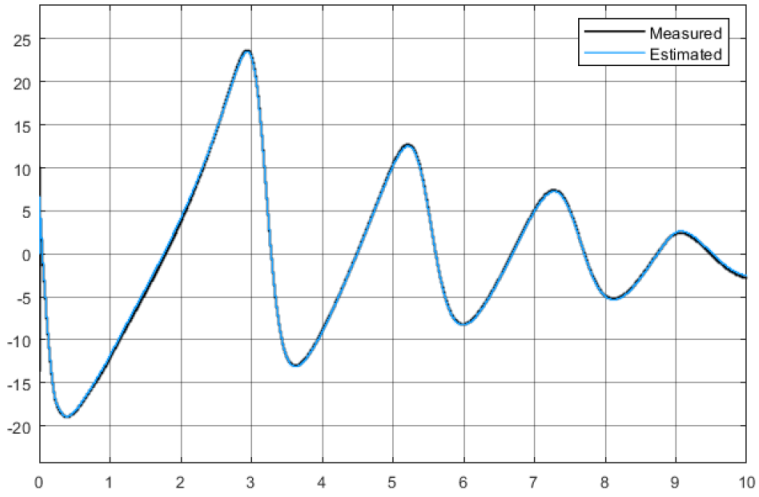

FIGURE 4.2: Simulated VSA and estimated VSA during the simulation. Vehicle velocity: 120km/h. Constant steering input: 120deg.

$$\dot{\psi}_{\text{desired}} = \gamma_{\text{desired}} = \frac{V_x}{(l_f + l_r) + k_u V_x^2} \delta_{\text{wheel}} \tag{4.3}$$

The understeer coefficient k_u is given by Equation 4.4.

$$k_u = m \frac{l_r C_r - l_f C_f}{2 L C_f C_r} \tag{4.4}$$

Here $L = l_f + l_r$ is used as the vehicle wheelbase. Note that the C_f and C_r are the cornering stiffness for each front and rear tire. The 2 in Equation 4.4 explains the effect of having two wheels at front and rear side of the vehicle. The desired side slip angle is shown in Equation 4.5.

$$\dot{\beta}_{\text{desired}} = \frac{l_r - \frac{l_f m V_x^2}{2 C_r L}}{L + k_u V_x^2} \delta_{\text{wheel}} \tag{4.5}$$

The desired VSA is a function of the driver's steering input, the vehicle's longitudinal velocity, and the vehicle parameters. The desired yaw rate and the desired VSA cannot always be achieved by the controller due to the frictional limitation between the road and the tires. Therefore, the desired yaw rate and the desired VSA are both bounded as explained by Rajamani[21].

$$\gamma_{upperbound} = 0.85 \frac{\mu g}{V_x} \tag{4.6}$$

$$\beta_{upperbound} = tan^{-1}(0.02 \mu g) \tag{4.7}$$

Therefore, the desired yaw rate of the vehicle model is taken to be the nominal value obtained by Equation 4.3 or 4.6 if the desired yaw rate exceeds the upper bound value. The desired VSA is determined as shown in Equation 4.7, so that it yields an upper bound of 10° at a friction coefficient of $\mu = 0.9$ and 4° at a friction coefficient of $\mu = 0.35$, which correspond to the desirable slip angle limits on dry road and slippery road covered with snow, respectively[21]. The effect of a given steering angle at different VSA was explored by Zanten, an inventor of the ESP at Bosch, in an attempt to find the characteristic VSAs, where the vehicle's steering capability vanishes[61]. The characteristic VSAs depend on the road tire friction coefficients; the characteristic VSAs were approximately ±12° and ±2° on dry asphalt and polished ice, respectively. The bounded VSA values suggested by Rajamani and Zanten match closely. As a result, Equation 4.7 will be used calculate the boundary values for the VSA in the controller design since Zanten's study does not provide the exact friction coefficients.

4.2 Vehicle Stability Region

It is necessary for the controller to monitor how stable the vehicle motion is, in order to control the vehicle motion for safety improvement. The phase-plane method is used to define the vehicle stability region described in [62], [63]. It will be a means for the controller to determine the vehicle stability. The phase-plane is defined in the $\beta - \dot{\beta}$ plane since the side slip motion of the vehicle is directly related to the vehicle lateral stability. Therefore, this phase plane is utilized in the controller design to keep the side slip motion of the vehicle within boundaries in which the vehicle remains stable. The phase-plane can be seen in Figure 4.3.

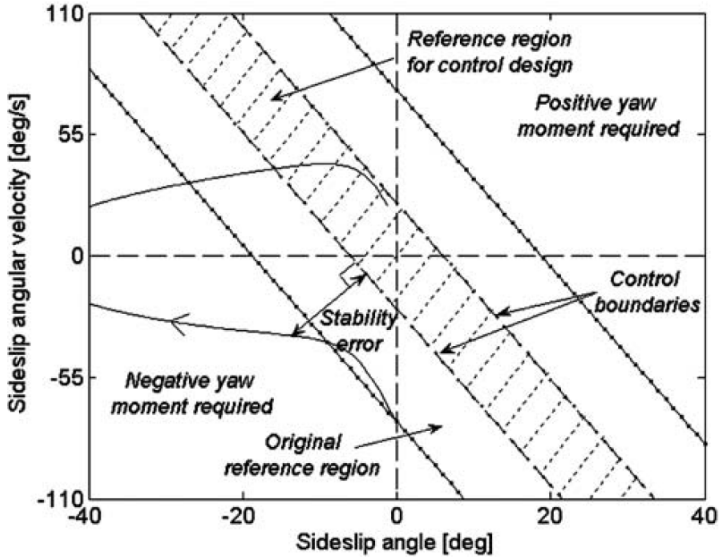

FIGURE 4.3: Reference stable region in the vehicle side slip phase plane for the controller design. Reproduced from He[49].

When the vehicle state is located within the boundaries, the vehicle is considered as stable by

the controller. In this region, safety is not a major concern since the vehicle is stable; however, the handling performance of the vehicle can be improved by the controller. When the vehicle state is outside the reference (stable) region, the vehicle instability can cause accidents on the road. Therefore, the primary goal of the controller is to pull the vehicle state back into the reference region if it is outside. The boundaries of the stable region are shown in Figure 4.3, as defined by He[49]. The boundaries are described using the stability index, χ, as seen in Equation 4.8, in which the units of β and $\dot{\beta}$ are $^\circ$ and $^\circ/s$, respectively.

$$\chi = |\frac{1}{24}\dot{\beta} + \frac{4}{24}\beta| < 1 \tag{4.8}$$

Adopting the stability index in the controller design enables the controller to quantitatively monitor the vehicle stability. In addition, the integration of AFS and DYC is possible since the vehicle stability can be described by the variable, which is described in detail in Chapter 4.5.

4.3 Active Front Steering (AFS) Control System

The AFS is used to improve the handling performance of a vehicle within the stable region. Lateral tire force and tire slip angles are assumed to be linear in the stable region, denoted as F_y and α, respectively. The following equations are used to predict the vehicle dynamics in the controller design.

$$F_{\text{y, front}} = -2C_f\alpha_f \tag{4.9}$$

$$F_{\text{y, rear}} = -2C_r\alpha_r \tag{4.10}$$

$$\alpha_f = \beta + l_f\frac{\gamma}{V_x} - \delta_{\text{wheel}} \tag{4.11}$$

$$\alpha_r = \beta - l_r\frac{\gamma}{V_x} \tag{4.12}$$

From Equations 4.9–4.12, one can see that the lateral force is a function of the road wheel angles. Therefore, AFS can generate a corrective road wheel angle to minimize the VSA. The bicycle model, which is discussed in Chapter 2, shows that the VSA and the lateral tire force are in the relationship of a first order system. However, the yaw angle and the yaw moment of the vehicle show the relationship of a second order system. Therefore, the ITSM and the NFTSM control strategies will be adopted to design the VSA and the yaw rate tracking controller, respectively.

4.3.1 Side Slip Angle Control

The tire lateral force equation from the bicycle model is rearranged to isolate the VSA on the left side. The VSA is replaced by the difference between the estimated VSA and the desired VSA, $\tilde{\beta} = \beta - \beta_{\text{desired}}$, which is the error to be minimized from the controller. In addition, unknown bounded function, $g_{\beta 1}$, is added to account for uncertainties and external disturbances during the nonlinear vehicle simulation.

$$\dot{\tilde{\beta}} = -\gamma + \frac{F_y^*}{mV_x} + g_{\beta 1} \tag{4.13}$$

The original tire lateral force notation, F_y, is replaced with F_y^*, in order to differentiate that the new lateral force, F_y^*, is generated from the controller to minimize the VSA error, $\tilde{\beta}$. The condition between the unknown bounded function and the controller parameter is shown in Equation 4.14.

$$|g_{\beta 1}| \leq k_\beta^{''}, k_\beta^{''} > 0 \tag{4.14}$$

According to the [58], the states of the system are chosen to be the VSA error and its rate.

$$\begin{aligned} x_1 &= \tilde{\beta}, \\ x_2 &= \dot{x_1} = \dot{\tilde{\beta}} \end{aligned} \tag{4.15}$$

The following ITSM surface $s_{\beta 1}$ is chosen to minimize the VSA error:

$$s_{\beta 1} = \tilde{\beta} - \tilde{\beta}(0) + \int_0^t \left(\frac{\alpha_\beta^{''}}{2}\tilde{\beta} + \frac{\beta_\beta^{''}}{2^{\gamma_\beta^{''}}}\tilde{\beta}^{\gamma_\beta^{''}}\right) dt \tag{4.16}$$

where $\tilde{\beta}(0) = 0$ is assumed, and $\alpha_\beta^{''}$, $\beta_\beta^{''}$, and $\gamma_\beta^{''}$ are parameters chosen to optimize the control response. Therefore, a control input, F_y^*, is expressed as

$$F_y^* = -mV_x\left(\frac{\alpha_\beta^{''}}{2}\tilde{\beta} + \frac{\beta_\beta^{''}}{2^{\gamma_\beta^{''}}}\tilde{\beta}^{\gamma_\beta^{''}} - \gamma + \frac{\alpha_\beta^{''}}{2}s_{\beta 1} + \frac{\beta_{\beta''}}{\sqrt{2}}\text{sgn}(s_{\beta 1}) + k_\beta^{''}\text{sgn}(s_{\beta 1})\right) \tag{4.17}$$

The Lyapunov function corresponding to this surface was defined in [18], and it is proved there that the system states will converge to equilibrium points in the fast finite time on this surface. Therefore, the corrective front wheel angle that controls the VSA error can be written as:

$$\delta_{w\beta} = \frac{1}{2C_f}(F_y^* + 2(C_f + C_r)\beta - \frac{2(l_rC_r - l_fC_f)}{V_x}\gamma) \tag{4.18}$$

4.3.2 Yaw Rate Control

Vehicle yaw moment equation from the bicycle model is rearranged to isolate the yaw acceleration on the left side. The yaw rate notation, γ, is replaced with the difference between the actual yaw rate and the desired yaw rate, $\tilde{\gamma} = \gamma - \gamma_{\text{desired}}$, which is the error to be minimized from the controller. Unknown and bounded function, g_ψ, is added to account for uncertainties and external disturbances, similar to how it was added in the VSA controller above.

$$\dot{\tilde{\gamma}} = \ddot{\tilde{\psi}} = \frac{1}{I_{zz}} M_{AFS} + g_\psi \tag{4.19}$$

The condition between the unknown bounded function and the controller parameter is shown in Equation 4.20.

$$|g_\psi| \leq k'_{\psi 1}, k'_{\psi 1} > 0 \tag{4.20}$$

According to Yang[57], the states of the system are chosen to be the yaw angle error and the yaw rate error.

$$\begin{aligned} x_1 &= \tilde{\psi}, \\ x_2 &= \dot{x_1} = \dot{\tilde{\psi}} = \tilde{\gamma} \end{aligned} \tag{4.21}$$

The following NFTSM surface is defined to minimize the yaw rate error[1]:

$$s_\psi = \tilde{\psi} + \alpha'_\psi |\tilde{\psi}|^{\gamma_{\psi 1}} \text{sgn}(\tilde{\psi}) + \beta'_\psi |\dot{\tilde{\psi}}|^{\gamma_{\psi 2}} \text{sgn}(\dot{\tilde{\psi}}) \tag{4.22}$$

where α'_ψ, β'_ψ, $\gamma_{\psi 1}$, and $\gamma_{\psi 2}$ are parameters chosen to optimize the control response. Therefore, a control input, M_{AFS}, is rewritten as:

$$M_{AFS} = -I_{zz} \left(\frac{1 + \alpha'_\psi \gamma_{\psi 1} |\tilde{\psi}|^{\gamma_{\psi 1} - 1}}{\beta'_\psi \gamma_{\psi 2}} \text{sgn}(\dot{\tilde{\psi}}) + k'_{\psi 1} \text{sgn}(s_\psi) + k'_{\psi 2} s_\psi \right) \tag{4.23}$$

The Lyapunov function was defined in [18], and it is proved that the defined system states will converge equilibrium points in the fast finite time on the NFTSM surface. Therefore, the corrective front wheel angle that controls the yaw rate can be written as:

$$\delta_{w\psi} = \frac{1}{2 l_f C_f} (M_{AFS} - 2(l_r C_r - l_f C_f)\beta + \frac{2(l_f^2 C_f + l_r^2 C_r)}{V_x} \gamma) \tag{4.24}$$

Note that the corrective angle for VSA defined in Equation 4.18 and the corrective angle for yaw rate defined in Equation 4.24 are distinct, i.e., the controller cannot simultaneously minimize both VSA error and yaw rate error, and a compromise is necessary.

[1]Note the use of functions of the form: $\text{sgn}(x)|x|^y$. This is equivalent to x^y if $x > 0$ or if y is an odd integer. The use of $\text{sgn}(x)|x|^y$ results in a function that behaves similarly to the odd integer power case (i.e., an odd function), even if y is chosen as an even integer or a real, where the simple power function can yield complex results (e.g. $(-2)^{2.5} \approx 5.66i$).

4.4 Direct Yaw Moment Control (DYC) System

The major objective of employing DYC in the IVDC controller is to control the VSA, so that the vehicle state goes back to the reference region. Outside the stable (reference) region, the VSA follows the dynamics of a second order system, with respect to M_{DYC}. Therefore, the NFTSM control strategy will be applied to design the VSA controller in DYC, instead of the ITSM control strategy, which is only available for first order systems.

4.4.1 Side Slip Angle Control

Modifying the bicycle model, the following equation is obtained:

$$\ddot{\tilde{\beta}} = -\frac{M_{DYC}}{I_{zz}} + \frac{\dot{F}_y}{mV_x} + g_{\beta 2} \tag{4.25}$$

where $g_{\beta 2}$ is an unknown bounded function to account for external disturbances and uncertainties, and M_{DYC} is the control input to minimize the VSA error. The unknown bounded function has the following condition, related to the controller parameter:

$$|g_{\beta 2}| \leq k'_{\beta 1}, k_{\beta 1} > 0 \tag{4.26}$$

The states of the system are the VSA error and its rate.

$$\begin{aligned} x_1 &= \tilde{\beta}, \\ x_2 &= \dot{x}_1 = \dot{\tilde{\beta}} \end{aligned} \tag{4.27}$$

The following NFTSM surface is defined to minimize the VSA error:

$$s_{\beta 2} = \tilde{\beta} + \alpha'_{\beta}|\tilde{\beta}|^{\gamma_{\beta 1}}\text{sgn}(\tilde{\beta}) + \beta'_{\beta}|\dot{\tilde{\beta}}|^{\beta_{\beta 2}}\text{sgn}(\dot{\tilde{\beta}}) \tag{4.28}$$

where α'_{β}, $\gamma_{\beta 1}$, $\gamma_{\beta 2}$, β'_{β}, and $\gamma_{\beta 2}$ are parameters chosen to optimize the control response. Therefore, the control input, M_{DYC}, is expressed as:

$$M_{DYC} = I_{zz}\left(\frac{1 + \alpha'_{\beta}\gamma_{\beta 1}|\tilde{\beta}|^{\gamma_{\beta 1}-1}}{\beta'_{\beta}\gamma_{\beta 2}}|\dot{\tilde{\beta}}|^{2-\gamma_{\beta 2}}\text{sgn}(\dot{\tilde{\beta}}) + k'_{\beta 1}\text{sgn}(s_{\beta 2}) + k'_{\beta 2}s_{\beta 2}\right) \tag{4.29}$$

The Lyapunov function and stability proof of the DYC is not discussed here; however, it is done similarly as mentioned in the AFS-NFTSM yaw rate controller.

4.4.2 Differential Braking System

The calculated yaw moment from the DYC, M_{DYC}, as a control input, is generated by employing the brake torques. Therefore, the differential braking system is chosen as the actuator. The individual differential braking system can be seen in Figure 4.4. The selection of individual wheels

to be used to generate the corrective yaw moment depends on the yaw moment generation ability of all four tires of the vehicle. A related study is done by Shelby[64]. When a vehicle is in an understeer condition, tire friction of the front wheels is typically close to saturation; therefore, the rear wheels are utilized for more effective yaw moment generation. Similarly, the front wheels are used to generate the corrective yaw moment during an oversteer condition. In this controller design, the vehicle motion is considered to be in an understeer condition when the absolute value of the actual yaw rate is smaller than the absolute value of the desired yaw rate calculated by the controller. Then, the vehicle motion is considered to be in an oversteer condition when the opposite is true, i.e., when the absolute value of the actual yaw rate is greater than the desired yaw rate. In order to prevent the undesired intervention of the DYC while the yaw rate difference is not significant, DYC is only activated when the difference between absolute values of actual and desired yaw rate values is greater than 5°/s. In addition, an average value of both front road wheel steering angles is used to determine the travel direction of the vehicle.

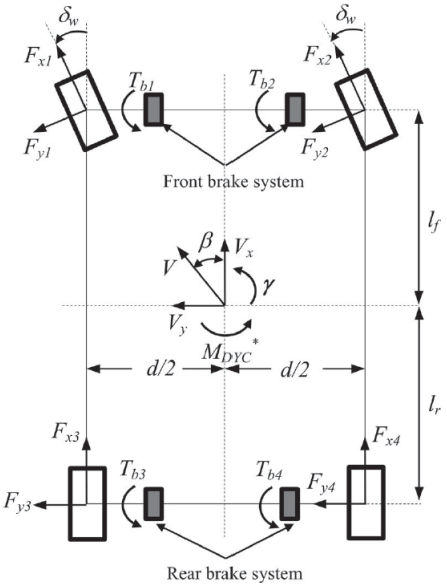

FIGURE 4.4: Individual differential braking system. Reproduced from Anwar[24].

When the vehicle turns left; counter-clockwise, the left rear brake is activated while the vehicle motion is in an understeer condition.

$$\begin{aligned} M_{DYC} &= \frac{d}{2} F_{x3} = \frac{T_{b3}}{R_w} \\ T_{b3} &= T_{LR} = \frac{2R_w}{d} M_{DYC} \end{aligned} \tag{4.30}$$

where M_{DYC} is the corrective yaw moment to be induced by the DYC, F_{xi} is the braking force on i-th wheel, and T_{bi} is the braking torque commanded by the DYC to each individual wheel. The braking torque on four corners also uses LR, RR, RF, LF as notations on the subscript, which are in order of left/right and front/rear.

When the vehicle turns right (clockwise), the right rear wheel is activated in understeer condition.

$$\begin{aligned} M_{DYC} &= \frac{d}{2} F_{x4} = \frac{T_{b4}}{R_w} \\ T_{b4} &= T_{RR} = \frac{2R_w}{d} M_{DYC} \end{aligned} \tag{4.31}$$

In an oversteer condition, the front wheels are braked to induce the corrective yaw moment, and the steering angle of front wheels must be considered in the calculation. The right front brake is activated when the vehicle is turning left (counter-clockwise).

$$\begin{aligned} M_{DYC} &= \left(\frac{d}{2} \cos(\delta_w) - l_f \sin(\delta_w) \right) \frac{T_{b2}}{R_w} \\ T_{b2} &= T_{RF} = \frac{R_w}{\frac{d}{2} \cos(\delta_w) - l_f \sin(\delta_w)} M_{DYC} \end{aligned} \tag{4.32}$$

where δ_w is the front road wheel angle. This value is received as the average value of the two front road wheel angles by the controller since the front wheel steering angles cannot be identical due to Ackermann steering geometry[2]. When the vehicle turns right (clockwise), the left front brake is activated in oversteer condition.

$$\begin{aligned} M_{DYC} &= \left(\frac{d}{2} \cos(\delta_w) - l_f \sin(\delta_w) \right) \frac{T_{b1}}{R_w} \\ T_{b1} &= T_{LF} = \frac{R_w}{\frac{d}{2} \cos(\delta_w) - l_f \sin(\delta_w)} M_{DYC} \end{aligned} \tag{4.33}$$

4.5 Integration of AFS and DYC

A key point in the design is that DYC can induce the corrective yaw moment through braking even when the effectiveness of the AFS is low due to the high VSA. However, its main drawback is that the DYC slows down the vehicle significantly while controlling the lateral motion of the vehicle. Therefore, DYC will not be used while the vehicle motion state is in the reference (stable) region, but will only be used when the vehicle state is outside the region, as discussed earlier.

As a result, a main objective of the controller when the vehicle motion state is within the reference region of the phase plane, is to improve the handling of the vehicle using AFS. The controller will start to utilize the DYC as the vehicle state is approaching to the boundaries of the reference region in the phase plane, as the lateral force of the tires, which are used by the AFS, approach saturation. A rule-based integration scheme, proposed by He[49], is used to integrate two subsystems while preventing undesired interference between them. The rule-based integration scheme is

[2]The geometry of the steering linkage is typically designed such that the inner wheel will steer at a larger angle than the outer wheel to account for geometry effects (the cornering radius of the inner and outer tires differ by the track width). The effect is only significant when using very large steer angles, e.g., maneuvering in a tight parking lot, and is negligible when the steering angle is small, as it is at highway speed.

based on fuzzy control logic, in an attempt to achieve a smooth transition between two standalone controllers.

The controller distributes the control effort between AFS and DYC by using an adaptation gain, ρ, that is based on the vehicle motion state in the phase plane; in this case χ, as defined in Equation 4.8. The adaptation gain based on the vehicle motion state is shown in Figure 4.5.

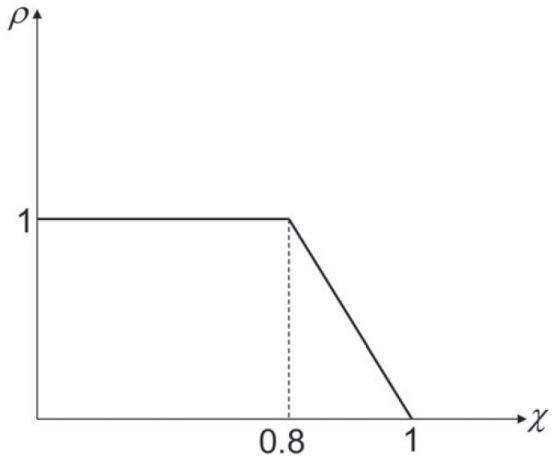

FIGURE 4.5: Adaptation gain ρ is used to achieve smooth transition between AFS and DYC for improving handling performance and improving the stability. Reproduced from Mousavinejad[18].

As a result, He's rule-based integration strategy can be implemented on the numerical calculation of the control outputs. The vehicle motion state in the phase plane approaches the boundaries of the stable region and eventually leaves the stable region. Therefore, the adaptation gain shows the increasing amount of control effort distribution towards the DYC, as χ increases. When the vehicle motion state is far enough from the stable region and χ is saturated at 1, only DYC will be activated to stabilize the vehicle, attempting to bring the vehicle motion state back inside the stable region. This integration scheme can be seen in the following equations:

$$\begin{aligned} M_z^* &= \rho M_{AFS} + (1-\rho) M_{DYC} \\ M_z^* &= M_{AFS}^* + M_{DYC}^* \end{aligned} \tag{4.34}$$

where corrective moments from AFS and DYC after the integration scheme is applied are denoted as M_{AFS}^* and M_{DYC}^*, respectively. Therefore, the corrective moment from AFS, M_{AFS}, shown in Equation 4.24 and the one from DYC, M_{DYC}, shown in Equation 4.29, are replaced with M_{AFS}^* and M_{DYC}^* in the controller design, respectively.

4.6 Block Diagram

Co-simulation is established between CarSim's nonlinear full vehicle model and the modified IVDC controller in Simulink, as seen in Figure 4.6. The vehicle model is represented by the S-function block, and it exports the steering wheel angle, lateral acceleration, longitudinal velocity and the yaw rate. The modified IVDC controller take these values to calculate the corrective control outputs to stabilize the vehicle lateral motion; brake torques from the DYC and corrective steering wheel angle from the AFS. Also, the road wheel angle that the controller uses is estimated by multiplying the steering ratio and the driver's steering wheel angle in the cabin.

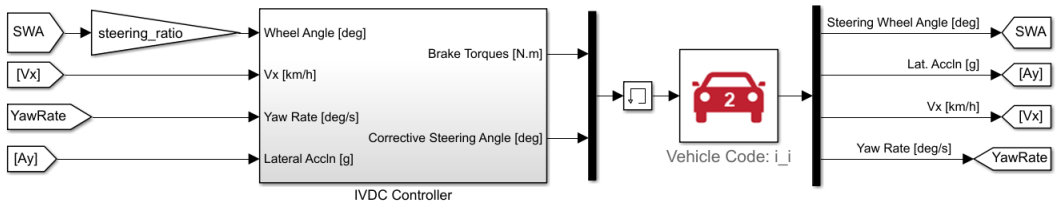

FIGURE 4.6: Co-simulation setup between the modified IVDC controller and CarSim S-function.

The modified IVDC controller consists of three subsystems and two main standalone controllers (AFS & DYC), variables calculated in the three subsystems are used in the two main standalone controllers. Note that the corrective steering angle is calculated by subtracting the initially estimated road wheel angle from the desired steering angle on the road wheels, then adding this single value to each left and right road wheel angles of the vehicle. Strictly speaking, this violates the Ackermann's steering geometry on real vehicles; however, it is sufficient to implement the logic of adding the corrective steering angle for the purpose of this research project.

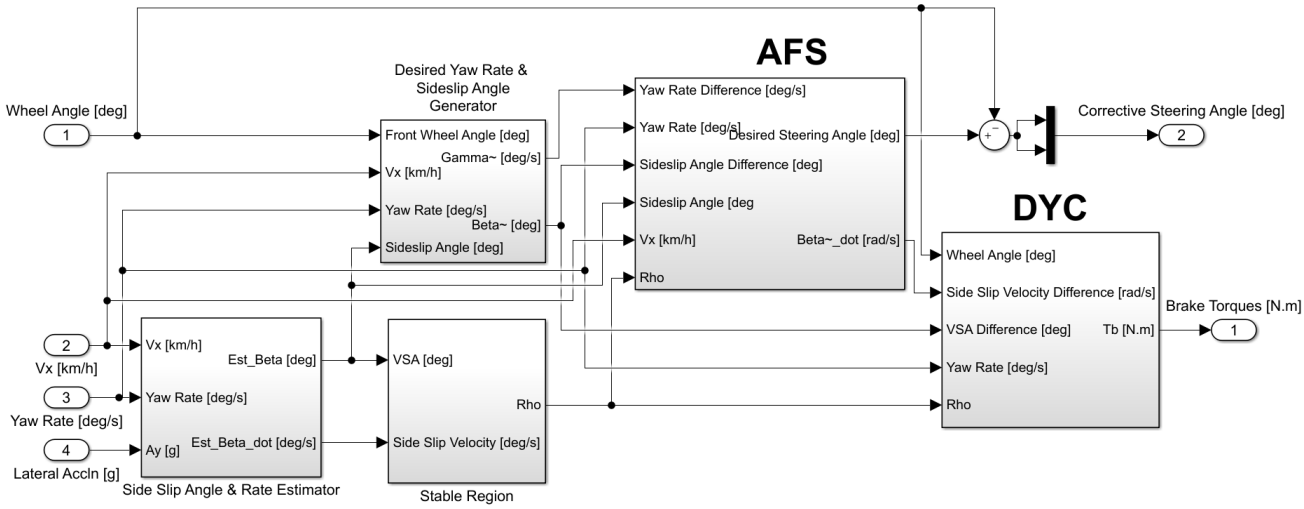

FIGURE 4.7: Structure of the modified IVDC controller.

Any calculations that involve angles use radians instead of degrees (°), so when the steering angle is sent to CarSim's S-function, the unit of angle is converted to degrees. A MATLAB file that sets the vehicle parameters, controller tuning parameters and unit conversion functions can be found in Appendix A. In addition, more block diagrams for each subsystems within the IVDC controller can be found in Appendix C.

4.7 Controller Tuning

This section explores the modification that are done to the IVDC controller model proposed by Mousavinejad[18]. There are many adjustable control parameters and numerical expressions that can be replaced with other methods in the controller. Thus, the choice of the controller parameters to be modified from the literature is determined by running simulations and observing undesired outputs, such as high frequency chattering, using the 'Scope' tool in Simulink, or simply simulation failure. In this research project, an iterative method is used for the determination of the modified parameters. In addition, determination of the control effort distribution between the yaw rate controller and the VSA controller in the AFS controller is described in this chapter. The effect of increasing the contribution of each individual controller is studied below.

4.7.1 Sign function and Chattering Issues

The nature of the sliding mode control (SMC) strategy is that the control effort is determined based on the location of the system state with respect to the control surface. As a result, numerical equations used for both ITSM and NFTSM contain the sign (sgn) function to determine the system state location, as seen in Equations 4.17, 4.22, 4.23, 4.28, and 4.29. Mathematically, this does not cause any issue in proving its functionality. However, implementing sign functions in numerical simulations can cause a high frequency chattering issue. During the research project, three options that can substitute for the sign function, including the sgn function itself, are compared to determine which method is the most suitable to reduce the chattering issue for the purpose of the research. The three options, the *sign* function, the *saturation* function, and the *exponential* function, are shown in Equation 4.35.

$$\begin{aligned} f(s) &= \text{sgn}(s) \\ f(s) &= \text{sat}(s) \\ f(s) &= \frac{e^{bs} - 1}{e^{bs} + 1} \end{aligned} \tag{4.35}$$

where b is the coefficient, and s is the variable of which the sign must be determined. The saturation function is saturated at -1 and 1.

A desired alternative option for the sign function must be sufficiently sensitive to the sign changes of a value to generate the control response towards the correct direction (+/-). At the

same time, the desired alternative option must not be as sensitive as the sign function to prevent the chattering phenomenon; a good alternative option should take longer time to change its value between positive and negative values, compared to the sign function. The characteristics of three options are compared, while the input pulse signal has a frequency of 0.1 Hz with three magnitudes of 1, 2 and 10. Figure 4.8 shows that the sign function changes its value between −1 and 1 instantly, while the saturation function behaves identical to the input signal when the input amplitude stays between −1 and 1. The saturation function's sensitivity to the sign change (speed of changing its value between −1 and 1) becomes more sensitive as the amplitude of the input signal becomes greater. The saturation function will cause varying magnitudes in control outputs, depending on the amplitude of the input signal feeding into the saturation function. Exponential function, however, is not dependent on or the least sensitive to the amplitude of the input signal. In addition, the exponential function does not change its sign instantly, but rather provides a lag time while changing its sign. Therefore, the exponential function is expected to be the most reliable option in the controller design since the same behaviour and sensitivity are expected at all time, and it is sufficiently sensitive to the sign of the input signal.

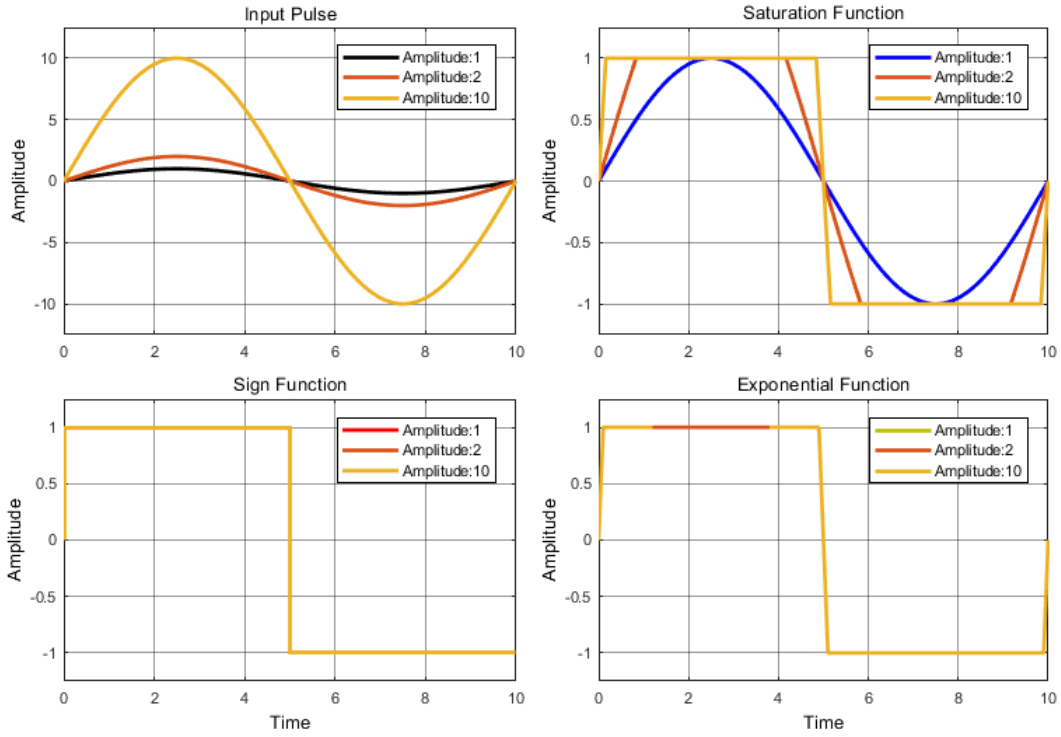

FIGURE 4.8: Comparison among three alternative options for the sign function generated from the input pulse in three magnitudes of 1, 2 and 10.

Three runs of the same simple simulation are conducted while adapting the sign function and the two other alternative methods to observe how three options affect the chattering phenomenon. The vehicle, equipped with the proposed IVDC controller, travelled at a constant speed of 120 km/h during the sine with dwell (SwD) event, with the steering wheel angle peak amplitude of 600°. The

effect of using the three options and how the chattering phenomenon can be avoided is observed. The difference between the actual and the desired vehicle yaw rate value is observed to compare the effect of the three methods. High frequency chattering is observed and the observed area is enlarged in Figure 4.9.

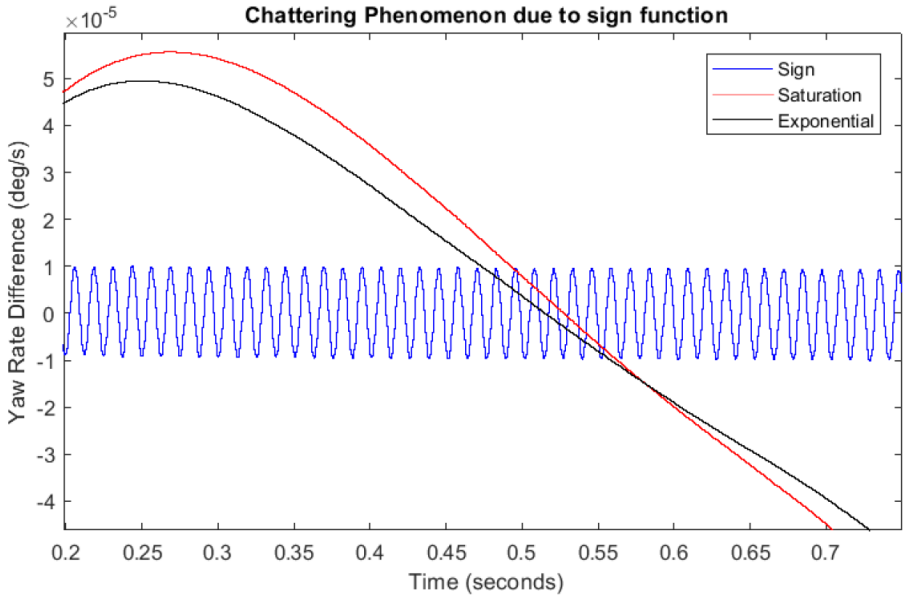

FIGURE 4.9: Yaw rate difference between the actual and the desired values of the vehicle when the controller design employs three different options for the sign function in the original design.

As seen in Figure 4.9, adopting the sign function caused the chattering phenomenon, and this was avoided by adopting the saturation or exponential functions. Another set of simulations of a closed loop double lane change (DLC) is performed to compare the saturation function and the exponential function. The vehicle was set to travel at a constant speed of 120 km/h with a peak lateral offset of 7.0 m from the the original longitudinal axis. The simulation failed when the sign function or saturation function are adopted to design the controller, since high frequency caused divergence in the solution. However, the simulation was run without failure when the exponential function was used. As a result, the exponential function is used to replace the sign function in the original controller design since it successfully and reliability prevented the chattering phenomenon in various simulation runs. The parameter for the exponential function, b, is set to be 100 in this controller design, which is determined through iterations for smooth response in the control outputs.

4.7.2 Control Parameters

Controller tuning parameters to be modified were chosen based on the observation over iterations of simulation. The tuning process started with the original control parameter setting from Mousavinejad[18]. Figure 4.10 shows the magnitude of every term in the bracket before they are

multiplied by the coefficients, which are controller tuning parameters. Figure 4.11 shows the magnitude of every term in the bracket that was used to calculate the lateral force in Equation 4.17. For example, in Figure 4.10, the first term is $\tilde{\beta}$ and the first term in Figure 4.11 is $\frac{\alpha_{\beta}''}{2}\tilde{\beta}$. Note that the fourth term is much higher than the other terms after coefficients are multiplied. Therefore, the parameter that was modified first was α_{β}''. This parameter in Equation 4.17, which calculates the lateral force as a control input, is multiplied to the ITSM surface in the AFS controller for the VSA control. This excessively huge tuning parameter caused the AFS to generate unrealistically huge steering angle to stabilize the vehicle for a given vehicle motion state, which led the simulation to stop before the simulation-end condition is met. After iterations of trial and error, knowing that the fourth term's magnitude must be lowered by lowering the α_{β}'', the controller tuning parameter of α_{β}'' is chosen to be 1.5. Similarly, other parameters are investigated, such as $\gamma_{\psi 2}$ and $k_{\beta 2}'$, and the new controller tuning parameters for the modified controller in this project are shown in Table 4.1.

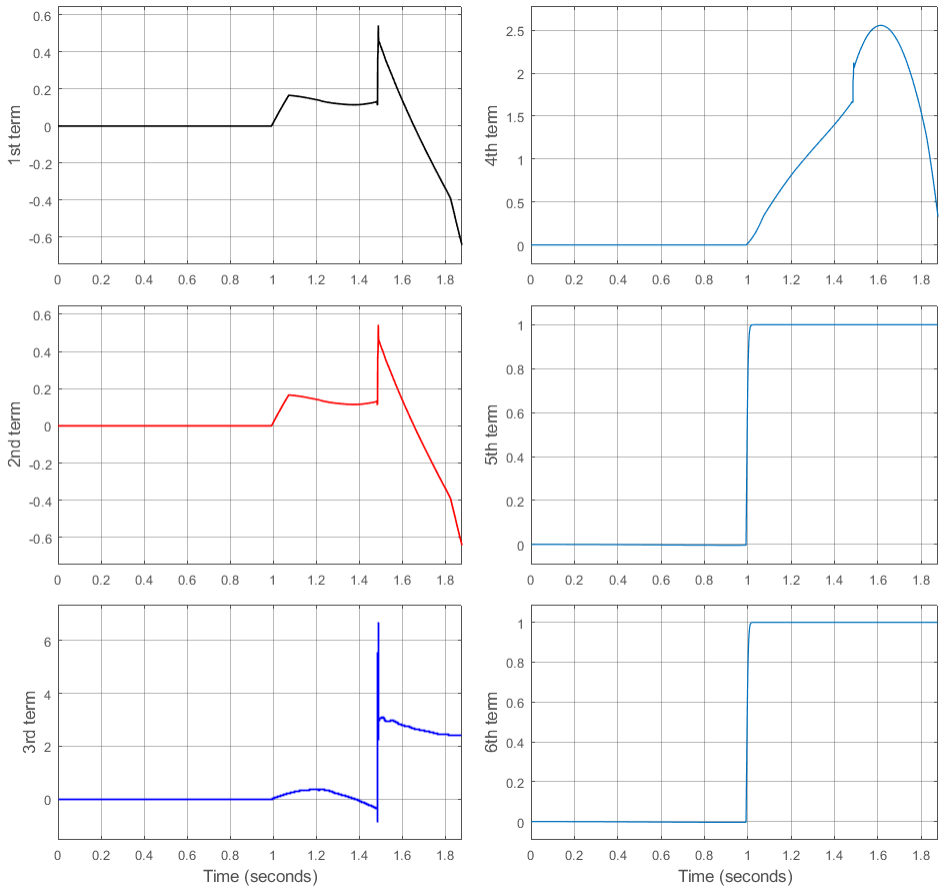

Figure 4.10: Magnitude of each term in Equation 4.17 before any control parameters are multiplied. SwD test at 120 km/h.

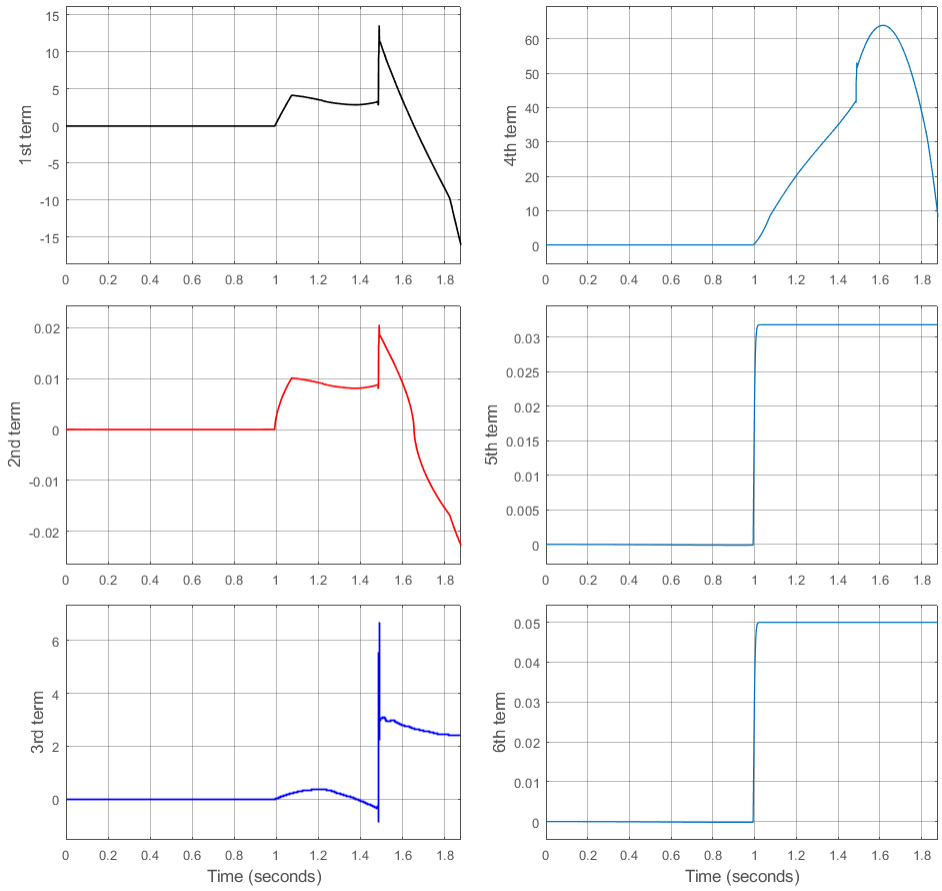

FIGURE 4.11: Magnitude of each term in Equation 4.17 after controller tuning parameters are multiplied. SwD test at 120 km/h.

TABLE 4.1: Modified IVDC controller tuning parameters.

Parameter	Value
$\alpha_{\beta}^{''}$	1.5
$\beta_{\beta}^{''}$	0.045
$\gamma_{\beta}^{''}$	0.6
$k_{\beta}^{''}$	0.05
$\alpha_{\psi}^{'}$	2.1
$\beta_{\psi}^{'}$	0.009
$\gamma_{\psi 1}, \gamma_{\psi 2}$	1.305, 1.01
$k_{\psi 1}^{'}, k_{\psi 2}^{'}$	0.001, 1.5
$\alpha_{\beta}^{'}$	2.1
$\beta_{\beta}^{'}$	1.2
$\gamma_{\beta 1}, \gamma_{\beta 2}$	1.305, 1.285
$k_{\beta 1}^{'}, k_{\beta 2}^{'}$	1.6, 1.0
$\alpha_{w}^{'}$	20
$\beta_{w}^{'}$	0.005
γ_{w1}, γ_{w2}	1.305, 1.285
$k_{w1}^{'}, k_{w2}^{'}$	0.002, 0.01

4.7.3 AFS Tuning

The resultant frontal corrective wheel angle generated by the AFS system is a combination of $\delta_{w\beta}$ and $\delta_{w\psi}$, which control the VSA and the vehicle yaw rate, respectively, and this is seen in Equation 4.36.

$$\delta_w = w_1 \delta_{w\psi} + w_2 \delta_{w\beta} \tag{4.36}$$

where w_1 and w_2 are the weighting factors.

One of the main contributions of this research project is to study the effect, caused from different weightings on each VSA-controlled and yaw rate-controller part of the AFS, and to choose the most optimal weighting ratios among the test sets.

The SwD test was performed to observe the performance of yaw rate tracking, VSA tracking, estimator of VSA and vehicle side slip velocity, average longitudinal velocity, and maximum lateral acceleration. The maximum steering input was set to be 600° with a constant longitudinal vehicle velocity of 120 km/h. The performance of each variable of interest was quantified by using the root mean square, as seen in Equation 4.37.

$$RMSE = \sqrt{\sum_{i=1}^{n} \frac{(y_{\text{simulated,i}} - y_{\text{desired,i}})^2}{n}} \tag{4.37}$$

The tests were performed at different combinations of weighting factors for the yaw rate controller and VSA controller. The results are compared to the reference vehicle model without the controller, and this can be seen in Table 4.2.

The first column in the table shows the AFS weighting coefficients for the yaw rate and VSA controllers. Therefore, the top row is VSA-control only, and only yaw rate is controlled in the bottom row. As a result, it is confirmed that the minimum yaw rate error was observed when only yaw rate was controlled in the AFS controller; similarly, the minimum VSA error was observed when only VSA was controlled by the AFS controller. This confirms the functionality of the individual stand-alone controllers in the AFS (yaw rate and VSA). Note that the VSA error was not as effectively reduced as the yaw rate error, even when only VSA was controlled. Estimator errors are shown as almost negligible. This ensures that the VSA and vehicle side slip velocity estimators are operating with high accuracy. Based on the observed average longitudinal speed, it is confirmed that the kinetic energy loss due to the intervention of the AFS controller is very low. In fact, it even improved the driver model's ability to maintain the longitudinal velocity closer to the target value of 120 km/h, compared to when the vehicle was not equipped with the IVDC controller. Minimum lateral acceleration was observed when only the vehicle yaw rate is controlled by the AFS controller. It is concluded that yaw rate controller is more effective than the VSA controller in tracking desired values. Therefore, a combination of $w_1 = 0.9$, $w_2 = 0.1$, is used for the AFS controller design since this results in highly efficient yaw rate error reduction along with the effect of

Table 4.2: Various combinations of the AFS weighting coefficients are compared during the SwD simulation.

AFS Coefficients (Yaw Rate, VSA)	RMSE-Yaw Rate (°/s)	RMSE-VSA (°)	RMSE-VSA Estimator (°)	RMSE-Side Slip Velocity Estimator (°/s)	Average Speed (km/h)	Maximum Lateral Acceleration (g)
Reference (No Controller)	12.0982	7.458	0.2361	0.2076	118.709	0.8171
0.0, 1.0	4.4304	5.1617	0.0379	0.1208	119.9053	0.7551
0.1, 0.9	3.3174	5.1670	0.0386	0.4281	119.9113	0.7625
0.2, 0.8	2.3405	5.3615	0.0179	0.0789	119.9156	0.754
0.3, 0.7	1.7814	5.5109	0.0127	0.1644	119.9173	0.7451
0.4, 0.6	1.5937	5.5941	0.0096	0.4415	119.9183	0.7403
0.5, 0.5	1.4562	5.6291	0.0083	0.3121	119.9187	0.7359
0.6, 0.4	1.3937	5.6525	0.0092	0.5124	119.919	0.7334
0.7, 0.3	1.2860	5.6612	0.0085	0.4245	119.9192	0.7227
0.8, 0.2	1.2272	5.6698	0.0098	0.4219	119.9193	0.7142
0.9, 0.1	1.1752	5.6784	0.0090	0.3970	119.9194	0.7061
1.0, 0.0	1.1296	5.6962	0.01100	0.4887	119.9195	0.6944

the VSA controller's contribution.

Chapter 5

Simulation Results and Discussion

This chapter will explore multiple simulation results to confirm that the integrated vehicle dynamics control (IVDC) controller presented in this project passes the performance requirement for the electronic stability control (ESC) to be approved by Federal Motor Vehicle Safety Standards (FMVSS) 126 and UN/ECE-R 13H regulations. Two studies are present in this chapter. One study is to consider if the target vehicle side slip angle (VSA) of the vehicle stability controller must be the steady state value or zero for the stabilization purpose since there are no clear indications on which is certainly better for the controller design. Second study was done to propose a new strategy for the current active front steering system (AFS) controller design in an attempt to change the fixed coefficient ratio between the yaw rate- and the VSA-standalone controller into the variable ratio, adapting to the vehicle motion state. Finally, the three sets of the double lane change (DLC) test are performed in a co-simulation environment with three different cases to compare the functionality of AFS and direct yaw moment control (DYC) of the presented IVDC controller.

5.1 ESC Homologation Process

One of main objectives of this research project is to ensure that the designed controller meets the regulation requirement set by FMVSS 126 and UN/ECE-R 13H for ESC homologation. Therefore, this section focuses on whether the modified IVDC controller can pass the ESC performance requirement defined by the two organizations mentioned above. A detailed description of how the modified IVDC controller intervenes in the vehicle motion during the simulation is described in Section 5.4. The two organizations share a very similar homologation process for ESC systems. The sine with dwell (SwD) maneuver is used to evaluate the performance of ESC in preventing vehicles from spinning out. The steering amplitude that will be used during the SwD test is decided by performing a slowly increasing steer (SIS) maneuver, prior to the SwD test. Vehicle responses from these tests will be further evaluated based on two criteria: yaw stability and responsiveness. Co-simulation is performed on the MATLAB/Simulink and CarSim platform. A nonlinear vehicle model and the modified IVDC controller described in earlier chapters are used for the simulation. A more detailed description of the homologation process used by the FMVSS and UN/ECE-R 13H can be found in [15], [65].

5.1.1 Slowly Increasing Steer (SIS) Maneuver

The first step of the SwD test for ESC homologation is to determine the steering amplitude, A, from the SIS maneuver test. The test begins with a vehicle coasting at 80 km/h within the deviation of 2 km/h without any steering action. Once the vehicle maintains the speed, the steering wheel angle is increased at a rate of 13.5°/s from no steering action. The steering amplitude of the interest, A, then is obtained when the lateral acceleration of the vehicle reaches 0.3 g (2.94 m/s^2).

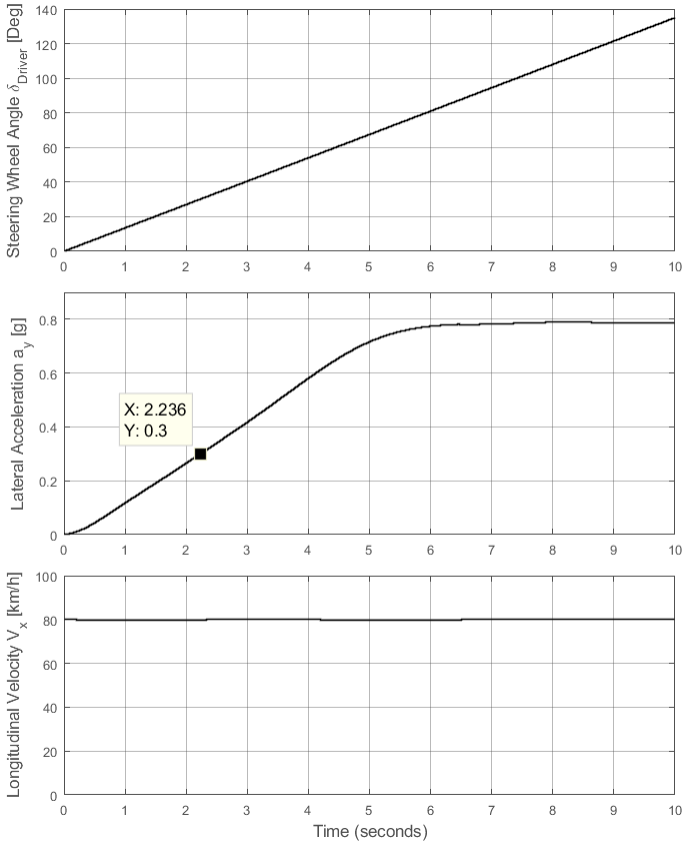

FIGURE 5.1: Result of the SIS maneuver test at V_x = 80 km/h. The target lateral acceleration a_y = 0.3 g is reached at A = 30.18°.

The lateral acceleration of the vehicle reached at a_y = 0.3 g at t = 2.236 seconds. The steering wheel angle from the driver at 2.236 seconds, A, is determined to be 30.18°.

5.1.2 Sine with Dwell (SwD) Test

The SwD test is performed to evaluate the ESC system based on yaw stability and responsiveness criteria. The test protocol defines that the vehicle travels at an entrance speed of 80 km/h then coasts without any throttle inputs. The steering input from the driver follows a 0.7 Hz sinusoidal pattern where the steering input is held constant at the second peak for 0.5 seconds for a dwell time. The input steering wheel angle peaks are identical in both peaks, and multiple runs of SwD tests are performed by varying this steering angle peak. The initial run has a steering amplitude of

$1.5A$. After the initial run, the steering amplitude increases by $0.5A$ from run to run. The maximum steering amplitude is the greater value of either 270° or $6.5A$. This research project will present the first and the last run since the last run is the most severe steering event. Therefore, initial run of SwD test will be performed with the steering amplitude of $1.5A$. As seen in Equation 5.1, the final run of the SwD test will have the maximum steering amplitude of 270°. Both runs will be performed with a vehicle model without the IVDC controller and the other vehicle model equipped with the IVDC controller for comparison.

$$6.5A = 6.5 * 30.18^\circ = 196.17^\circ < 270^\circ \tag{5.1}$$

The SwD test results will be evaluated based on the yaw stability criteria and responsiveness criteria as seen below. Figure 5.2 shows the steering wheel angle input and the yaw rate of interest, described in the criteria, during the SwD test simulation.

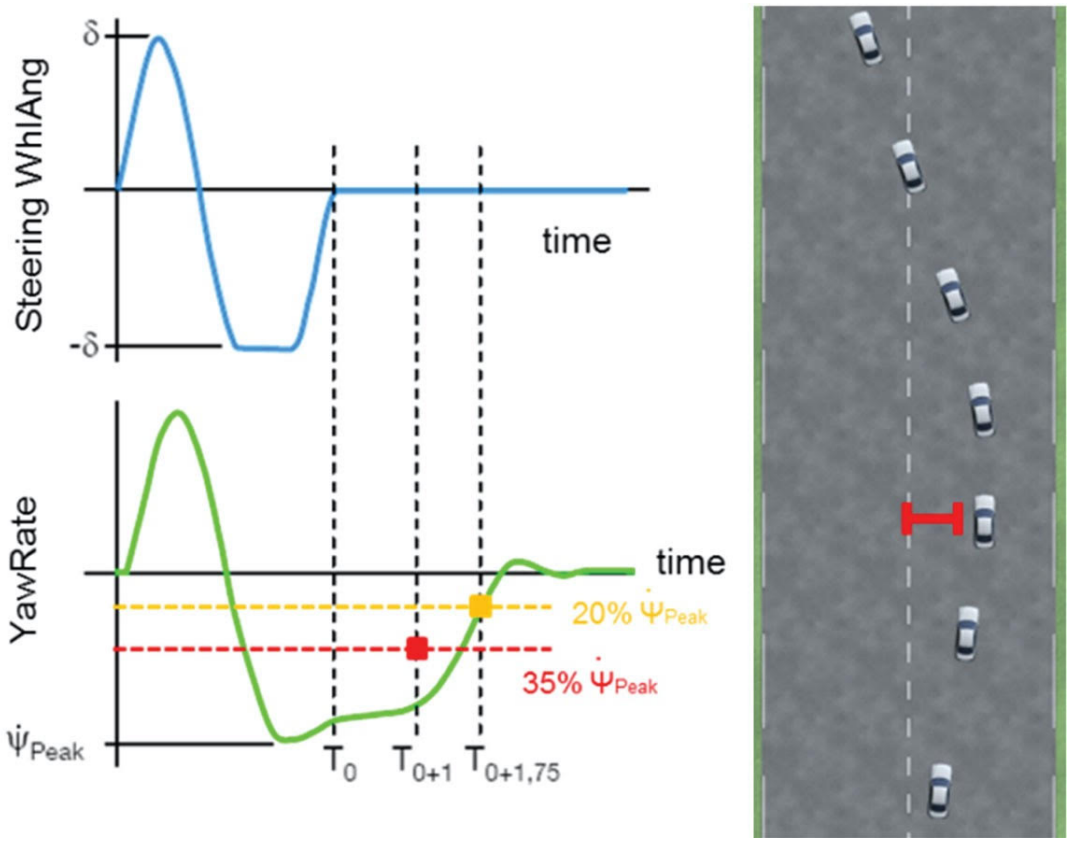

FIGURE 5.2: Steering wheel angle input and yaw rate to be simulated during the SwD test. Reproduced from Lutz[66].

Directional or yaw stability criterion are as follows, where T_0 is the time when the steering input becomes zero:

- The yaw rate recorded at 1 second after the completion of steer (COS), $\dot{\psi}_{T_{0+1}}$, must be less than 35% of yaw rate peak, $\dot{\psi}_{\text{peak}}$
- The yaw rate at 1.75 seconds after the COS, $\dot{\psi}_{T_{0+1.75}}$, must be less than 20% of yaw rate peak, $\dot{\psi}_{\text{peak}}$

Both T_{0+1} and $T_{0+1.75}$ in the yaw stability criterion are decided to be the point of measures based on the statistical analyses performed by NHTSA. According to the study, there is a 95% chance that the vehicle will not spin-out, which is defined as the difference between the final heading angle and the initial heading angle being greater than 90°, if the remaining yaw rate at 1 second after COS is less than 35%. The same prediction was made when the remaining yaw rate at 1.75 seconds after COS is less than 20%.

The responsiveness criterion is:

- The lateral displacement of the vehicle centre of gravity from the initial straight path must be at least 1.83 m for vehicles with a gross vehicle mass of 3500 kg or less, when computed 1.07 seconds after the initiation of the steer. This criteria applies only when the steering amplitude is greater than 180°.

The lateral displacement is a direct indication of obstacle avoidance ability of a vehicle. Therefore, it is prone to assume that the maximum lateral displacement must be a measure to determine the ability of a vehicle to avoid obstacles. However, the maximum lateral displacement and the maximum steering angle do not occur simultaneously; it occurs later in the maneuver. In addition, the time when the maximum lateral displacement is measured for different vehicles will vary. Therefore, it makes the most sense to measure the lateral displacement at the same time, early in the maneuver, so that there are no deviations in the evaluation criteria while testing different vehicles, see [15]. The vehicle model used in this research project has a mass of 1300 kg.

The first set of the SwD test is performed while the vehicle model is not equipped with the IVDC controller and the steering amplitude is $1.5A = 45.27°$. The COS time is $t = 1.93267$ seconds. The second set of SwD tests had the same steering amplitude of $1.5A$, but this time the vehicle is equipped with the IVDC controller. The first and second set of the SwD tests are presented to show the characteristics of the SwD test and how the vehicle responds to the steering input, as shown in Figures 5.3 and 5.4. The third and fourth sets of the SwD test has the most severe steering input; 270°. The third set has the vehicle model without the IVDC controller, and the fourth set was performed with the IVDC controller. The results of the third and the fourth sets are seen in Figures 5.5 and 5.6. The SwD test results for the ESC homologation purpose are presented in Table 5.1.

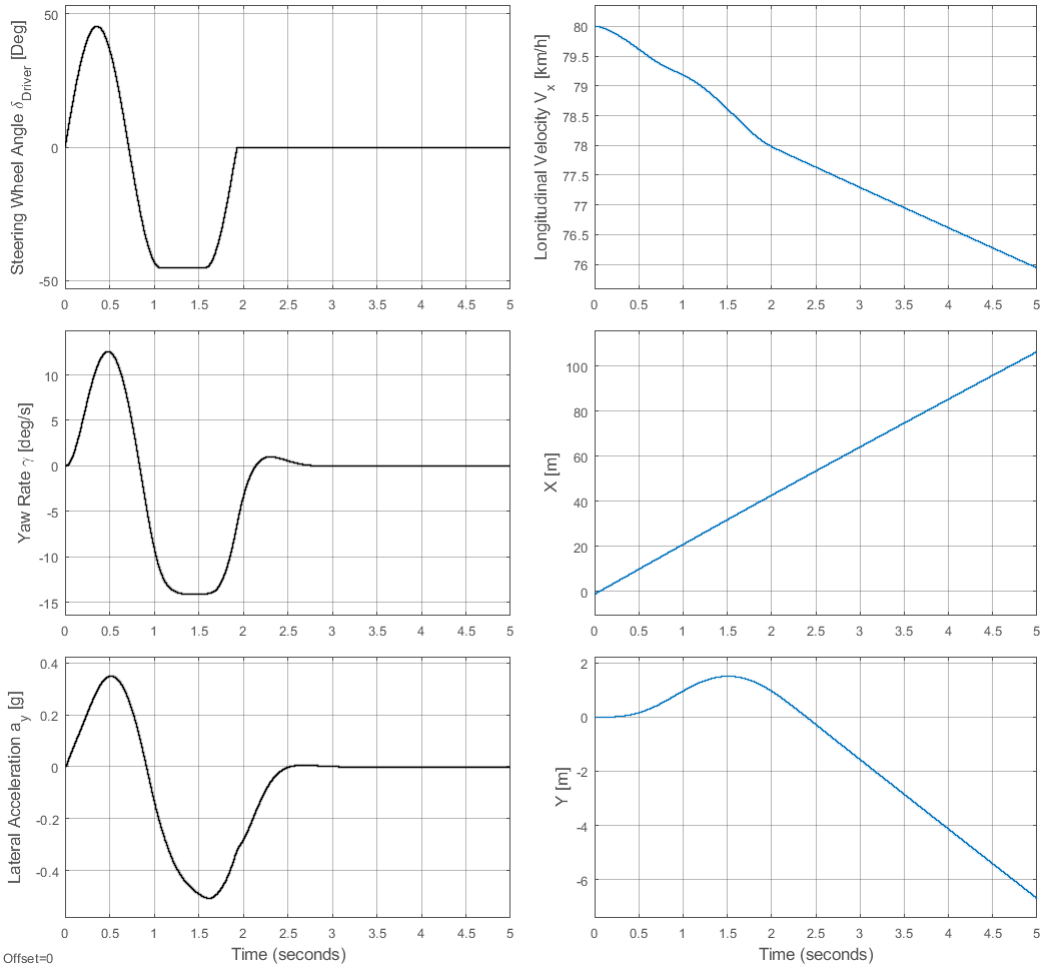

FIGURE 5.3: SwD Test: Run 1 with steering amplitude of $1.5A = 45.27^{\circ}$. The vehicle model is not equipped with the IVDC controller.

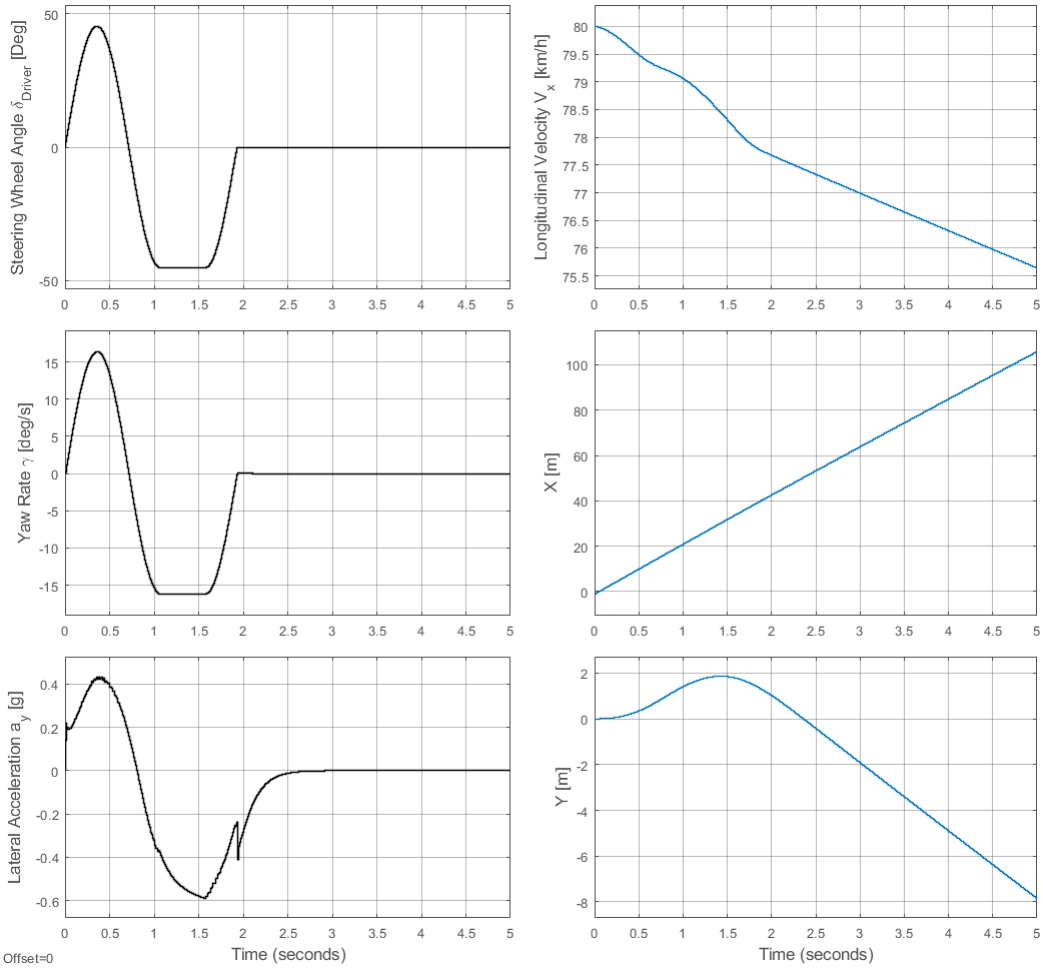

FIGURE 5.4: SwD Test: Run 2 with steering amplitude of $1.5A = 45.27^{\circ}$. The vehicle model is equipped with the IVDC controller.

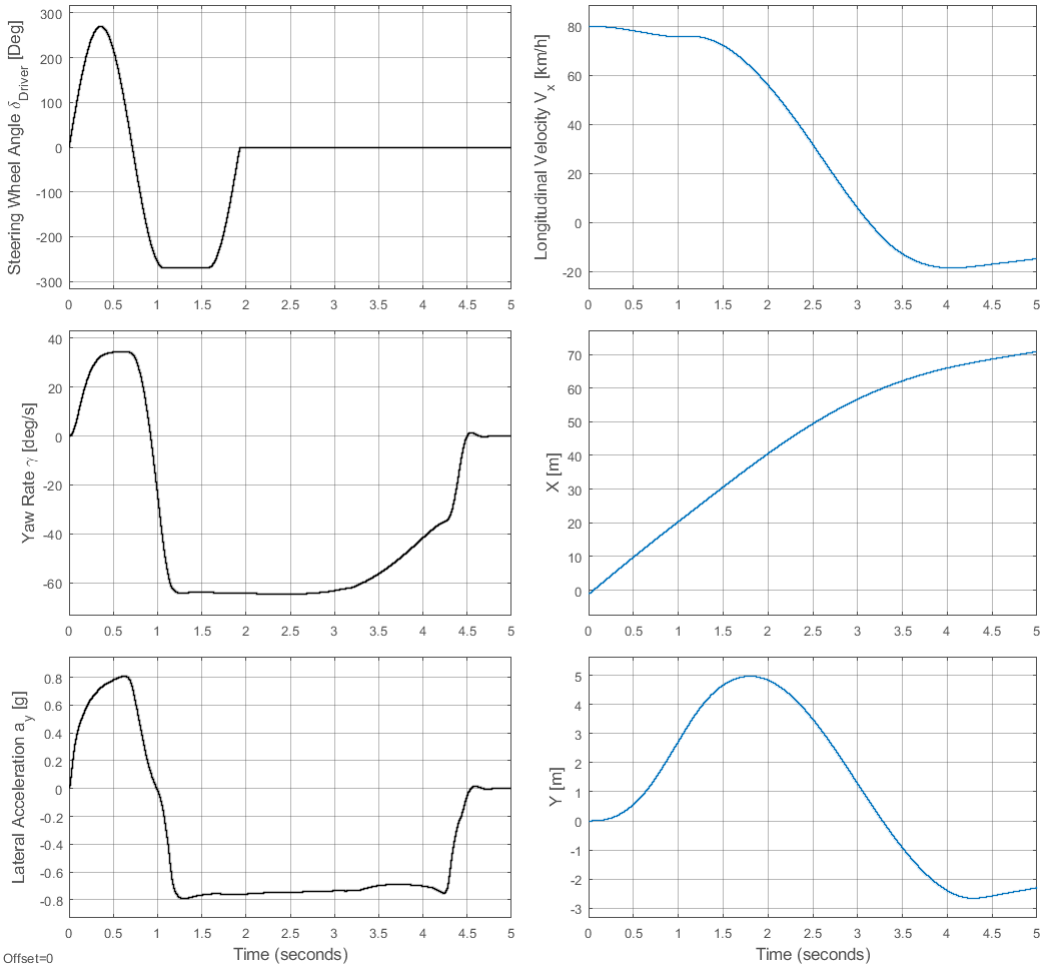

FIGURE 5.5: SwD Test: Run 3 with steering amplitude of 270°. The vehicle model is not equipped with the IVDC controller.

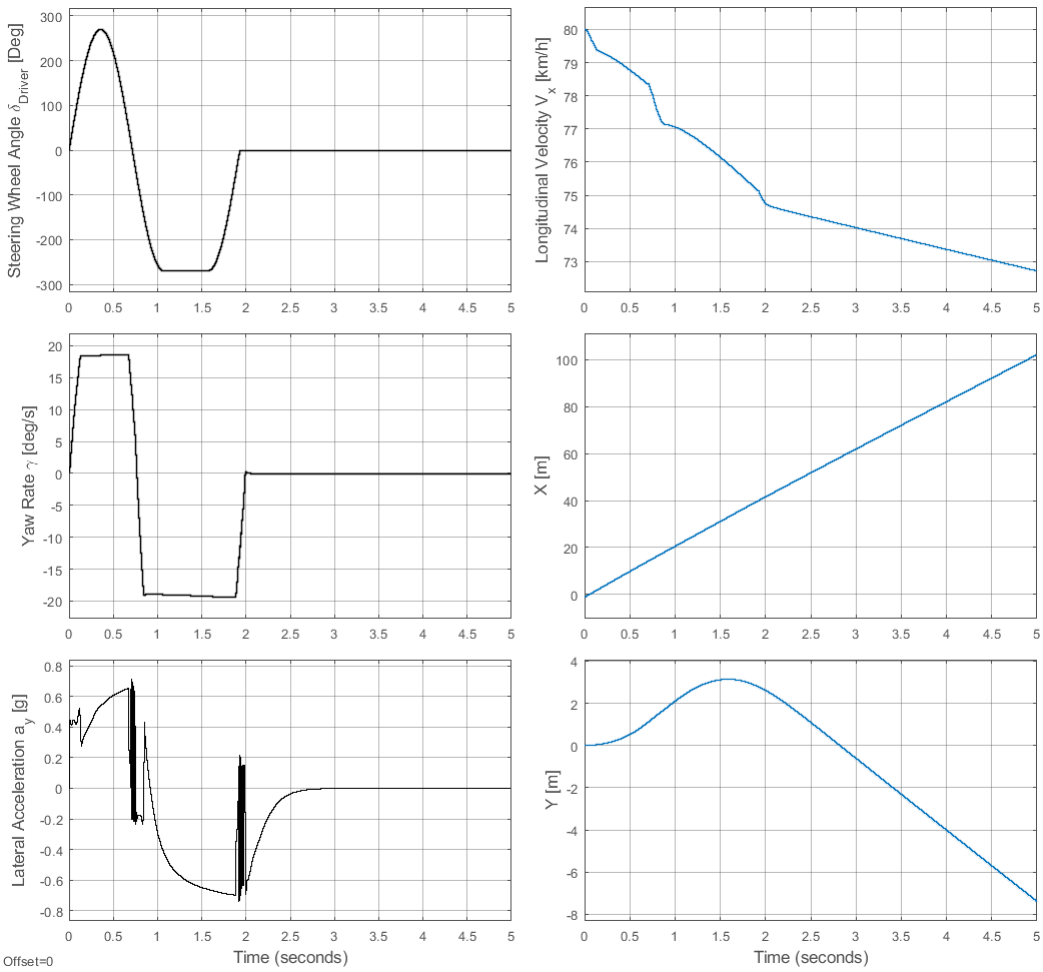

FIGURE 5.6: SwD Test: Run 4 with steering amplitude of 270°. The vehicle model is equipped with the IVDC controller.

Table 5.1: SwD Test Results.

Test #	δ_{peak} [°]	IVDC	$\dot{\psi}_{\text{peak}}$ [°/s]	$\dot{\psi}_{T_{0+1}}$ [°/s]	$\dot{\psi}_{T_{0+1.75}}$ [°/s]	$Y_{T_{1.07}}$ [m]	$\frac{\dot{\psi}(T_{0+1})}{\dot{\psi}_{\text{peak}}}$ [%]	$\frac{\dot{\psi}(T_{0+1.75})}{\dot{\psi}_{\text{peak}}}$ [%]
1	45.27	Not equipped	−14.1288	−0.0536	−0.0257	1.092	0.3794	0.1819
2	45.27	Equipped	−16.2166	0.0051	0.0045	1.533	0.0314	0.0277
3	270.0	Not equipped	−64.6661	−63.597	−46.1061	3.072	98.35	71.30
4	270.0	Equipped	−19.4040	−0.019	−0.0188	2.313	0.0979	0.09689

From Figure 5.3, it is observed that the vehicle travels at an entrance speed of 80 km/h, then coasts without any throttle. The peak yaw rate of 14.1288°/s is achieved at the steering amplitude of 45.27°. The COS occurred at $t = 1.93267$ seconds; however, the yaw rate of the vehicle continues to increase until approximately $t = 2.2$ seconds. The physical interpretation of this section of the graph is that the steering wheel is turned straight, but the vehicle still maintains the inertia of rotation leading to the yaw rate not reaching zero simultaneously with respect to the steering wheel angle. Lateral displacement in this run is not meaningful since the steering amplitude is less than 180°.

During the second run of the SwD test, the most obvious difference when compared to the first run is that the yaw rate lag is substantially reduced. The yaw rate of the vehicle equipped with the IVDC controller in this run almost becomes zero simultaneously with respect to the steering wheel angle. The stabilizing effort of the IVDC controller during this time also appears in the lateral acceleration at around $t = 2$ seconds. This was caused by the controller providing corrective steering wheel angle to control the vehicle yaw rate. As a result, the maximum lateral displacement of this run is higher than the first run at $t = 1.07$ seconds. The intervention of the IVDC controller cost a small kinetic energy loss based on the final longitudinal velocity in this run being lower than the first run. However, the speed loss is a negligible amount.

Figure 5.5 shows the vehicle behaviour at the most severe steering amplitude of 270° while the vehicle model is not equipped with the IVDC controller. It is observed that the vehicle without the controller struggled to return to the zero yaw rate after the COS, implying that the vehicle skidded sideways. The slipping vehicle caused the longitudinal velocity graph to reach negative values since the vehicle is not travelling forward while it is slipping. The acceptable yaw rate at $t = 1$ second after the COS, in order to pass the NHTSA's yaw stability performance criteria, must be −22.6331°/s. However, the yaw rate at this time is still −63.597°/s, which is 98.35% of the peak yaw rate. The lateral displacement is greater in this run, compared to the first two runs; however, it is due to the significantly increased steering amplitude. Therefore, this does not necessarily indicate the vehicle in this run showed a great obstacle avoidance, especially since its lateral acceleration and yaw rate took a very long time to reach zero after the COS.

On the last run of the SwD test, the vehicle was given the most severe steering amplitude, as in the third run; however, the vehicle this time is equipped with the IVDC controller. Similarly

to the second run, the vehicle yaw rate shows a very similar pattern with respect to the steering wheel angle input, leading the yaw rate to reach zero almost at the same time as the COS. Flat sections in the vehicle yaw rate are observed during the peak of the steering amplitude. These are caused by the IVDC controller which tries to limit the desired yaw rate at the friction limit. Based on how the yaw rate is controlled over the entire simulation, this limit value of the yaw rate that used by the controller seems to work properly. The controller's corrective outputs caused the oscillations in the lateral acceleration. The controller successfully prevented the vehicle from spinning out, based on the controlled yaw rate and the lateral acceleration. The longitudinal velocity did not drop significantly even during the intervention of the controller, meaning that the controller worked efficiently; it does not cause the huge loss of longitudinal kinetic energy while controlling the lateral motion of the vehicle. The peak yaw rate during this run was observed to be -19.4040°/s, while $\dot{\psi}_{T_{0+1}}$ and $\dot{\psi}_{T_{0+1.75}}$ are -0.019°/s and -0.0188°/s respectively. This resulted in values of 0.0979% and 0.09689% for the target yaw rate percentage, compared to the peak yaw rate while the acceptable values are 35% and 20%, respectively. In addition, the vehicle still maneuvered sufficiently quick to be considered as avoiding the obstacle by having $Y_{T_{1.07}} = 2.313$ m > 1.83 m.

5.2 Target Vehicle Side Slip Angle for Vehicle Stability Controller Design

This section focuses on providing meaningful contents in answering a question that arises during the design stage of the vehicle stability control system. Vehicle side slip angle (VSA) is the angle deviation between the facing direction of the vehicle and the actual traveling direction of the vehicle, so called drift angle. The IVDC controller has two standalone controllers of which aims to control the VSA. The target VSA for each standalone controllers is the steady state value of the VSA, predicted by the bicycle model. The bicycle model is based on the vehicle parameters, longitudinal speed and steering wheel angle. Rajamani [21] describes that usage of the steady state value of the VSA is a more suitable option for the purpose of the vehicle dynamics control, rather than assuming the desired VSA to be zero. However, he cites no supporting studies to provide evidence for this claim.

In this section, two sets of the DLC test are simulated. The steering input during the test can be seen in Figure 5.7. The same vehicle model in CarSim will be used for both cases. The same controller design will be used with different settings. The first simulation will be performed while the controller has a target desired VSA of the steady state value provided by the bicycle model, and the second simulation is run while the controller has a new target desired VSA of zero; no drifting at all. A comparison of the simulation results from both cases should generate meaningful outcomes to help decide which target VSA is more suitable for the proposed IVDC controller. This result may expand further to help decide the target VSA for vehicle stability controller design in general. The testing condition is set for both cases as follows:

- Test type: Double lane change (DLC) maneuver
- AFS setting: 0% Yaw rate control (w_1 = 0.0), 100% VSA control (w_2 = 1.0)
- DYC: activated
- Steering amplitude: 200°/s
- Vehicle velocity: constant at 120 km/h
- Case 1: target VSA = steady state value of VSA
- Case 2: target VSA = 0°

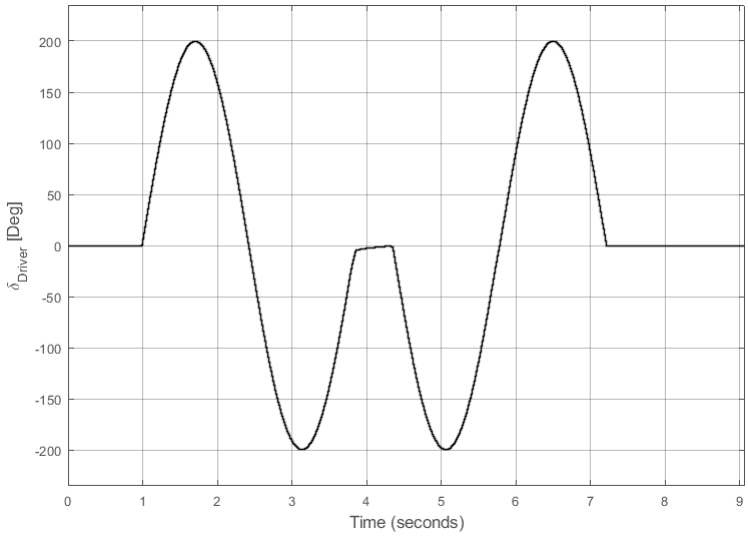

FIGURE 5.7: Steering input of DLC test with steering amplitude of 200°.

The vehicle model without the IVDC controller is used for this study as a reference. As seen in Figures 5.8, 5.9, and 5.10, the vehicle without the controller exhibits huge yaw rate peaks, and it drifted so much that the VSA estimator is showing a very different value with respect to the simulated VSA. The AFS controller is generating such a huge magnitude of corrective angle, the y-axis of the corrective steering angle shows a power of five. The DYC calculated the yaw moment and the corresponding brake torques are shown in Figure 5.9; however, these values did not affect the vehicle motion during the simulation since the DYC is deactivated. It is observed that the vehicle longitudinal velocity decreased significantly and changed sign at a certain point. This is because the vehicle spun out. This shows that the given DLC test setting is severe enough to make the vehicle without any stability control spin out.

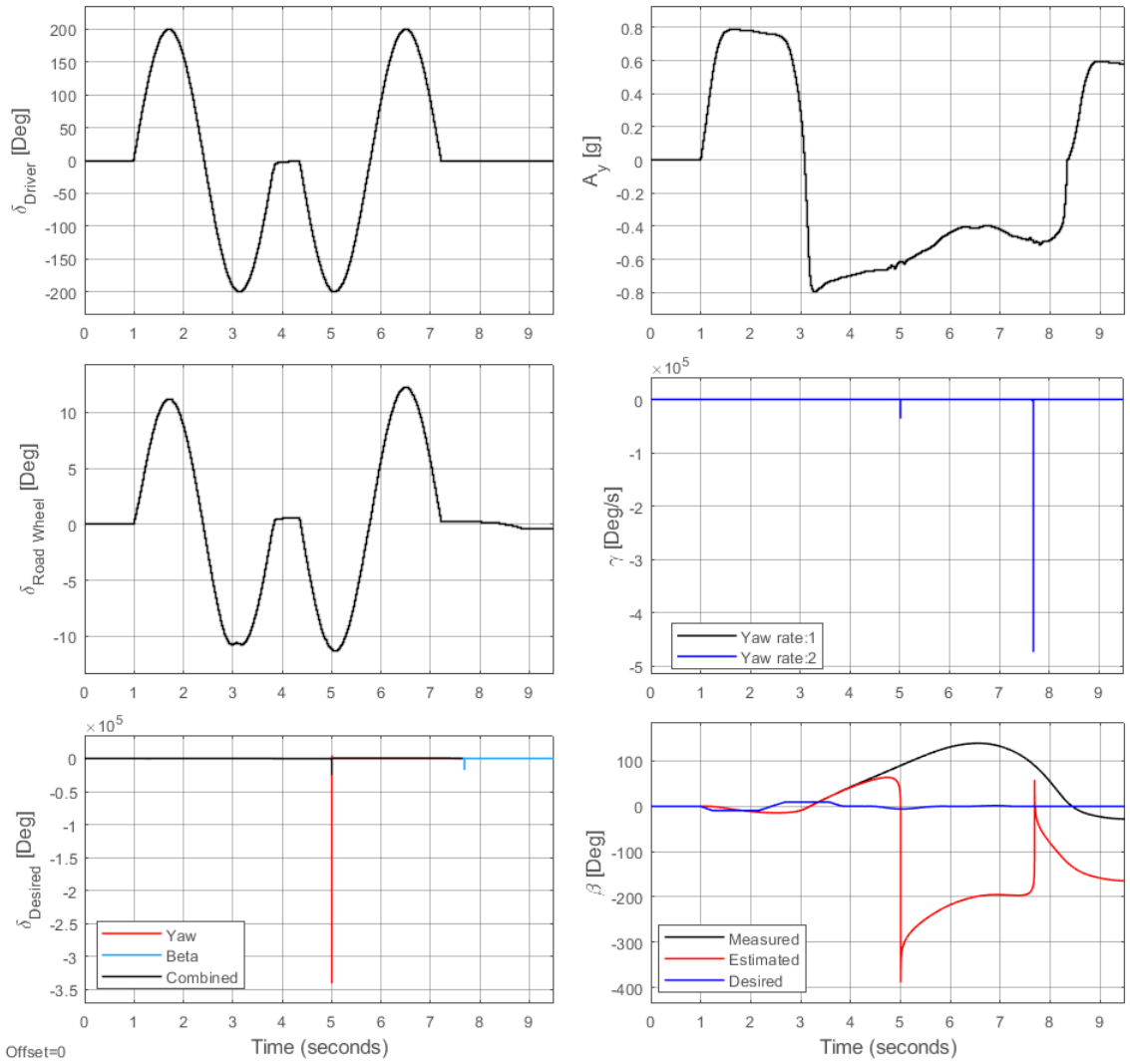

FIGURE 5.8: DLC simulation result of a reference vehicle model without the IVDC controller. Vehicle spun out. A significant amount of the wheel corrective angle is calculated, but AFS is deactivated. Measured values are the simulated values from the virtual vehicle.

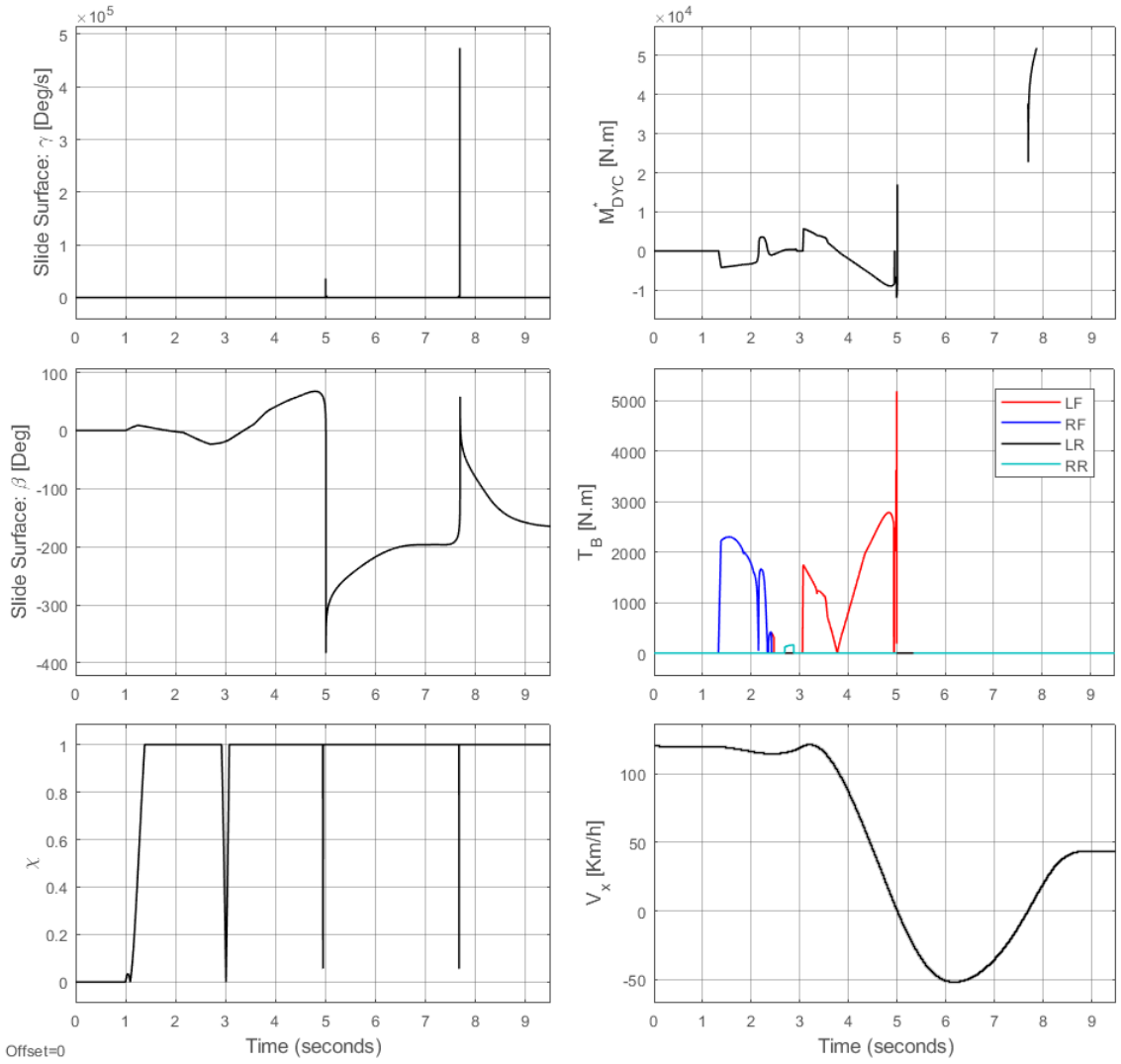

FIGURE 5.9: DLC simulation result of a reference vehicle model without the IVDC controller. The DYC controller calculated the required corrective moment but it is not applied to the vehicle since the DYC is deactivated.

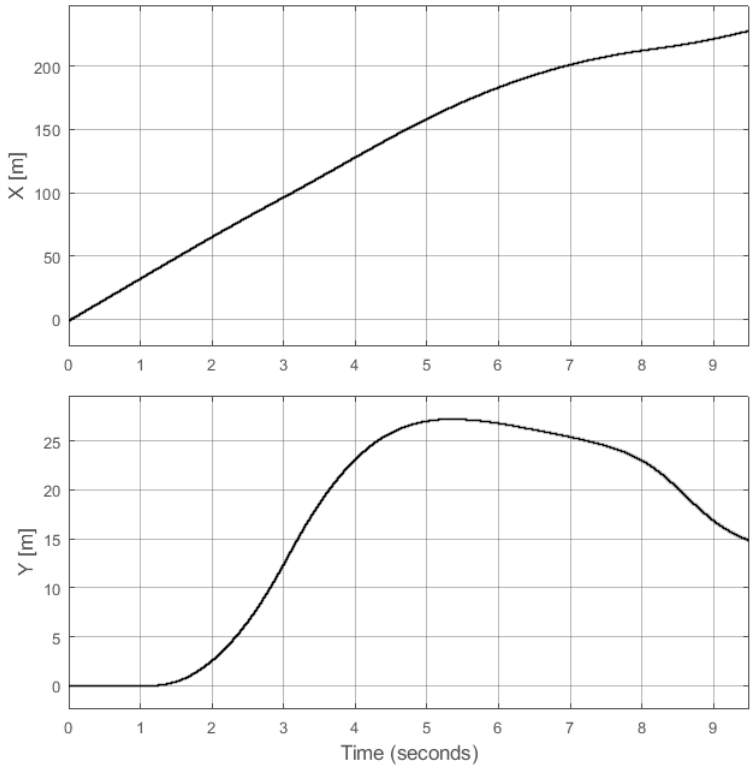

FIGURE 5.10: DLC simulation result of a reference vehicle model without the IVDC controller. A vehicle shows a great lateral slip, and it did not come back near the initial axis of y=0.

5.2.1 Case 1: DLC test with a $\beta_{\text{desired}} = \beta_{\text{steady state}}$

In case 1, the VSA standalone controllers in the AFS controller and the DYC controller have the same VSA target as described in Chapter 4, the steady state value predicted by the linear bicycle model. The sliding mode control strategy is designed to control the dynamic system so that the sliding surface approaches towards zero at all time. The ITSM control strategy in the VSA standalone controller has a sliding surface, $\tilde{\beta} = \beta - \beta_{\text{steady state}}$. The VSA controller in the AFS controller will generate the lateral tire force as a control input so that the actual VSA approaches to the steady state value by providing the corrective wheel steering angle. The yaw rate standalone controller in the AFS controller is deactivated in this study in order to observe the simulation results solely from the VSA controller, without any of yaw rate controller. The DYC controller generates the yaw moment in an attempt to control VSA, but note that its control objective is not the yaw rate. The simulation results of case 1 are shown in Figures 5.11, 5.12, and 5.13.

It is observed that the road wheel angle is corrected by the AFS controller to control VSA. The bottom left corner of Figure 5.11 shows three different graphs. Each line is the corrective road wheel angle generated by the standalone controllers. The black line that combines the effect of the yaw rate-control and VSA-control in the AFS design shows an identical corrective road wheel angle, compared to the 'Beta' line (VSA-controller) since the yaw rate controller in the AFS is deactivated. The simulated yaw rate of the vehicle shows deviation from the desired yaw rate, but it shows a matching trend over the entire simulation. The desired VSA shows higher value than the simulated or estimated VSA, while the simulated VSA is showing delay compared to the desired VSA. The controller is keeping the VSA within the boundaries of $\pm 5^{\circ}$, which enables the vehicle to have steer-ability. This is also proven by not having a spin out. Figure 5.12 shows the sliding surfaces of both the yaw rate control and the VSA control do not exhibit huge peaks, but seem to stay within or near the range of 20°/s and 10° for yaw rate and VSA, respectively. The DYC is activated to support the AFS to generate the corrective yaw moment to match the desired VSA. The vehicle longitudinal speed is maintained near 120 km/h even with the intervention of the DYC controller. As seen in Figure 5.13, the vehicle came back to near the initial axis ($y = 0$) of the travel after the steering event.

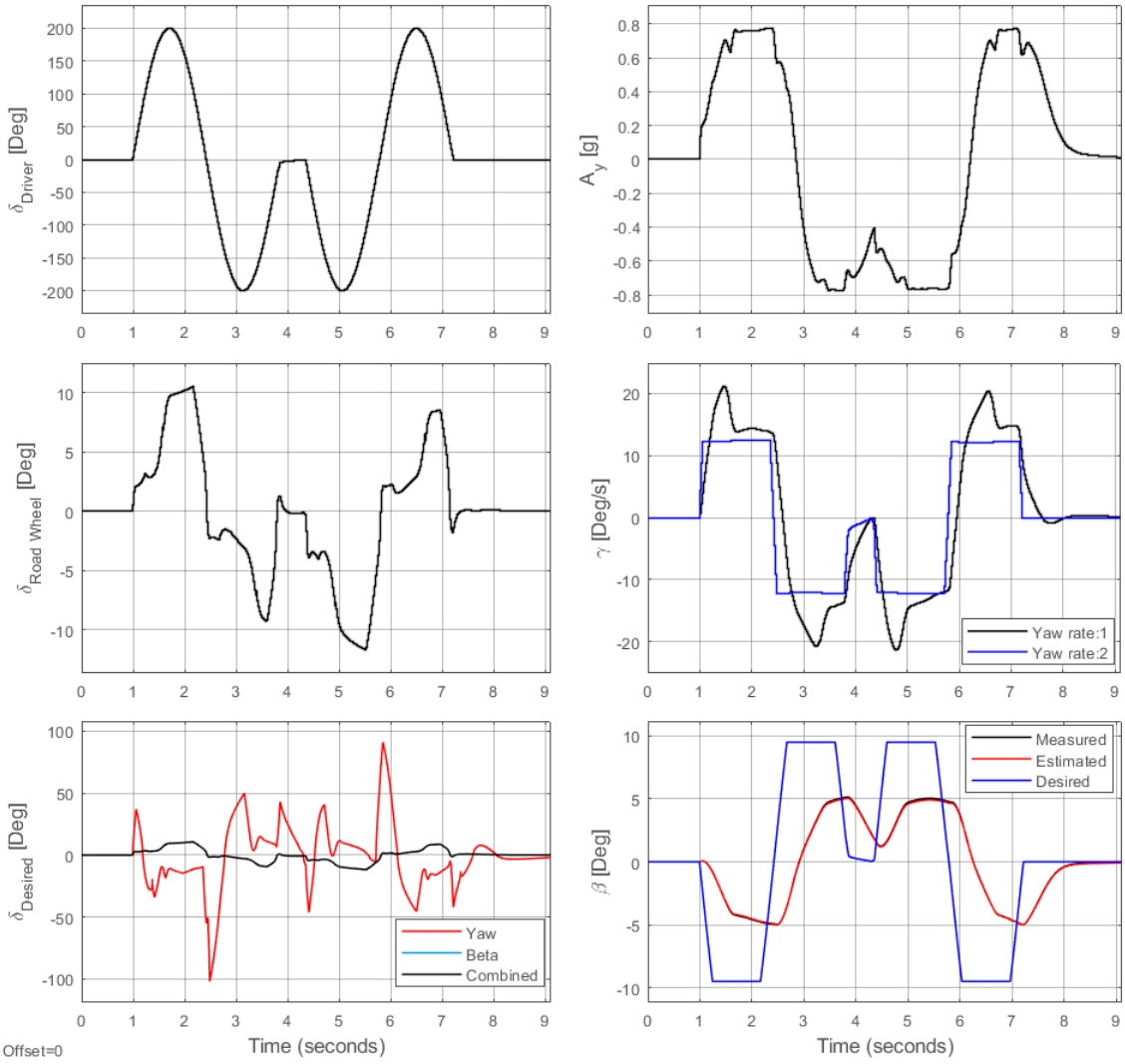

FIGURE 5.11: Case 1: DLC simulation results (1 of 2). Yaw rate:1 = simulated yaw rate. Yaw rate:2 = desired yaw rate. Measured values are the simulated values from the virtual vehicle.

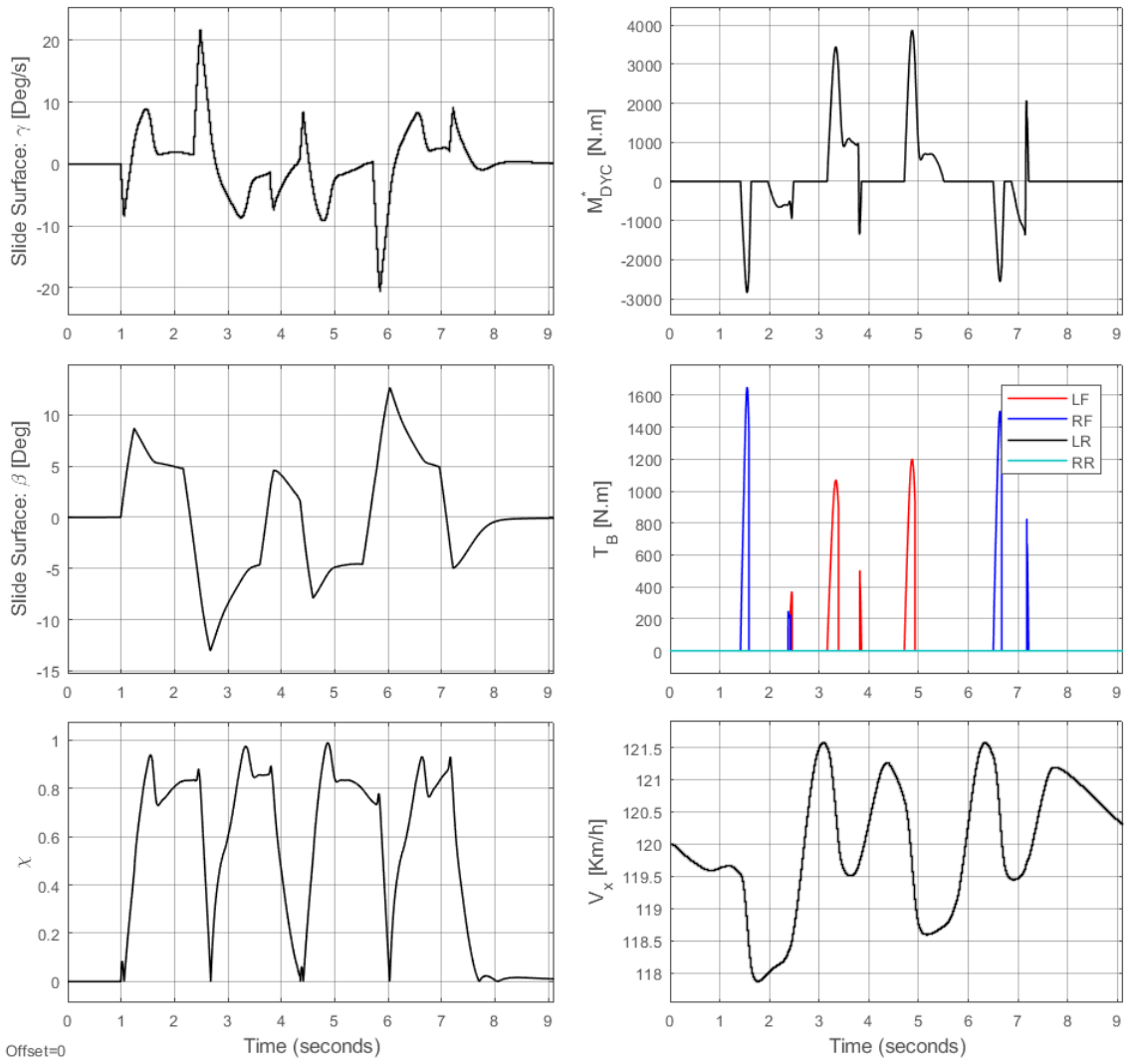

FIGURE 5.12: Case 1: DLC simulation results (2 of 2).

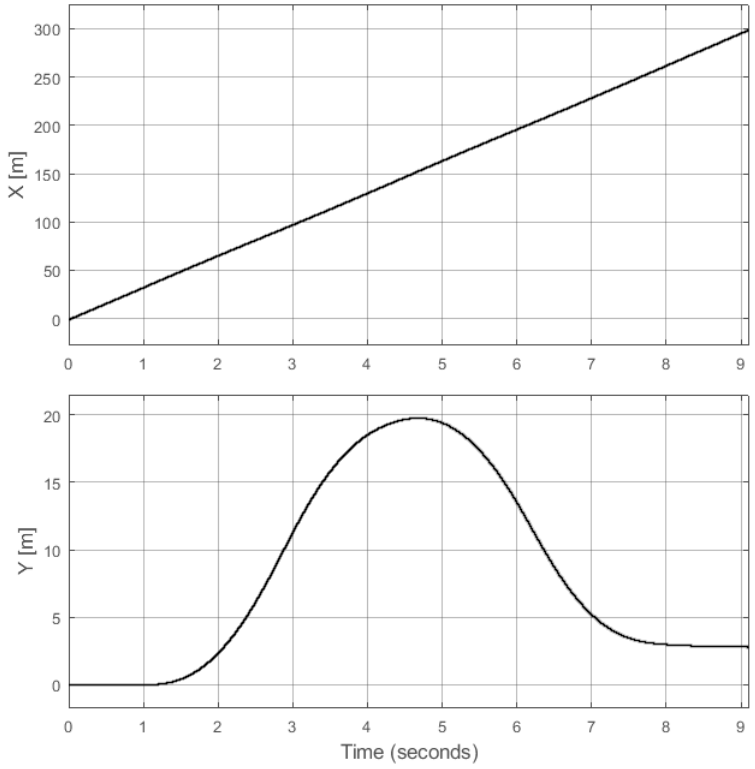

FIGURE 5.13: Case 1: Vehicle travel coordinates over time. The controller vehicle in this case came back to near the starting line of $y = 0$.

5.2.2 Case 2: DLC test with a $\beta_{\text{desired}} = 0$

Case 2 sets the IVDC controller to have a desired VSA of zero. Therefore, the state of the control systems in both the VSA standalone controller in AFS and DYC controller becomes $\tilde{\beta} = \beta - 0$. The AFS then will try to generate the lateral tire forces to counter any current VSA, bringing it to zero. Similarly, DYC will generate a yaw moment to make VSA zero. The simulation results of case 2 are presented in Figures 5.14, 5.15, and 5.16. The yaw rate controlled corrective wheel angle at the bottom left corner of Figure 5.14 do not affect the vehicle behaviour since the yaw rate controller in the AFS controller is deactivated.

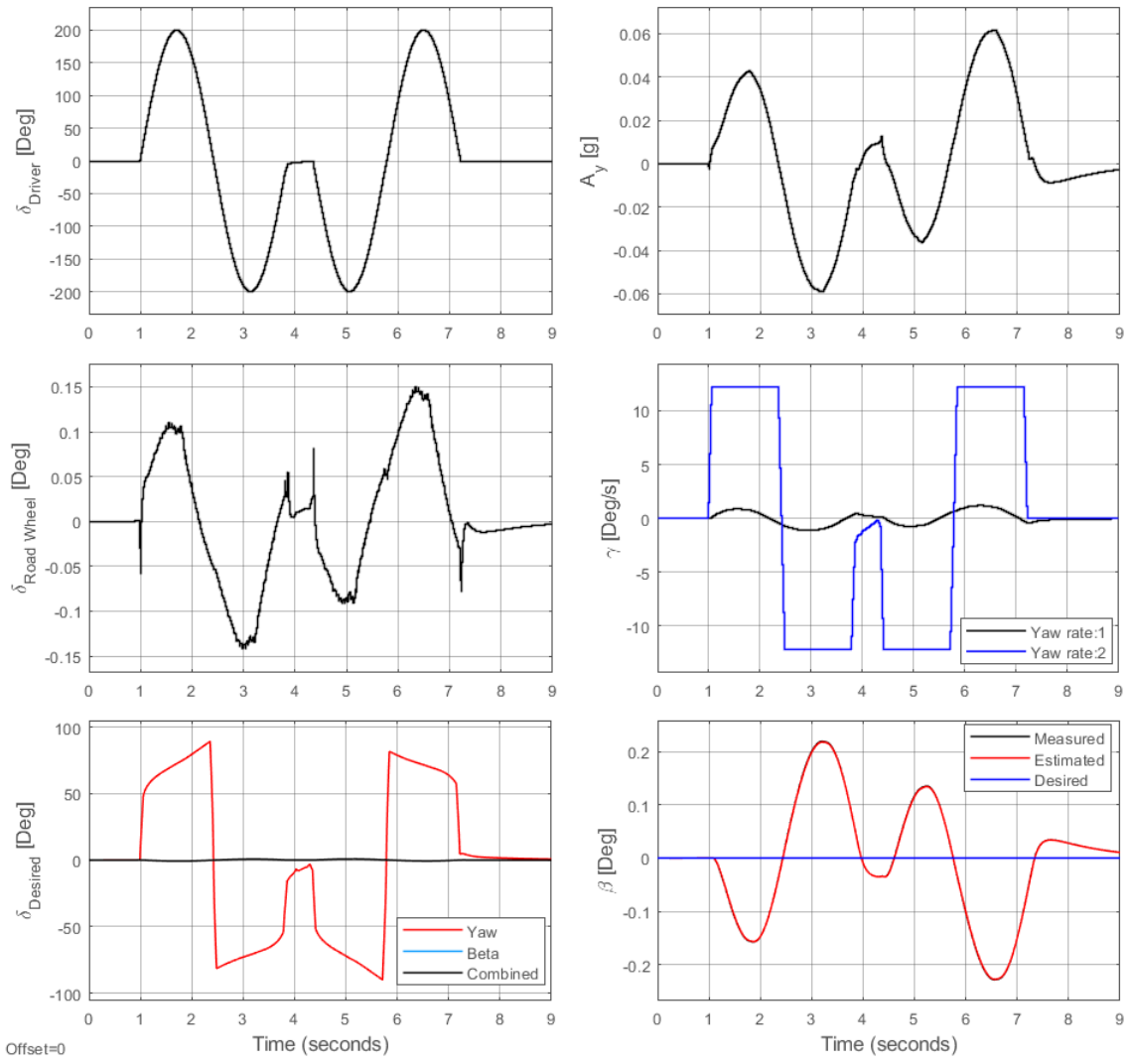

FIGURE 5.14: Case 2: DLC simulation results (1 of 2). Measured values are the simulated values from the virtual vehicle.

From the simulation results, interesting phenomena are observed. Significantly decreased yaw rate is observed along with very small road wheel steering angle. The physical interpretation of these phenomena is that while AFS tries to make the VSA go to zero, it instantly makes the small

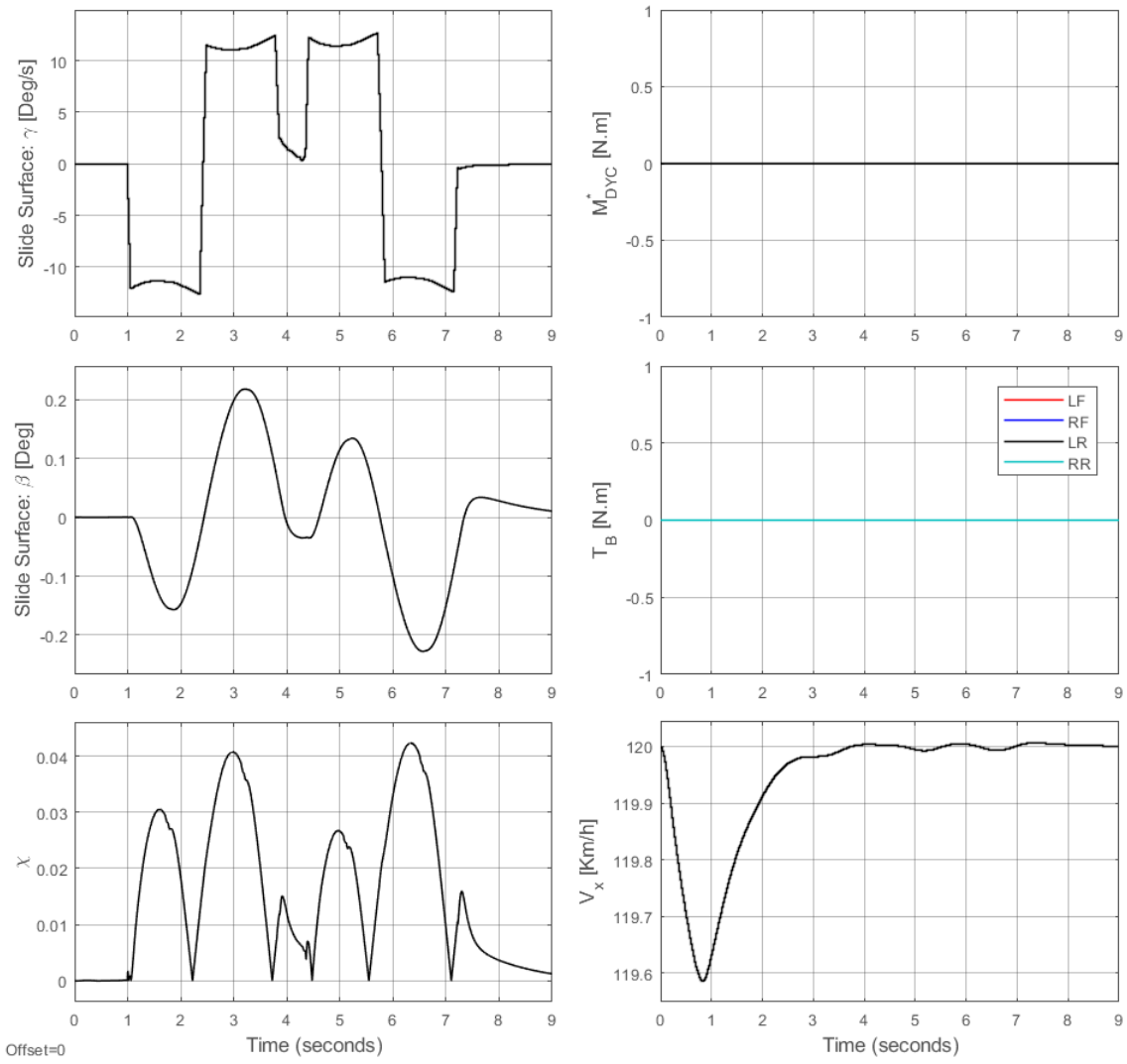

FIGURE 5.15: Case 2: DLC simulation results (2 of 2).

wheel angle so that the deviation between the travel direction and the heading direction stays small. Theoretically, it was expected that the VSA controller will generate corrective wheel steering angle so that the vehicle follows an intended path with small or almost zero-VSA. However, the VSA controller in the AFS controller corrects the road wheel angle to lead the vehicle to the slipping direction. As a result, it is not the controller that is changing the vehicle behaviour actively, but it is rather the controller driven by the natural phenomenon of slipping while the vehicle travels. This characteristic of zero target VSA has resulted in that the vehicle barely exhibits any motion due to small wheel angle, yaw rate, and this can be found in Figure 5.16. While the case 1 showed the lateral displacement of almost 20 m, the case 2 showed a peak lateral displacement of only 0.4 m.

In conclusion, it is obvious that the steady state VSA is much more suitable than the zero-VSA as a control target for the vehicle stability controller design. The choice of steady state VSA

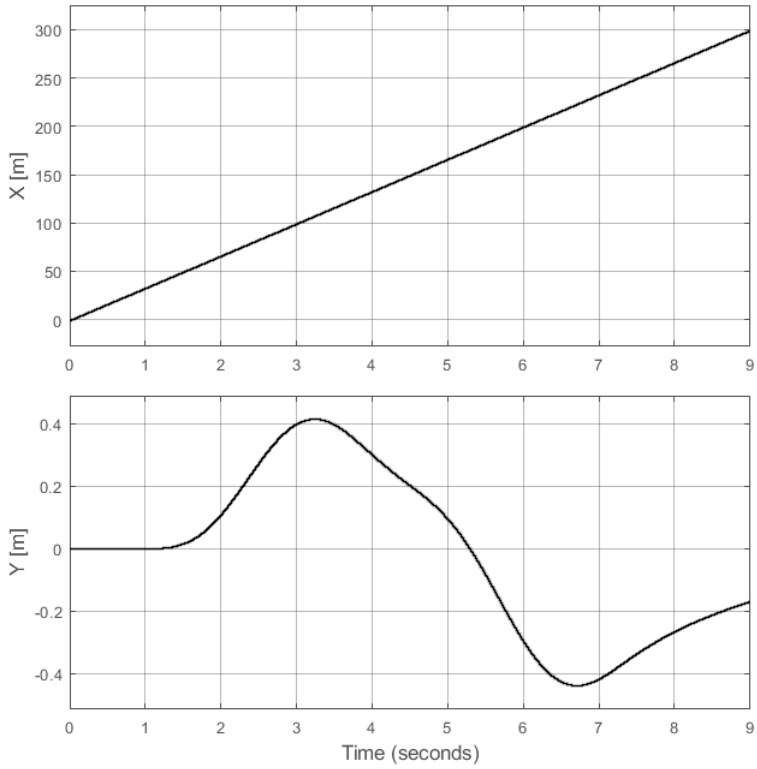

FIGURE 5.16: Case 2: Vehicle travel coordinates over time

value as the target is shown to keep the actual VSA within a good range so that the vehicle keeps the steer-ability during the simulation. Note that the zero VSA target may lead one to think that the vehicle will travel while following the intended path without any slipping. However, if zero-VSA is implemented as the control target, the controller will not change the vehicle motion to what the driver desired, but it rather will make the vehicle motion to be dominated by the natural phenomenon of slipping, leading the vehicle to have barely any lateral motion.

5.3 Variable Control Effort distribution vs Fixed Control Effort Distribution of the AFS Controller

The AFS controller presented in this work has two standalone controllers that each generate a corrective steering angle in attempts to control both yaw rate and VSA. The AFS controller uses a linear combination of corrective wheel angles generated by the yaw rate standalone controller and the VSA standalone controller. In an earlier chapter, an iterative method was taken to explore the effect of varying the linear coefficient for both yaw rate controlled steering angle and VSA controlled steering angle, in order to find an efficient linear combination between these two variables. The determined ratio between the yaw rate and VSA standalone controllers is $9 : 1$, since increasing the coefficient for the VSA-controller did not improve the desired VSA tracking performance as much as it did for the yaw rate tracking. The priority between two control objectives

is subjective to change at different time during different dynamic events. Therefore, the idea of adopting the stability index, χ, which describes how stable the vehicle is, is proposed as the means to determine the contribution of each standalone controller in the AFS controller. As the stability index becomes higher, the VSA must be controlled since it is approaching the boundary of the reference region. Therefore, the proposed method of generating the resultant corrective wheel angle is shown as follows:

$$\delta_w = (1 - \chi)\delta_{w\psi} + (\chi)\delta_{w\beta} \tag{5.2}$$

This section explores whether the proposed method of calculating the resultant corrective wheel angle in the AFS controller would show more promising vehicle stabilizing performance than the fixed linear combination method. In order to compare the proposed method and the conventional method, the following testing conditions are set:

- Test type: Double lane change (DLC) test
- DYC: deactivated
- Steering amplitude: 200°/s
- Vehicle velocity: constant at 120 km/h
- Case 1: Linear setting $\delta_w = w_1\delta_{w\psi} + w_2\delta_{w\beta}$
- Case 2: Variable setting $\delta_w = (1 - \chi)\delta_{w\psi} + (\chi)\delta_{w\beta}$

The reference vehicle model during this test has spun out exhibiting a huge yaw rate. The full simulation results can be referred to Figures 5.8, 5.9, and 5.10 in Section 5.2, as the identical test setting was used without the intervention of any controllers there.

5.3.1 Case 1: DLC test with a fixed linear setting

The first case in which the AFS controller has the linear combination of coefficients $w_1 = 0.9$ and $w_2 = 0.1$, for yaw rate controller and VSA controller, exhibits very good yaw rate tracking; therefore, the sliding surface for the yaw rate stays near zero for most of the simulation time. The resultant steering correction angle, δ_{desired}, consists of 90% of $\delta_{w\psi}$ and 10% of $\delta_{w\beta}$. The VSA tracking is not as good as the yaw rate tracking, as seen in Figure 5.17; however, it was confirmed that increasing w_2 does not improve VSA tracking significantly. Note that the VSA is controlled so that it stays within the range between ±5°, which provides a good steer-ability for the vehicle on the road. Figure 5.18 shows that the sliding surface of the VSA also shows a trend that it tries to bring the sliding surface towards zero. The trajectory of the vehicle over the simulation shows a good return to the initial axis without any spinning out, as seen in Figure 5.19.

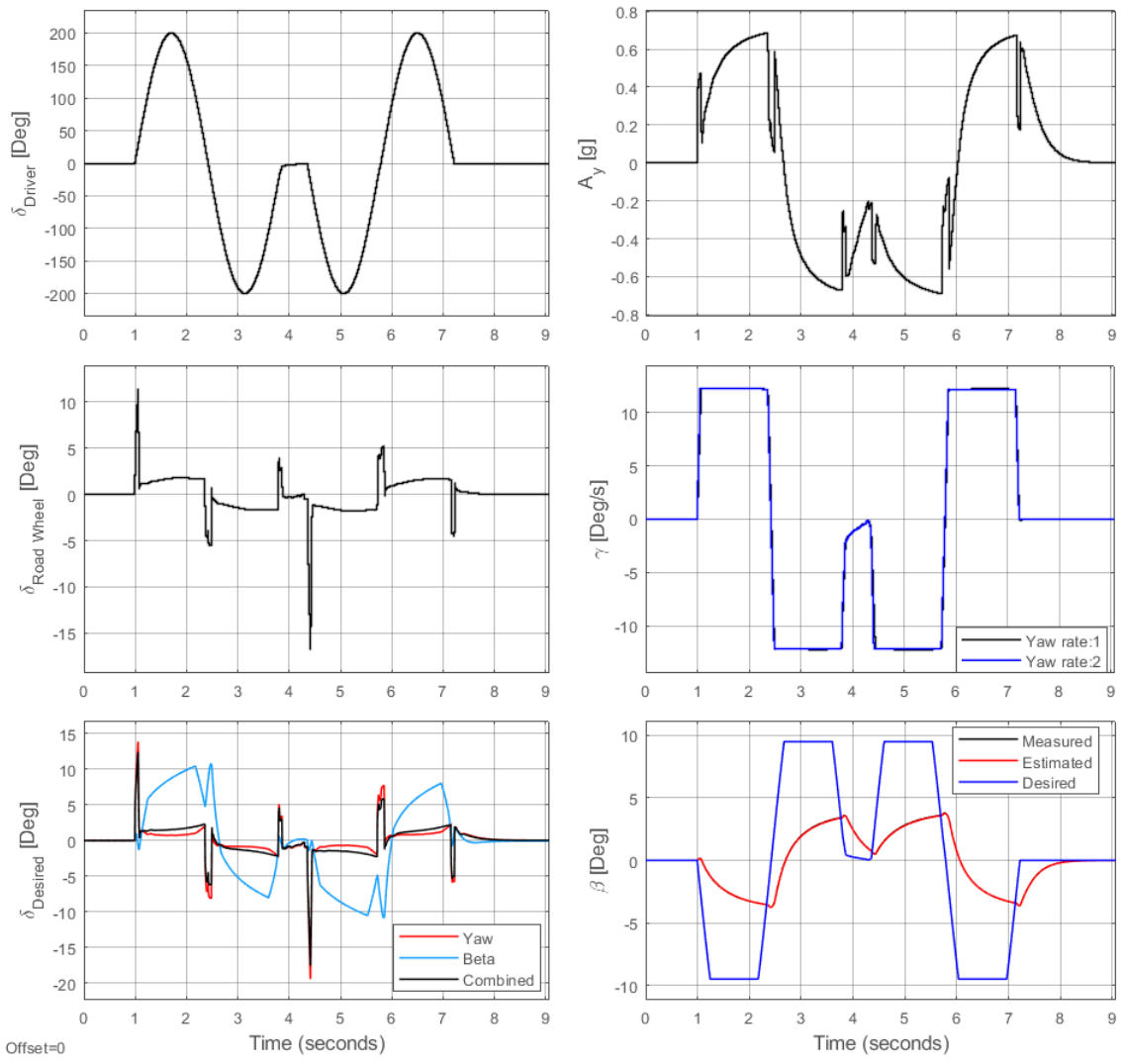

FIGURE 5.17: Case 1: DLC simulation results (1 of 2). Measured values are the simulated values from the virtual vehicle.

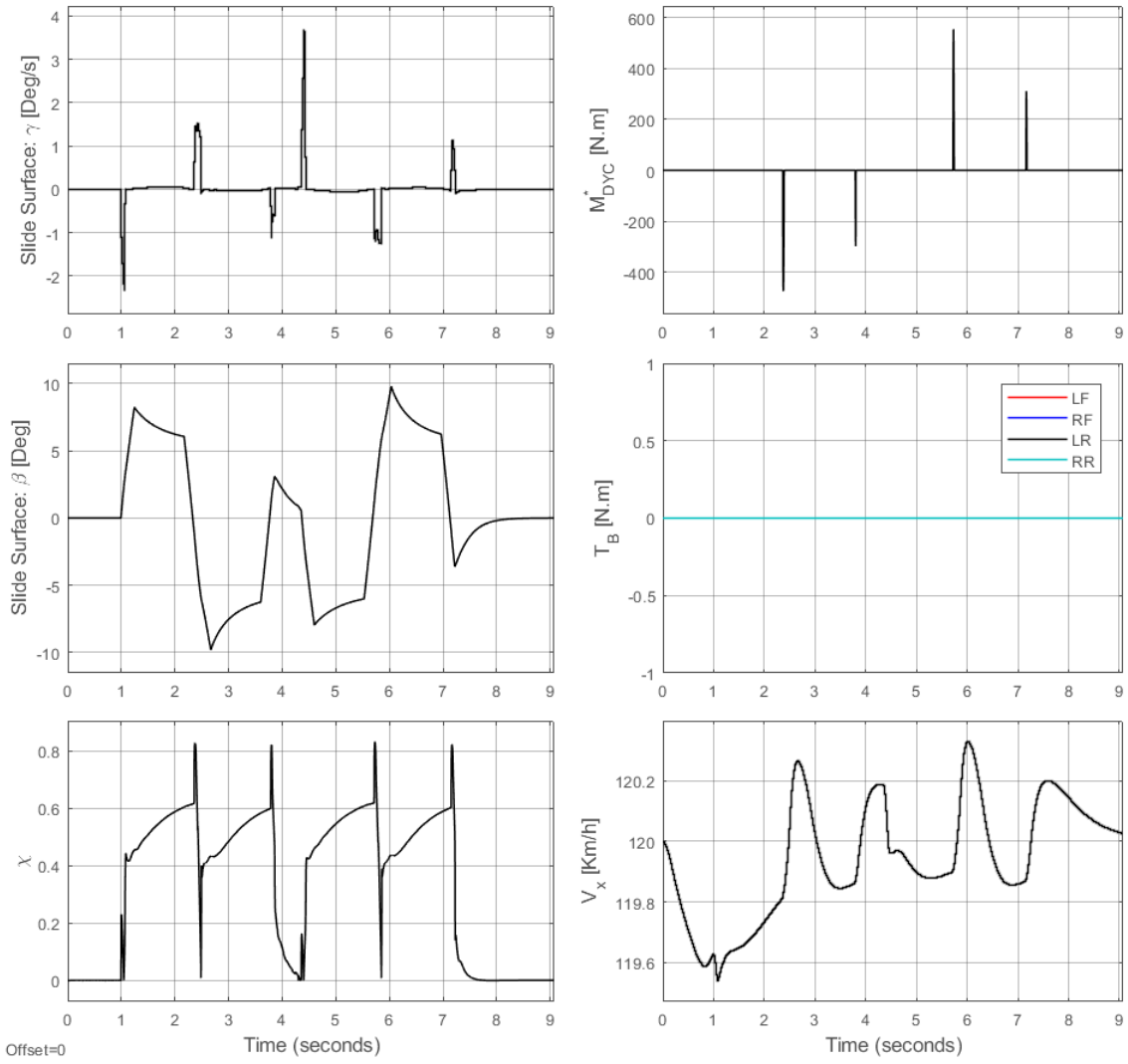

FIGURE 5.18: Case 1: DLC simulation results (2 of 2) Sliding surface for the standalone yaw rate controller stays near zero for most of the simulation time.

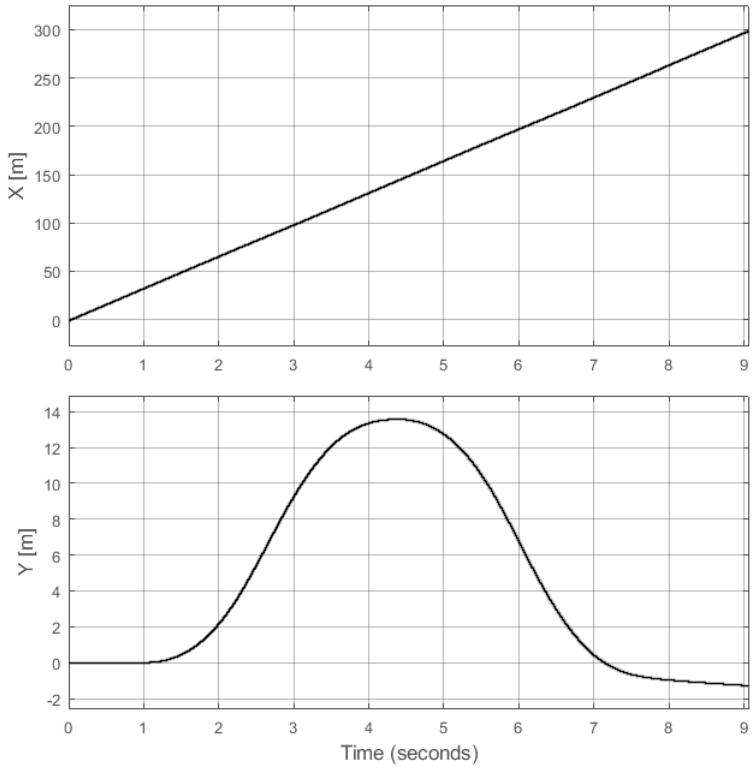

FIGURE 5.19: Case 1: Vehicle travel coordinates over time.

5.3.2 Case 2: DLC test with a variable setting

The second case adopts the proposed Equation 5.2 as the method of calculating the resultant corrective steering wheel angle in the AFS controller. The yaw rate tracking performance in case 2 seemed to be operating well to keep the simulated yaw rate of the vehicle close to the desired yaw rate. However, the yaw rate tracking performance in case 2, compared to the one in case 1, seemed worse but acceptable. The stability index shows that the maximum value of stability index, χ, in case 2 is higher than case 1, as shown in Figure 5.21. This means that the vehicle motion state in case 2 was less stable than the one in case 1; the vehicle motion state of case 2 at some points in the phase plane is near the unstable region. The stability index, χ, tends to generate spikes as the corrective action affects the vehicle. Shortly after, the stability index drops significantly after the corrective action from the controller stabilizes the vehicle. As the vehicle motion state becomes unstable, stability index χ grew, increasing the effect of the VSA-controller in the AFS controller. However, increasing the effect of the VSA-controller is not as effective as the yaw rate-controller. As a result, the yaw rate tracking performance became worse and the stability index χ kept growing. This caused the calculation of the corrective braking torques T_B since the yaw rate error became greater than the threshold value as seen in Figure 5.21, showing the braking torques that are calculated by the DYC subsystem in case 2. The DYC was deactivated, and therefore the observed braking torques did not affect the vehicle behaviour; however, this information implies that the vehicle was sufficiently unstable that the DYC system was activated and calculated a corrective yaw moment and braking torques. Figures 5.19 and 5.22 show the vehicle travel trajectories. According to these two figures, the vehicle model equipped with the controller in case 1 setting maintained the straight heading direction after the maneuver, while the vehicle model with the controller in case 2 setting travelled more off course. The simulation results from both cases are quantified by measuring the root mean square error (RMSE) of yaw rate, VSA, VSA-estimator and vehicle side slip velocity estimator, and average longitudinal velocity to quantify the kinetic energy loss and maximum lateral acceleration in an attempt to explain that one case is better than the other case more quantitatively. The summary of the simulation results are shown in Table 5.2.

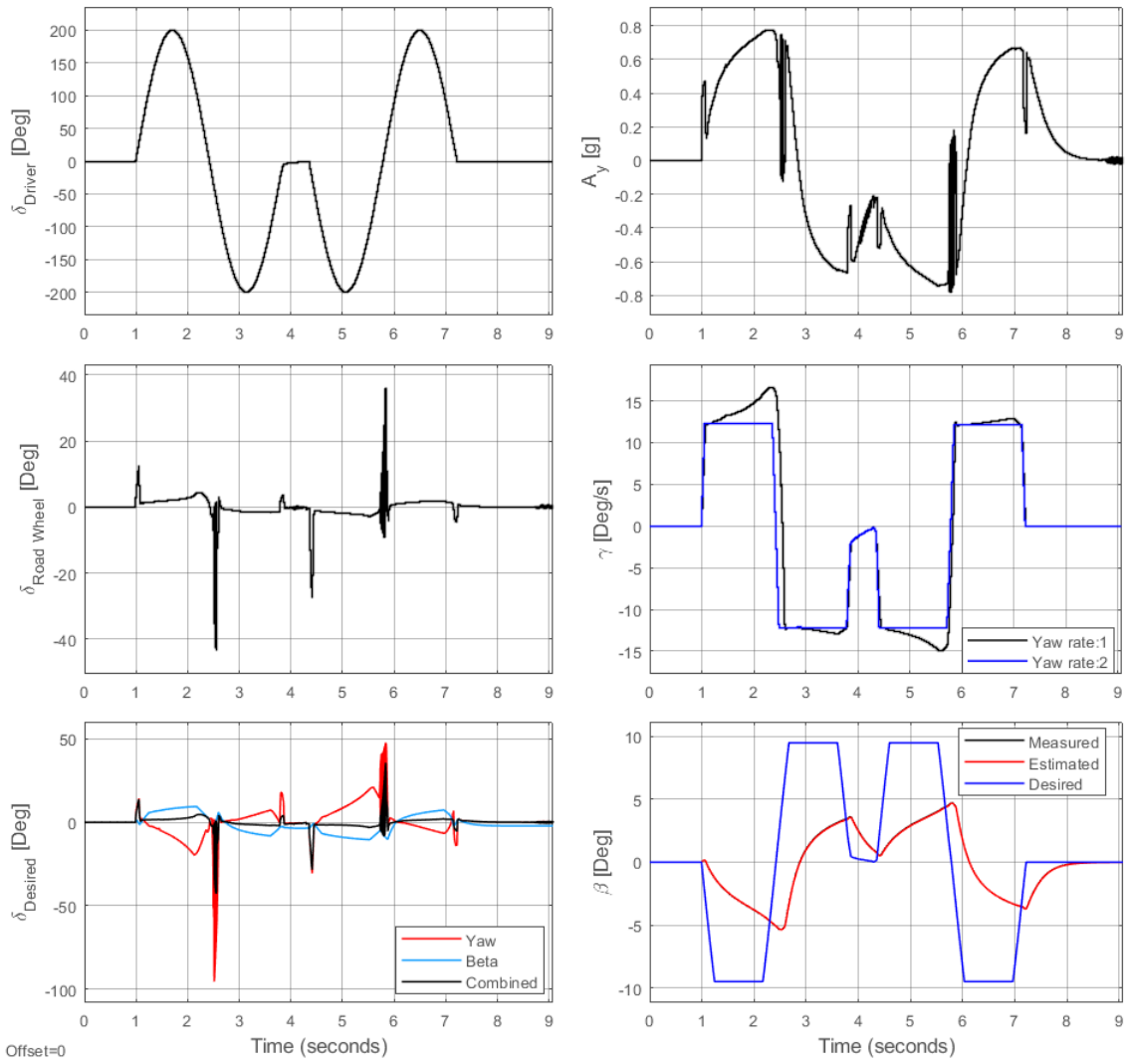

FIGURE 5.20: Case 2: DLC simulation results (1 of 2) Yaw rate tracking is still very good, but greater deviations are observed in case 2, compared to case 1. Measured values are the simulated values from the virtual vehicle.

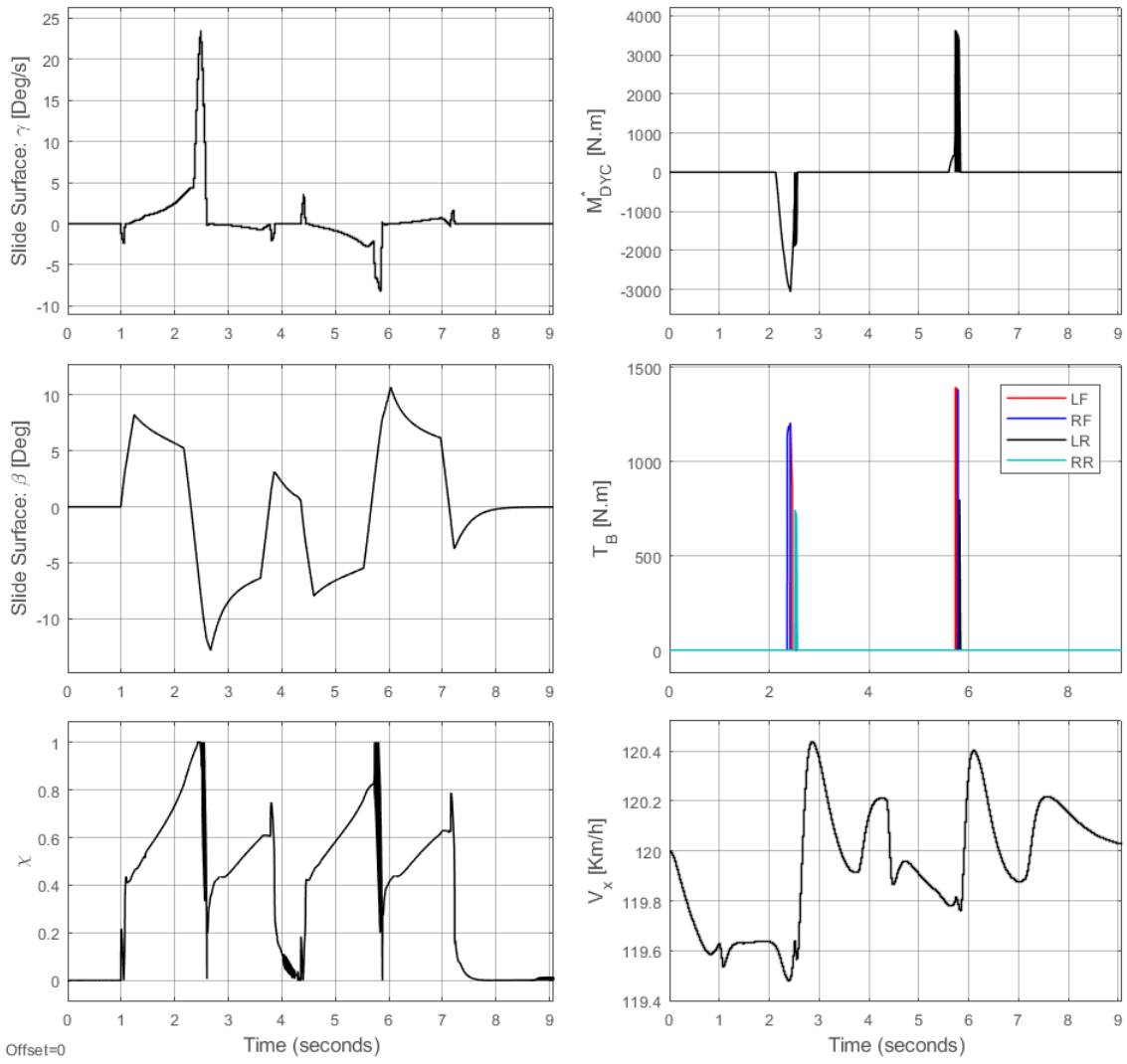

FIGURE 5.21: Case 2: DLC simulation results (2 of 2). The corrective braking torque appeared here did not affect the vehicle motion, but it is shown in the figure to imply that the corrective yaw moment would have been generated by the DYC system due to the vehicle stability index exceeding 0.8 and yaw rate error being greater than 5°/s.

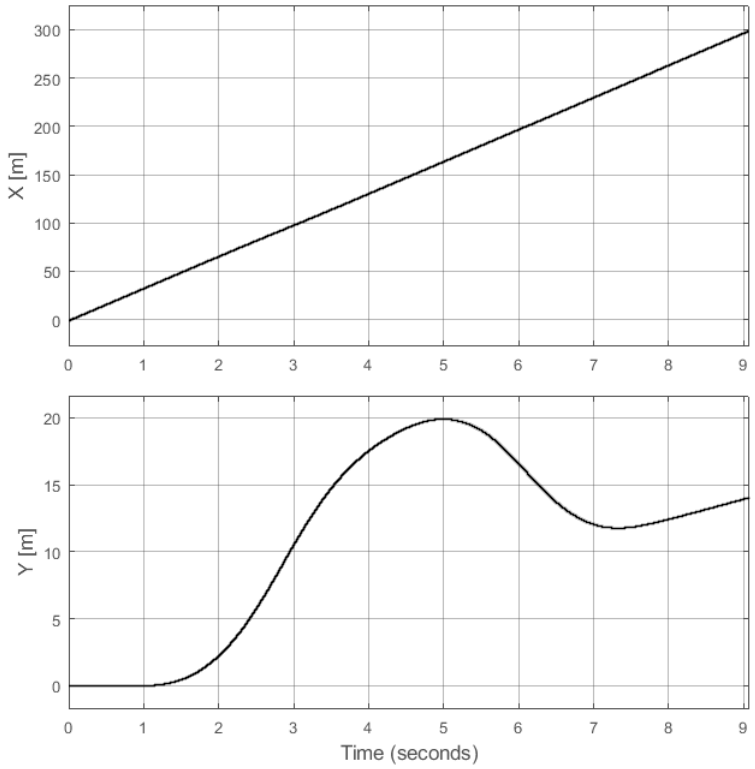

FIGURE 5.22: Case 2: Vehicle travel coordinates over time.

Table 5.2: DLC Test Results: Case 1 uses a linear combination and case 2 uses a variable AFS coefficient of stability index, χ.

Test #	AFS Setting (w_1, $w2$)	RMSE-γ (°/s)	RMSE-β (°)	RMSE-β Estimator (°)	RMSE-$\dot{\beta}$ Estimator (°/s)	$V_{x,avg}$ (km/h)	$a_{y,max}$ (g)
1	0.9, 0.1	0.3550	5.0024	0.7604	0.5415	119.9425	0.6891
2	1-χ, χ	2.9177	5.3493	0.9352	5.9368	119.9425	0.7814

As a result of the comparison, case 1 shows better yaw rate tracking performance by having a very small value of RMSE for yaw rate; 0.3550°/s, compared to case 2 in which the RMSE value for yaw rate is 2.9177°/s. Case 1 also showed better VSA tracking performance of 5.0024°, which is less than in case 2, 5.3493°, even though case 1 only has 10% contribution of the VSA-standalone controller in the AFS controller for the resultant corrective wheel steering angle. The VSA and vehicle side slip velocity estimators seem to operate very accurately in both cases. The average longitudinal velocity in both cases were identical; therefore, it cannot be concluded which method costs more longitudinal kinetic energy loss. The maximum lateral acceleration was observed to be lower in case 1 by 11.8%, compared to case 2. The case 2 method was proposed in an attempt to cope with multiple control objectives flexibly during the simulation; however, the non-linearity added in this proposed method caused instability in correcting the vehicle behavior. As proofs for this conclusion, the proposed method (case 2) shows greater maximum lateral acceleration, worse yaw rate tracking, worse VSA tracking and most importantly worse ability to follow the intended path, based on the driver's steering input. As a result, the proposed method of calculating the resultant corrective wheel steering angle is worse than the original method of calculating it by using a fixed linear combination between two corrective steering angles from two standalone controllers.

5.4 Comparison of Standalone Controllers Performance

The IVDC controller in this research project integrates multiple standalone controllers; AFS and DYC. This section describes how the AFS controller and the DYC controller stabilize the lateral motion of the vehicle as individual controllers, but also as the combined IVDC, using a dynamic event that is a more severe maneuver than the one used for the ESC homologation process. A vehicle model without any controllers was tested in this section as a reference, then a vehicle model is equipped with three combinations of the controllers during each of three simulation cases to observe the performance of individual controllers (AFS and DYC) and integrated controllers (AFS+DYC). The testing condition is set for three cases as follows:

- Test type: Double lane change (DLC) maneuver with steering amplitude of 600°
- Road: Dry asphalt road with $\mu = 0.85$
- AFS setting: 90% Yaw rate control ($w_1 = 0.9$), 10% VSA control ($w_2 = 0.1$)
- Vehicle velocity: constant at 120 km/h
- Case 1: AFS is activated. DYC is deactivated
- Case 2: AFS is deactivated. DYC is activated
- Case 3: AFS and DYC are both activated

The steering input for this simulation is shown in Figure 5.23. The DLC simulation setting is set to finish at $t = 10$ seconds providing sufficient time to observe any vehicle motions due to inertia after the COS, at $t = 7.22$ seconds.

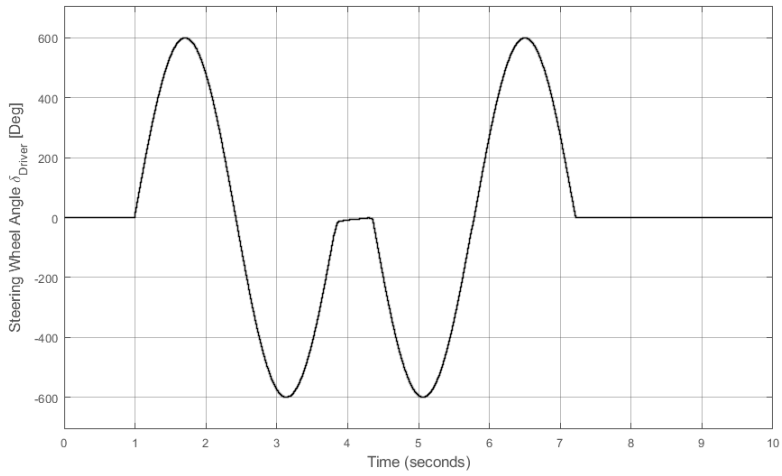

FIGURE 5.23: Steering input data during the DLC test with an amplitude of 600°. Zero steering input is maintained for about 3.8 seconds after the COS to observe any residual vehicle motion from steering and braking actuation.

The reference vehicle model without any controllers spun out, causing the simulation to stop computations at around $t = 5$ seconds. Figure 5.24 shows that the simulated VSA keeps increasing at a fast rate leading to a change of sign of VSA near $t = 5$ seconds, since the vehicle lost control and kept spinning . This caused the sliding surface of the VSA controller to grow as seen in

Figure 5.25. The stability index is saturated at 1 most of the simulation time, which indicates great instability of the reference vehicle model without any controllers. Any correction outputs from AFS and DYC controllers shown in the figures in this section show the calculated values in each controllers based on the state of vehicle motion. Whether it was actuated to stabilize the vehicle or not depends on the controller setting in each set of simulation runs. For instance, a corrective steering wheel value, δ_{desired} and a corrective yaw moment, M^*_{DYC}, and brake torques, T_b, were not actuated to affect the steering system or differential braking system to stabilize the reference vehicle in this run.

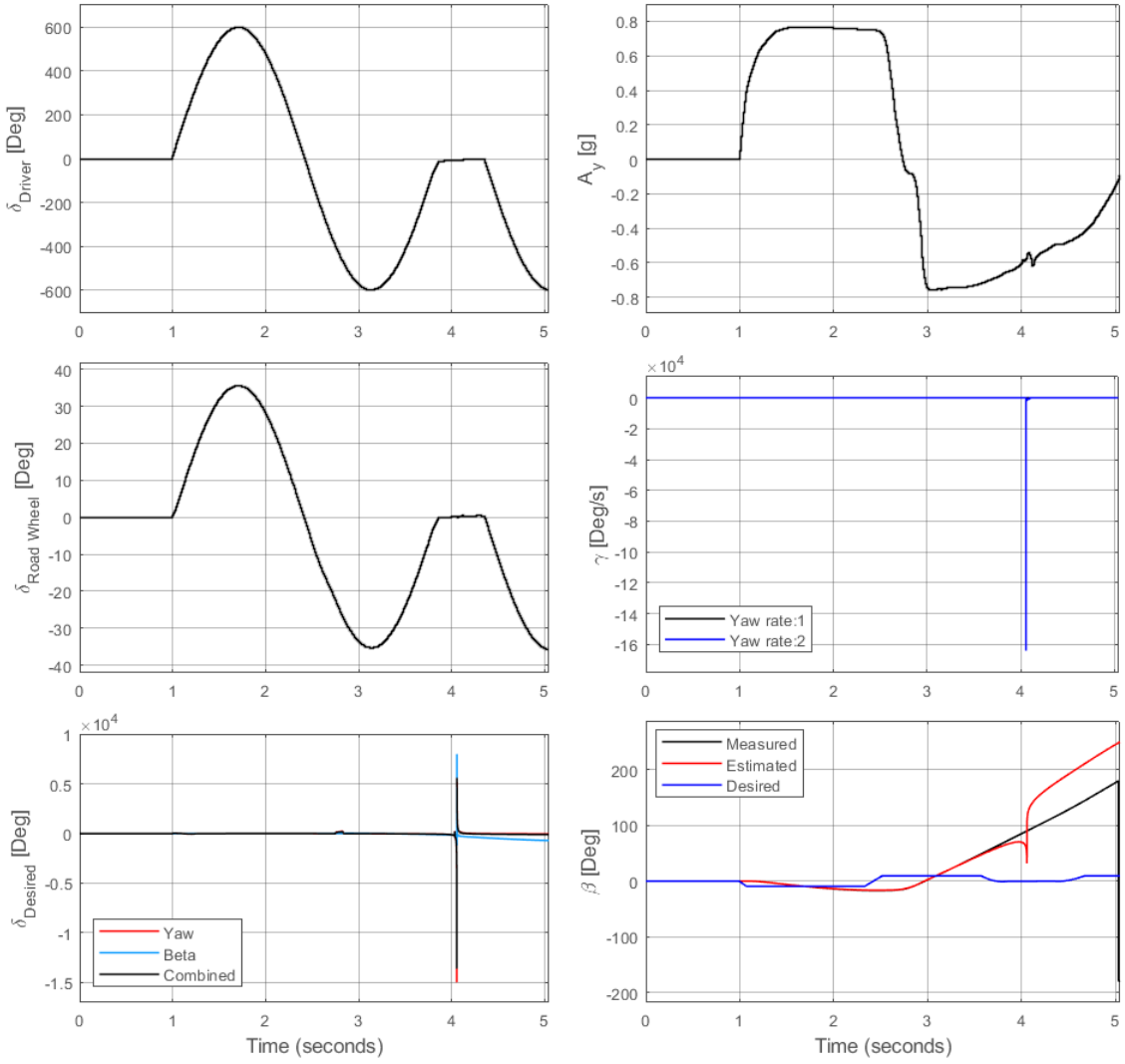

FIGURE 5.24: DLC simulation results (1 of 2) of reference vehicle model. The vehicle model spun out causing peaks in yaw rate. Corrective steering angle shown here did not affect the vehicle motion, but it is calculated in the AFS controller in the background. Measured values are the simulated values from the virtual vehicle.

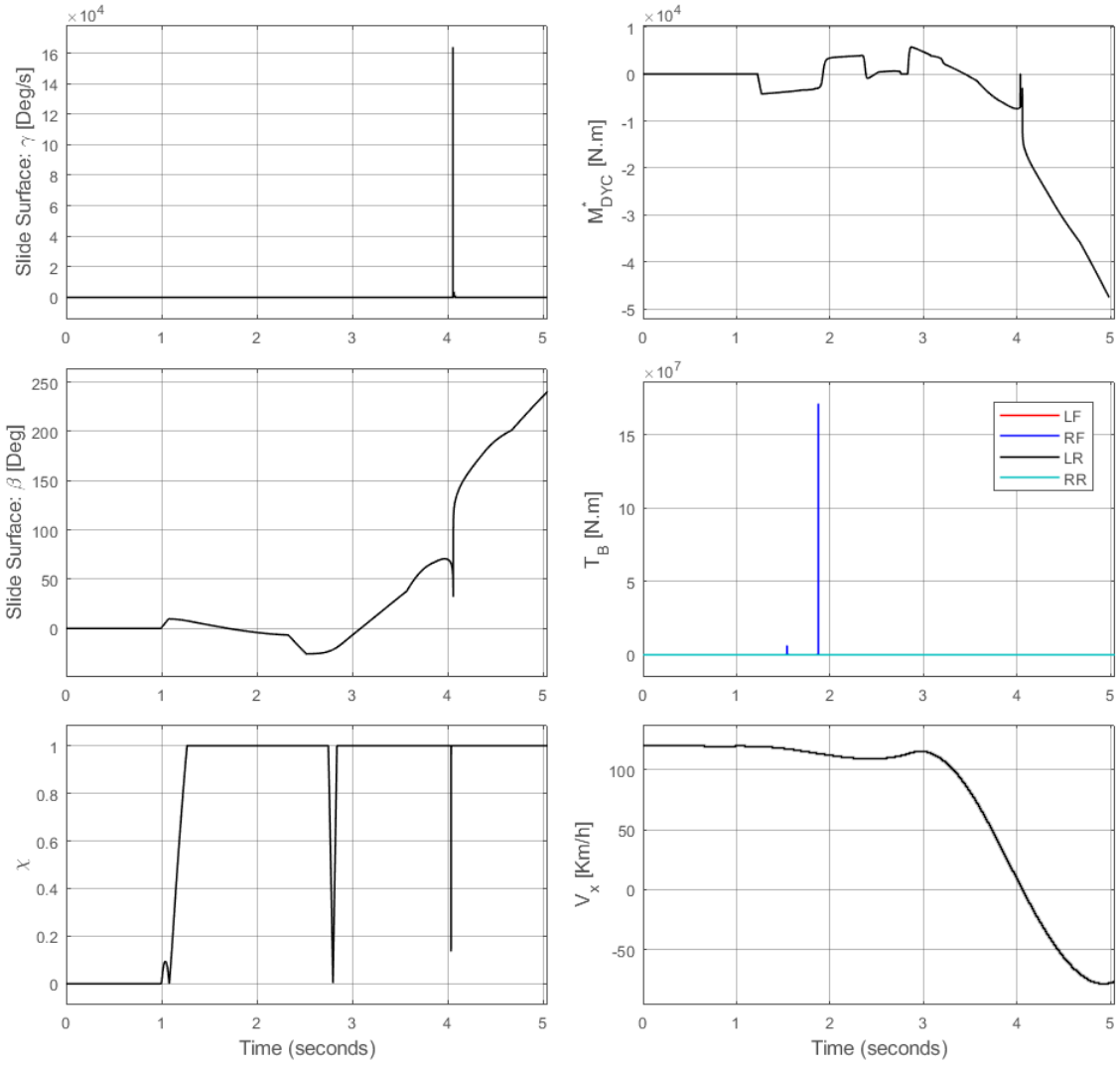

FIGURE 5.25: DLC simulation results (2 of 2) of reference vehicle model.

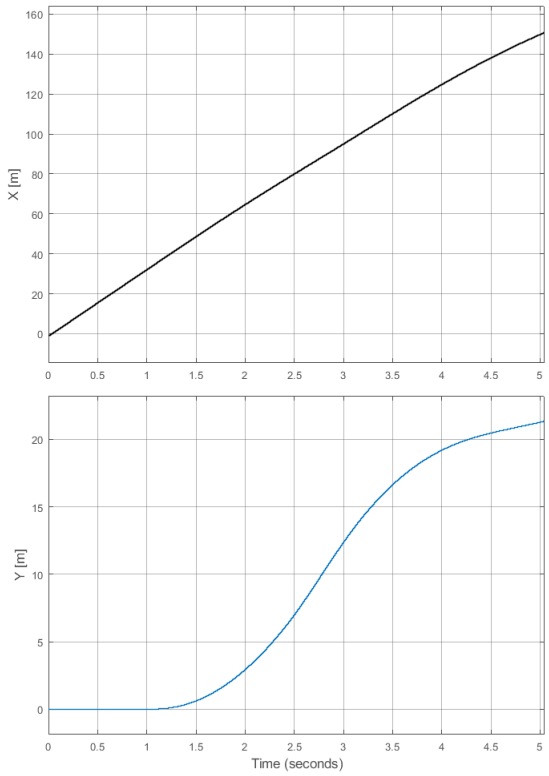

FIGURE 5.26: Reference vehicle travel coordinates over time Sliding surface for the VSA controller, VSA error between simulated and desired VSA values, grows over the simulation.

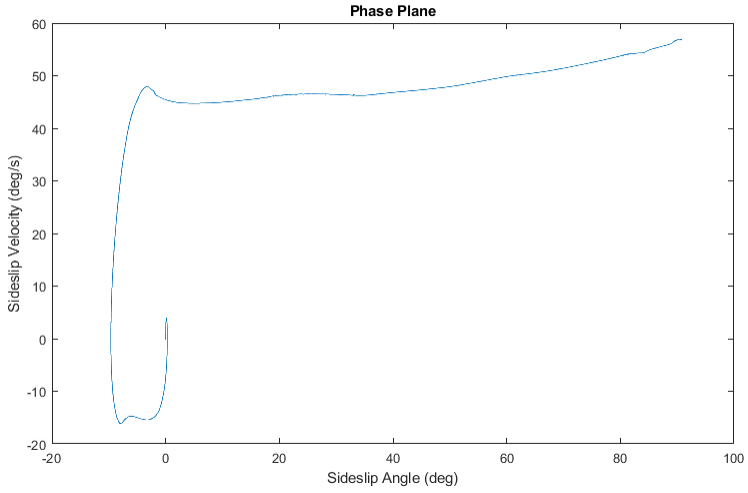

FIGURE 5.27: Phase plane of the reference vehicle during the DLC test. VSA and side slip velocity increased significantly as the vehicle spun out.

5.4.1 Case 1: DLC test with a vehicle equipped with the AFS controller

The first case has only the AFS controller activated, compared to the reference vehicle model. The AFS controller is set to take 90% of yaw rate controlled corrective steering angle and 10% of VSA controlled corrective steering angle. With only the AFS controller activated during the severe maneuver, the simulation did not fail since the vehicle did not spin out. The value of ρ was set to be constant at 1 during this run so that the corrective yaw moment is entirely sourced from the AFS controller. If ρ is not changed to a fixed value, but remained as a variable, the corrective yaw moment that would have been generated by the AFS controller will be reduced when the vehicle motion state is near the stable region boundaries, as seen in the stability index equation.

Figure 5.28 shows that the AFS controller corrected the vehicle yaw rate to match the desired yaw rate very closely during the simulation. The VSA stays within the upper and lower boundaries of 4° amplitude while the saturation boundaries for the VSA have an amplitude of 10°, which is calculated based on the road surface friction coefficient. The sliding surface for the yaw rate controller in the AFS controller stays near zero at all time. When the yaw rate difference shows a peak, corrective wheel steering angles are generated to bring the sliding surface (yaw rate difference) to zero promptly.

The corrective yaw moment and braking torques generated from the DYC controller are shown in Figure 5.29, but these are calculated values in the background of the DYC controller, not affecting the vehicle motion. The AFS controller generates the corrective wheel angles to bring the vehicle motion state towards the stable region when the vehicle motion state leaves the stable region as seen in Figure 5.31; the stability index shows peaks and converges to 1 during this time as seen in Figure 5.29.

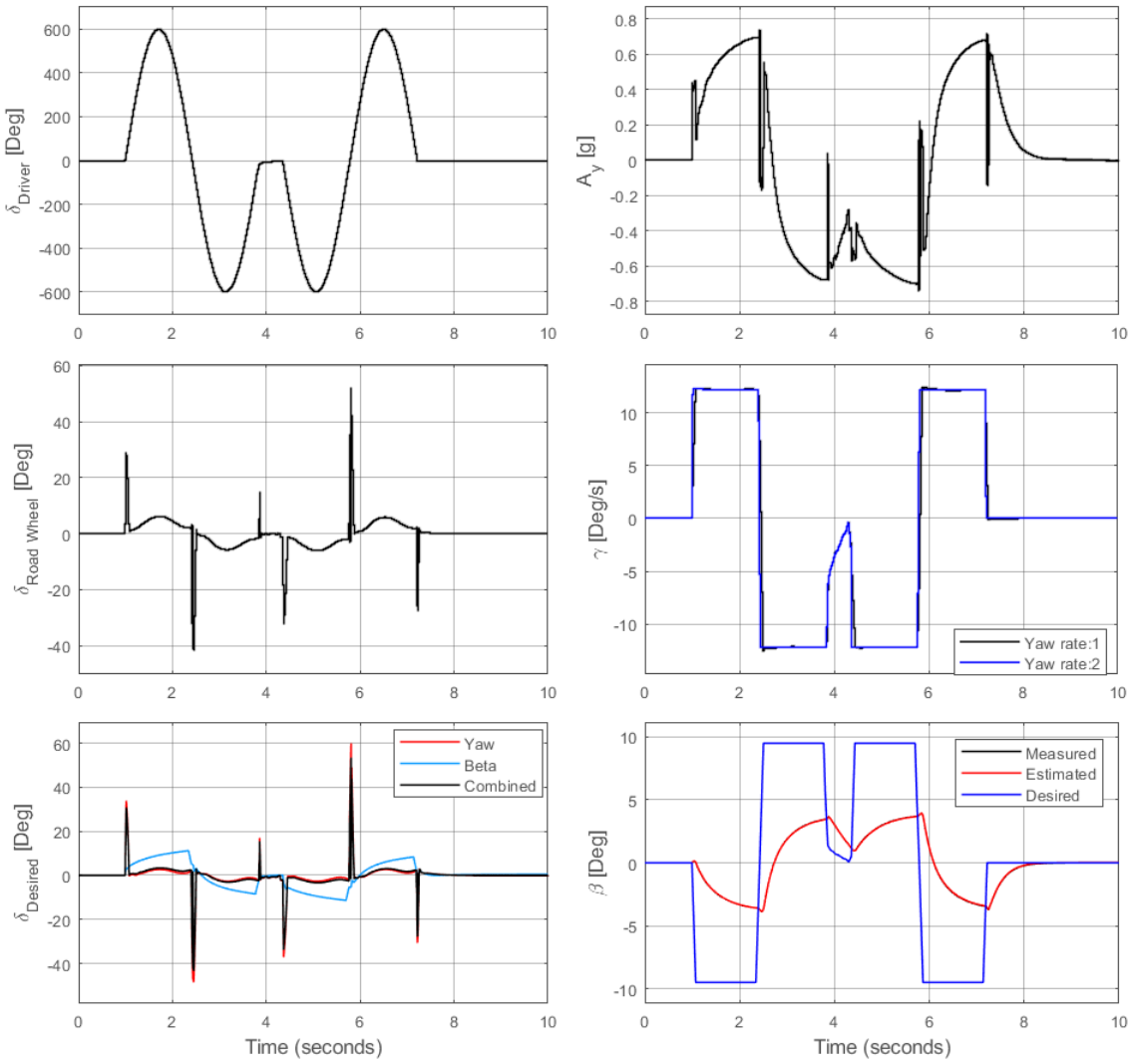

FIGURE 5.28: Case 1: DLC simulation results (1 of 2). Yaw rate is matched to the desired yaw rate. Corrective wheel steering angles are generated when the steering angle changes direction to counter the inertia. Measured values are the simulated values from the virtual vehicle.

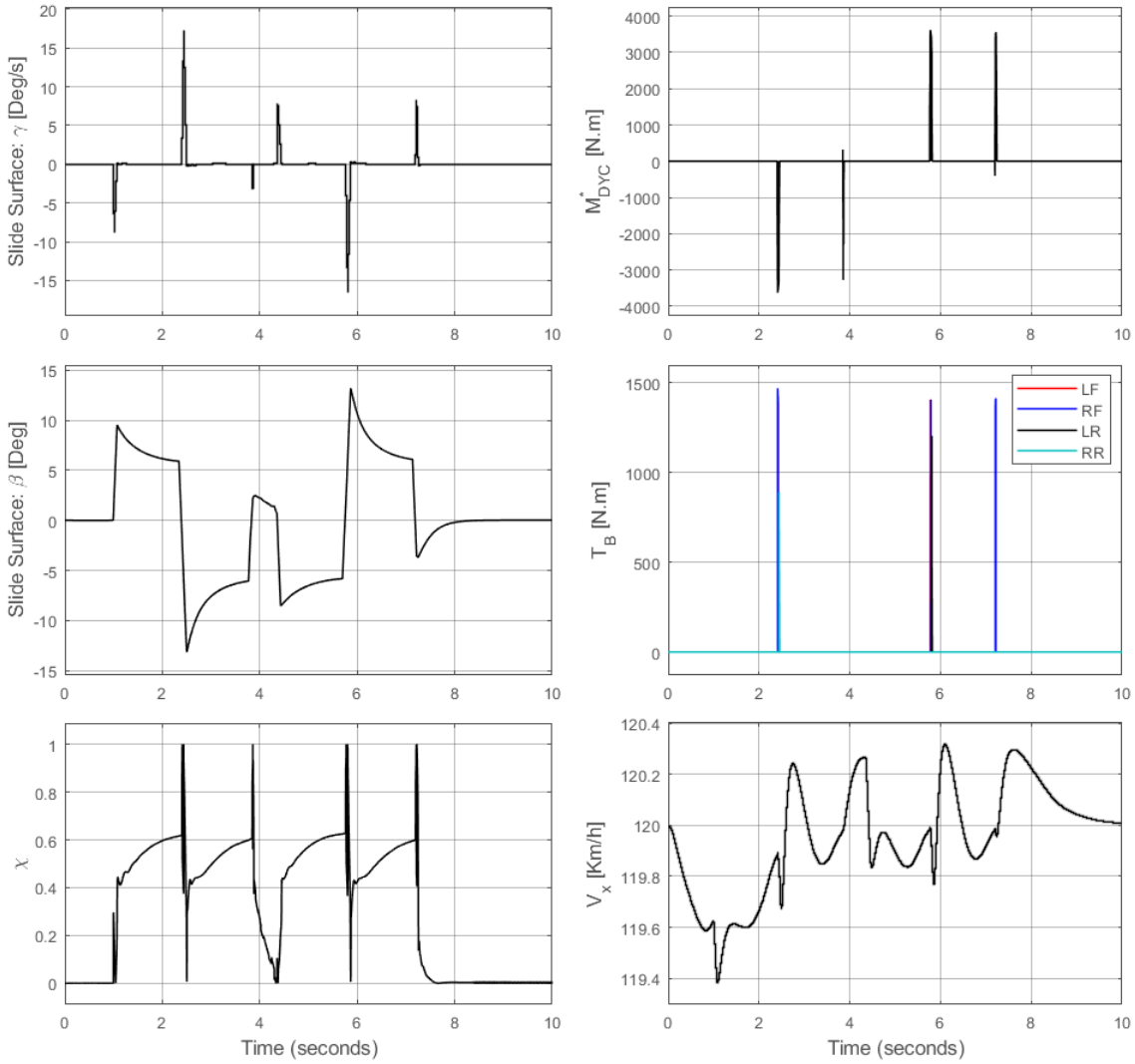

FIGURE 5.29: Case 1: DLC simulation results (2 of 2) Corrective moments and braking torques shown here are only calculated values inside the DYC controller, but the DYC did not affect the vehicle motion.

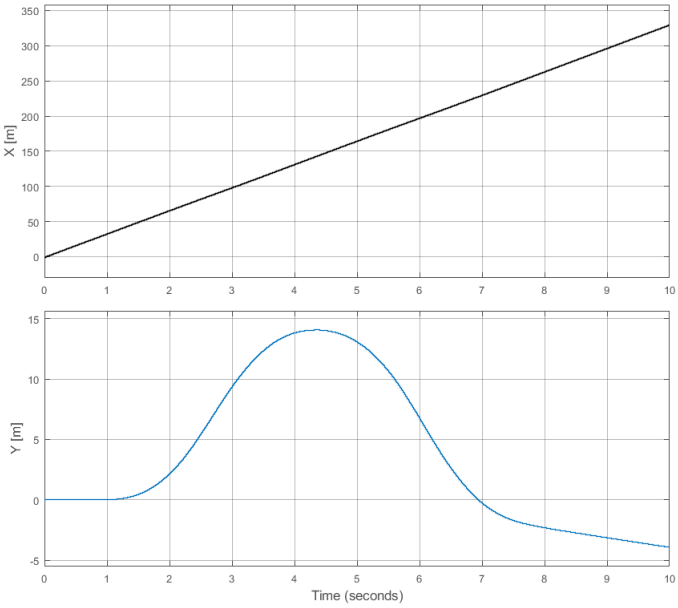

FIGURE 5.30: Case 1: Vehicle travel coordinates over time. The vehicle is heading slightly towards the right at the end of the simulation.

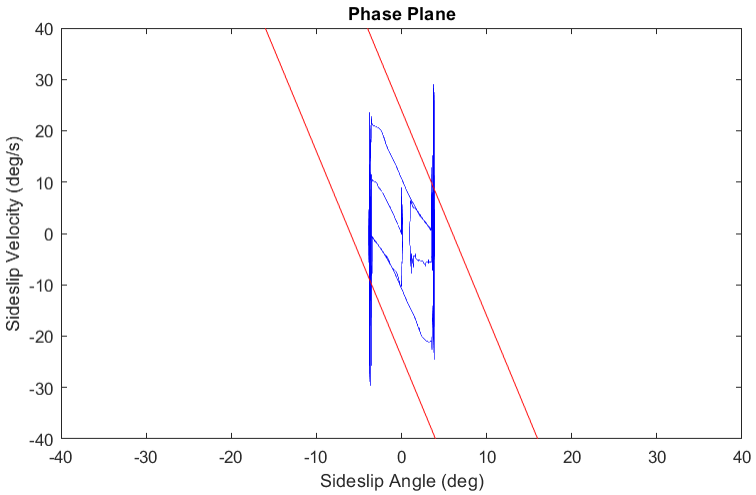

FIGURE 5.31: Case 1: Phase plane. Red lines are stable region boundaries. The DYC would have been activated once the vehicle state left the stable region, but only AFS generated the corrective steering wheel angle to bring the vehicle motion state back into the stable region.

5.4.2 Case 2: DLC test with a vehicle equipped with the DYC controller

During the case 2 simulation, the vehicle is equipped with the only DYC controller. The ρ is set to be zero during this run, similar to how it was set during the case 1 run. Figure 5.32 shows that the yaw rate of the vehicle does not match the desired value without the support of the AFS controller. This led the vehicle to travel towards the lateral direction at the end of the simulation, which shows that equipping the vehicle with only DYC does not provide good path following performance. However, it was not expected that the DYC will provide good handling performance since its primary goal is to maintain stability. This is also proven by the fact that the vehicle model with the DYC controller maintained its stability to finish the simulation without any major spinning out.

Figure 5.33 shows the intervention of the individual braking systems. The selection of individual wheels to be braked to provide the corrective yaw moment to control VSA is determined based on the yaw rate difference between simulated and desired values, vehicle steering direction and if the vehicle is in oversteer or understeer condition. The notation of the individual wheels is named so that the first letter implies left or right and the second letter means front or rear. It is observed that the corrective braking torques dropped the entrance speed of 120 km/h by almost 20 km/h within 4 seconds.

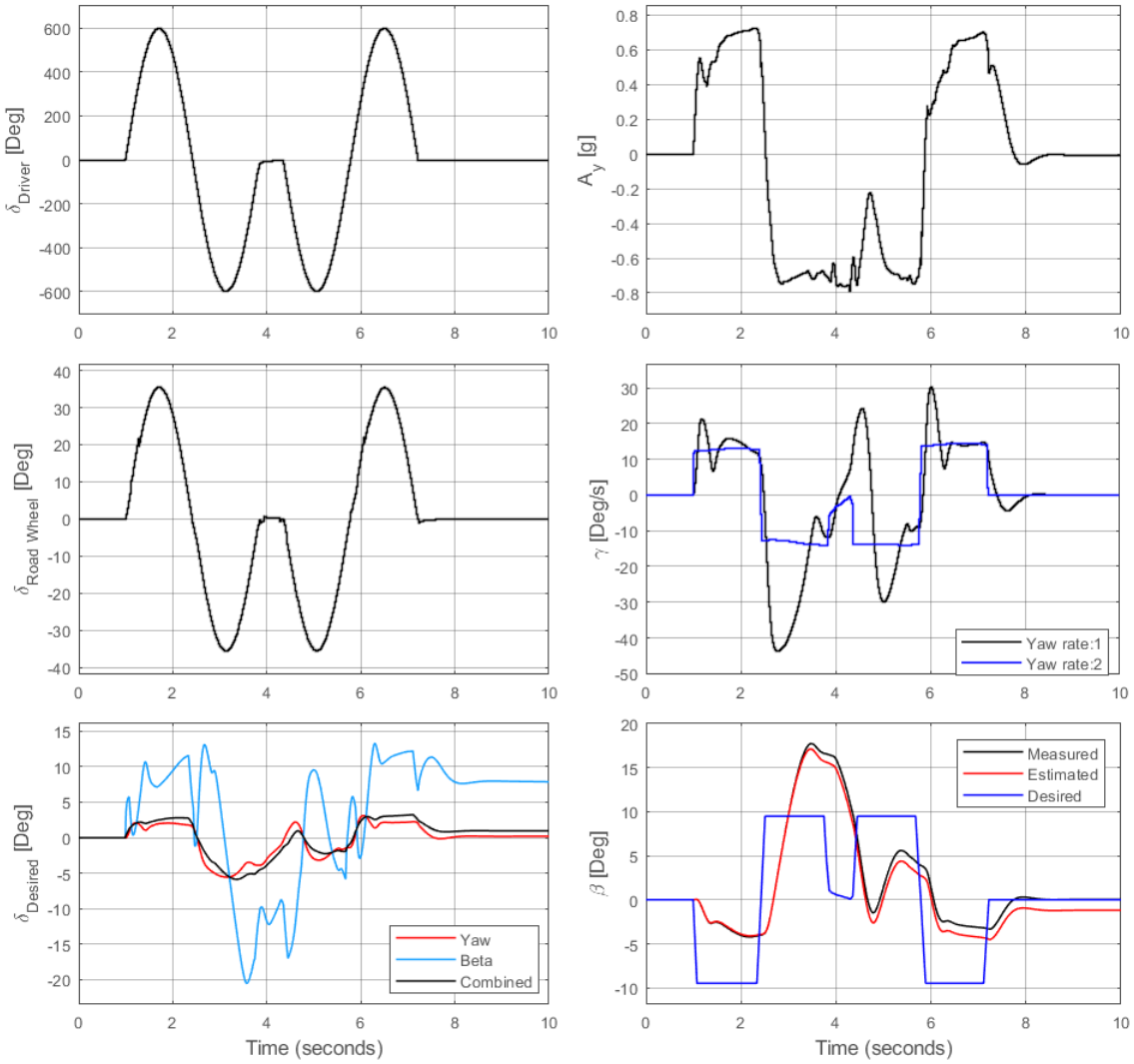

FIGURE 5.32: Case 2: DLC simulation results (1 of 2). The corrective wheel angle, δ_{desired} presented here do not affect the vehicle motion since the AFS controller is deactivated. Measured values are the simulated values from the virtual vehicle.

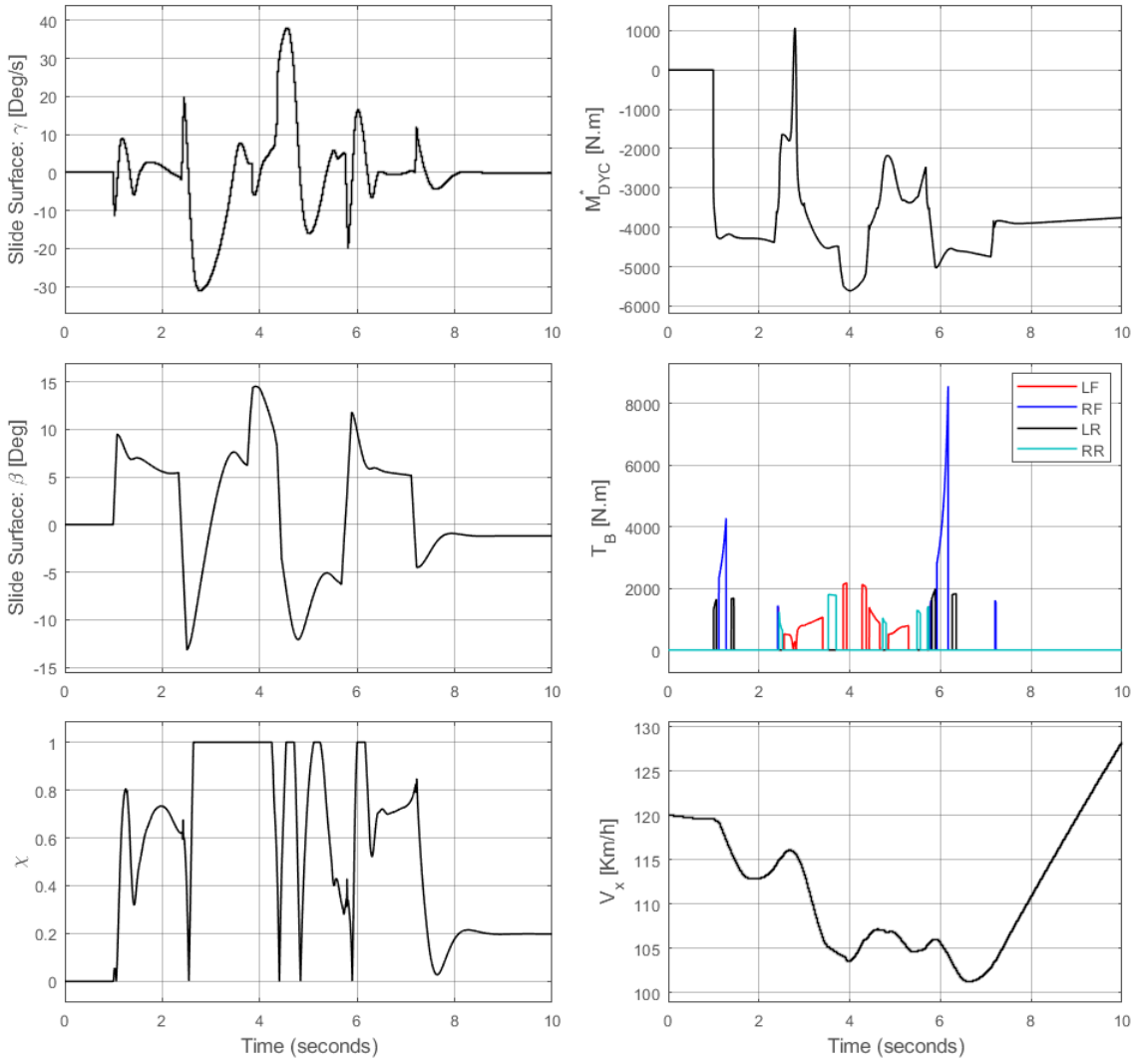

FIGURE 5.33: Case 2: DLC simulation results (2 of 2).

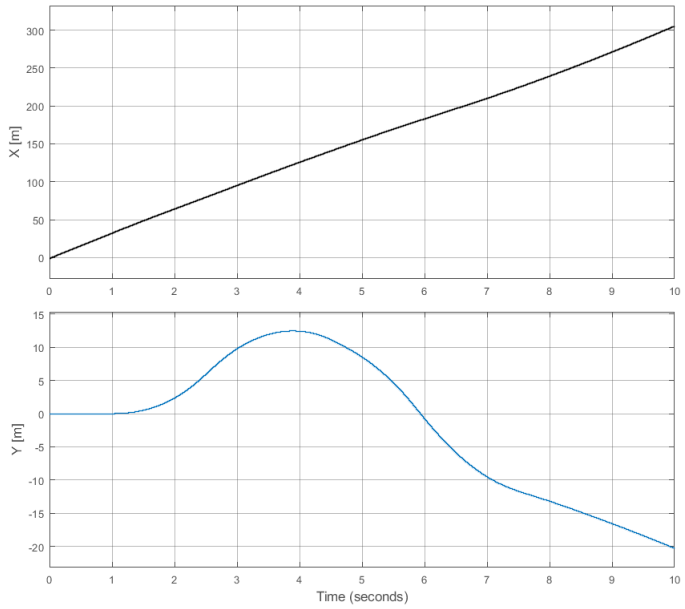

FIGURE 5.34: Case 2: Vehicle travel coordinates over time. The DYC controller did not provide good path following performance, but its primary goal is to keep the vehicle stable.

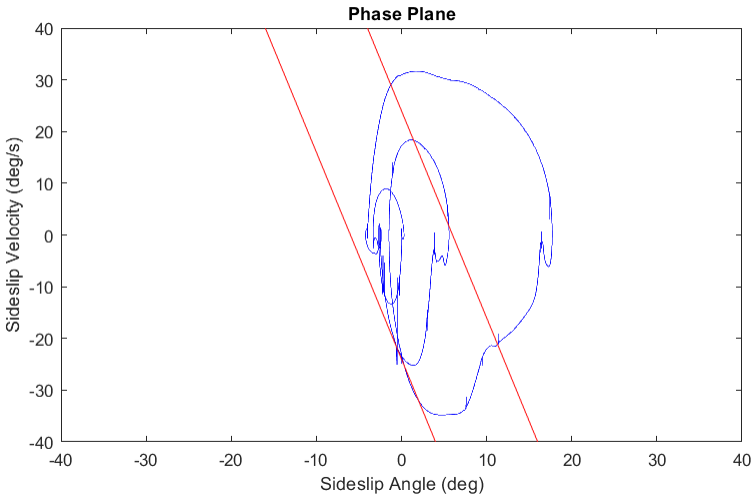

FIGURE 5.35: Case 2: Phase plane. Red lines are stable region boundaries. The DYC was activated when the state was outside the stable region.

5.4.3 Case 3: DLC test with a vehicle equipped with the IVDC controller (AFS+DYC)

During the third case, the AFS and DYC controllers are both activated using the rule-based integration scheme. The controller setting used here is identical to the one used in Section 5.1. Figure 5.36 shows that the yaw rate follows the desired value for the entire simulation. The corrective wheel angle shows very similar trends, compared to the first case. The VSA is always maintained within the boundaries of ±5°, while providing the good steer-ability. Braking torques are generated by the DYC controller when the vehicle motion state leaves the stable region. In case 3, these values all affected the vehicle motion in creating the corrective yaw moment to stabilize the vehicle. Figure 5.39 shows that the vehicle motion state is located within the stable region most of the time.

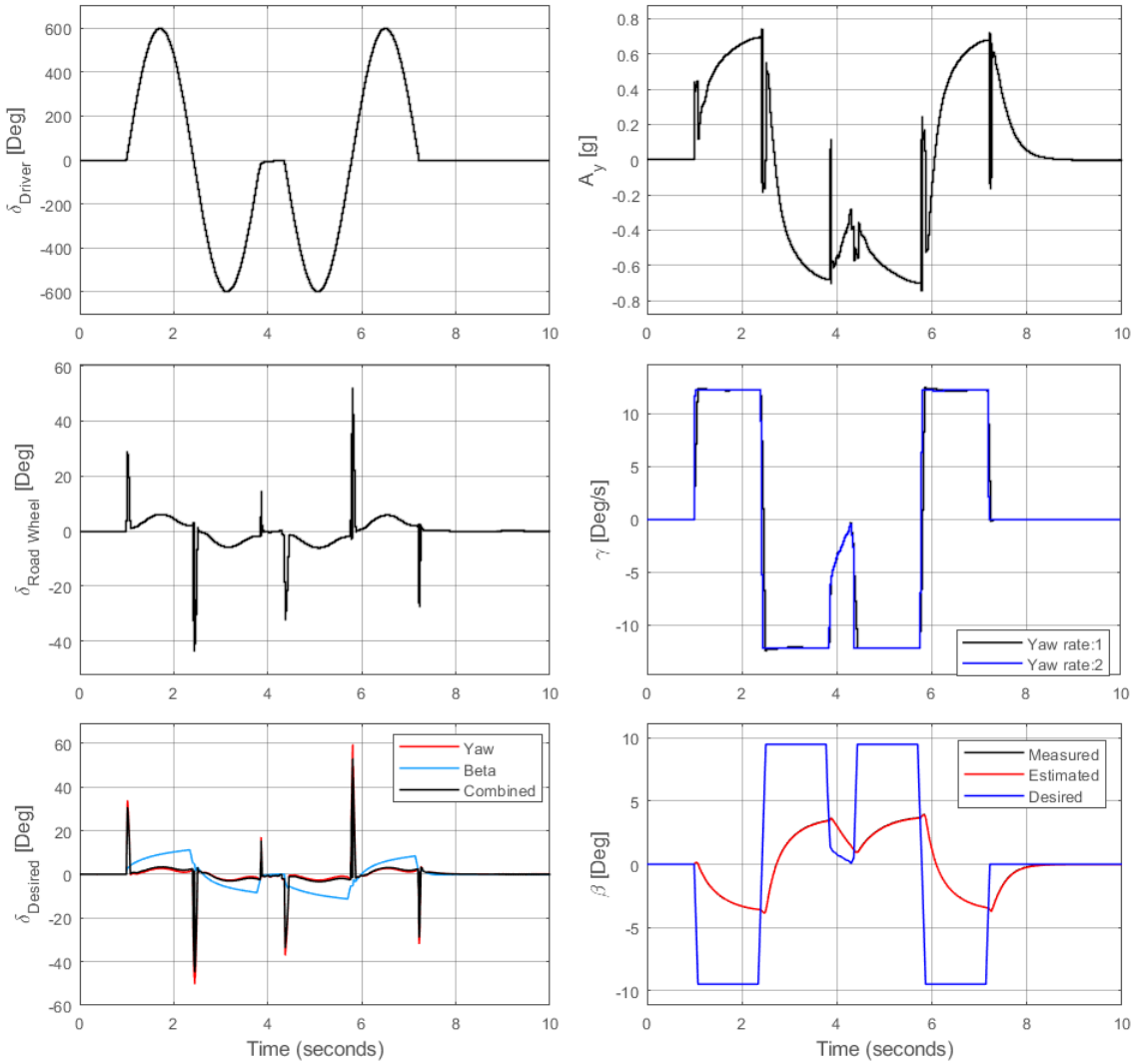

FIGURE 5.36: Case 3: DLC simulation results (1 of 2). Measured values are the simulated values from the virtual vehicle.

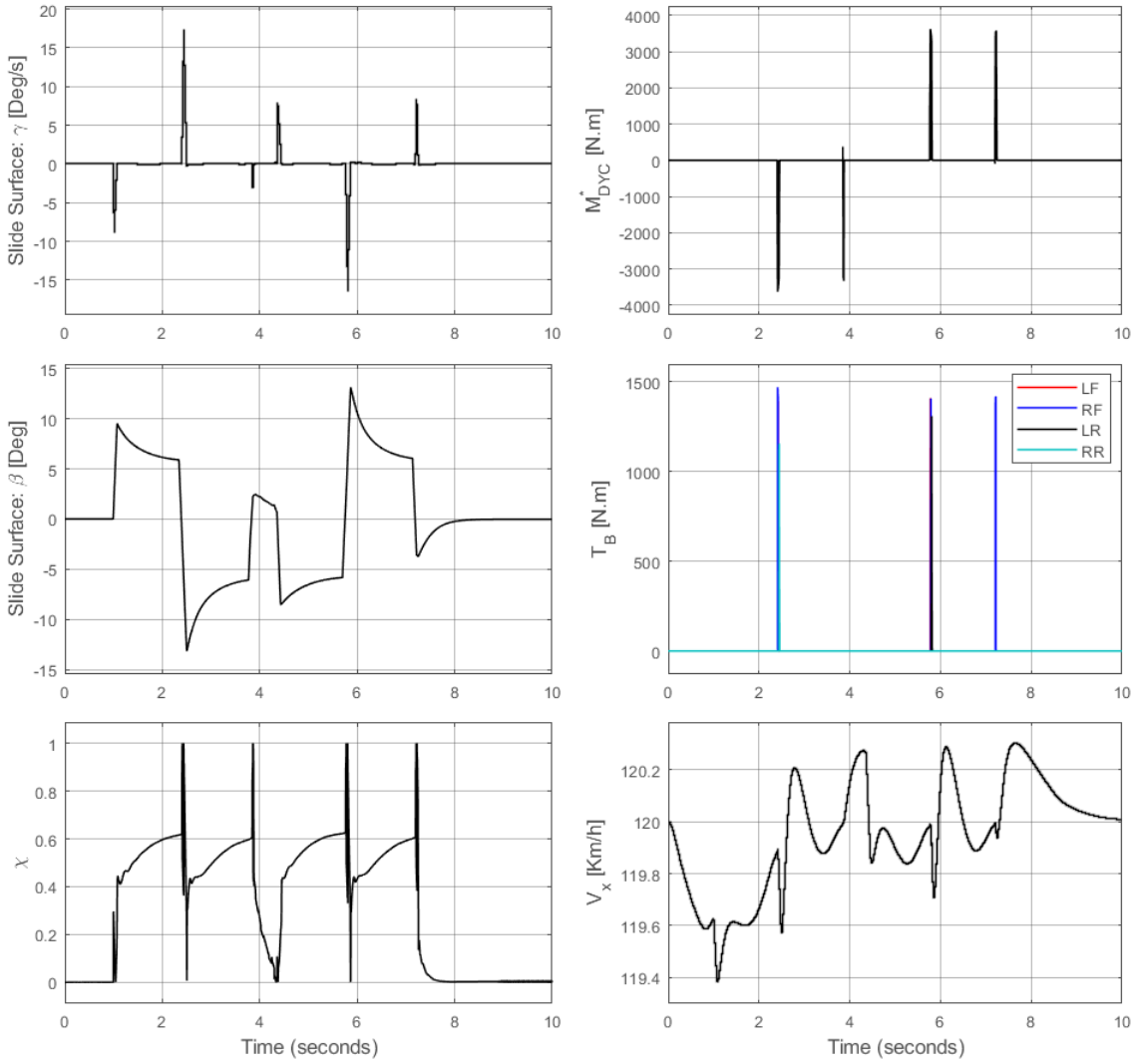

FIGURE 5.37: Case 3: DLC simulation results (2 of 2). Individual braking torques were generated shortly. The second corrective yaw moment peak from the M^{*}_{DYC} did not generate the braking torque at the same time since the yaw rate threshold of $5^{\circ}/s$ was not reached.

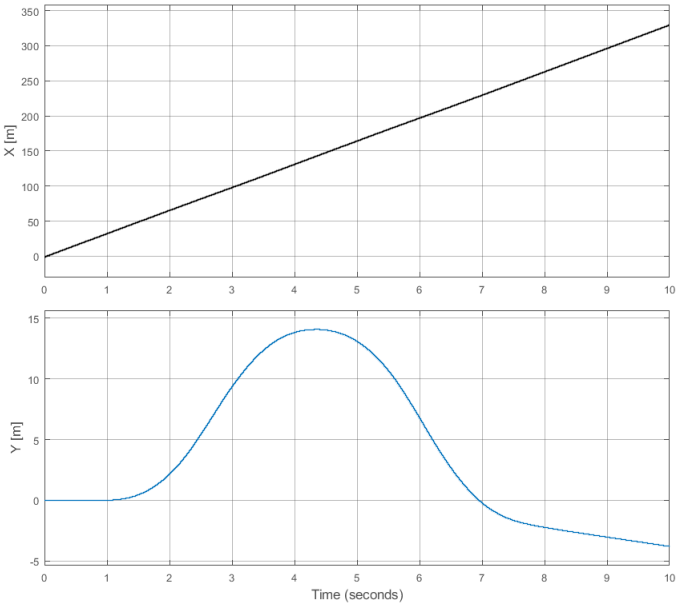

FIGURE 5.38: Case 3: Vehicle travel coordinates over time.

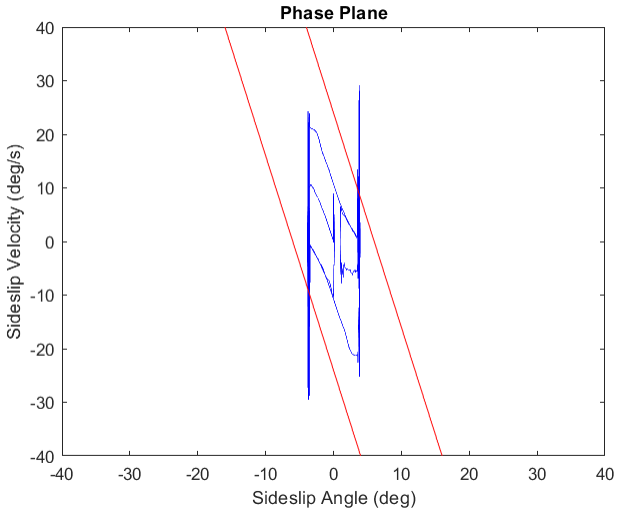

FIGURE 5.39: Case 3: Phase plane.

Table 5.3 shows the performance of the controllers in each case, assessed quantitatively by examining the RMSE of the yaw rate and VSA.

The reference vehicle model without the controller exhibited a very large yaw rate difference of 1648.5°/s, which caused the failure of the simulation, as the vehicle spun out. The accuracy of the estimator for the VSA and vehicle side slip velocity decreased significantly as the vehicle motion state becomes unstable.

Case 1 shows that the AFS provides good handling improvement on the vehicle motion. This was achieved by robust yaw rate tracking, which led to a very small yaw rate error; the RMSE of vehicle yaw rate is 1.5655°/s. The VSA was controlled so that it remains within the range where the vehicle still has steer-ability. The vehicle velocity was not substantially affected during the AFS-intervention, which led the average speed of the vehicle to remain at 119.9489 km/h.

Case 2 shows that the DYC provides good stabilizing performance, which prevented the vehicle from spinning out. This eventually enabled the simulation to finish on time, instead of failing due to spinning out. However, the DYC does not provide as good handling performance improvement as the AFS controller, which is related to the ability to follow the intended path. The handling performance is evaluated by the yaw rate tracking performance. The DYC controller showed greater RMSE of yaw rate, 10.6688°/s, compared to the one seen in case 1 with the AFS controller, 1.5655°/s. The VSA estimator showed a substantial error of 21.0674°. A noticeable difference between the simulated VSA and the estimated VSA can be observed when the vehicle stability index is high in Figure 5.32. Adopting the individual braking system as the only actuator to stabilize the vehicle resulted in the average longitudinal speed of the vehicle during the simulation showing a value of only 111.5858 km/h, lower than any other cases.

Case 3 shows that implementing both AFS and DYC provides good handling performance improvement, proven by the low RMSE of yaw rate, 1.5609°/s. In addition, the stability of the vehicle is well maintained by having a much smaller RMSE of VSA, 5.4740°, compared to the one observed in the reference vehicle without any controllers, 63.76090°. When the vehicle motion state left the stable region, it is confirmed that the differential braking system was actuated to provide better stability, as seen in Figure 5.37. However, the average longitudinal speed of the vehicle in this case was not decreased as much as it did when the vehicle was adopting the braking system only in case 2. While VSA is well maintained within the boundaries, calculated by the road wheel friction, the vehicle shows good traction, which leads to a good steer-ability. In this case, high lateral acceleration often means that the vehicle can exit corners quickly. Since cases 1 and 3 show a very good yaw rate tracking while maintaining the VSA within the boundaries between ±4°, higher lateral acceleration means that the vehicle has the capability to better avoid obstacles. The difference between lateral acceleration in case 1 and case 3 is very small, but case 3 shows a higher value.

TABLE 5.3: DLC test results comparison among different controller settings: only AFS activated, only DYC activated, both of AFS and DYC activated.

Test #	AFS, DYC	RMSE-γ (°/s)	RMSE-β (°)	RMSE-β Estimator (°)	RMSE-$\dot{\beta}$ Estimator (°/s)	$V_{x,avg}$ (km/h)	$a_{y,max}$ (g)
0	None	1648.5	63.7609	36.8698	94.8323	73.1863	0.7663
1	AFS	1.5655	5.4757	0.8065	5.5219	119.9489	0.7454
2	DYC	10.6688	6.2157	21.0674	3.0025	111.5858	0.7908
3	AFS, DYC	1.5609	5.4740	1.0067	6.2456	119.9489	0.7491

Chapter 6

Conclusions and Recommendations

6.1 Summary

In this thesis, a nonlinear full vehicle model in CarSim was developed to match the pre-validated 8 degrees of freedom (DOF) full vehicle model. Many more vehicle parameters are considered in commercial multi-body dynamics (MBD) software, CarSim. Therefore, two simulation tests (Constant steering input & Slowly increasing steering input) were performed to show how the steering ratio and the cornering stiffness of a vehicle can be chosen when the vehicle model becomes more complex. A modified benchmark controller that integrates active front steering system (AFS) and direct yaw moment control (DYC) was proposed for the integrated vehicle dynamics control (IVDC) controller. Three studies were done in the controller tuning process. The first study was done to solve the chattering issue, caused by the sign function in sliding mode control (SMC) strategy. The second study explored the effect of the controller tuning parameters, which caused undesired control outputs with excessive magnitudes. The third study during the controller tuning process explored the effect of linear coefficients for corrective steering angles to choose the optimal combination using an iterative approach. A new method of calculating the resultant corrective steering angle in the AFS controller, using the stability index, was proposed. One of main objectives was to ensure that the modified IVDC controller passes the ESC homologation process set by Federal Motor Vehicle Safety Standards (FMVSS) 126 and UN/ECE-R 13H. Various simulation tests were performed including the regulation test (SwD) and more severe maneuvering test to check the controller's performance in stabilizing the lateral dynamics of the vehicle model. Additional study is done in Chapter 5 to explore which target vehicle side slip angle (VSA) is more suitable for the vehicle stability controller design.

6.2 Conclusions

The following conclusions are drawn from the results of the co-simulation tests:

- Using the exponential function successfully resolved the chattering issues caused by the sign function involved in sliding mode control strategies. The saturation function showed

improvement in reducing the chattering issues; however, the saturation function still caused the chattering issues during the simulation, which led to the simulation failure. The saturation function showed high sensitivity to the amplitudes of the input signal, which led to the conclusion that its sensitive characteristic is not desired in the vehicle stability controller design. In addition, the exponential function has a coefficient that can be tuned for the suitable sensitivity for different dynamic systems.

- When controller tuning parameters were studied, the $\alpha_{\beta}^{''}$ tuning parameter was identified as causing overly aggressive correction outputs from the original design, which destabilized the vehicle before the tuning process. The AFS controller successfully generated corrective steering angles to improve the handling performance of the vehicle if the parameters are properly tuned.
- When using an iterative method to evaluate the effect of fixed coefficients for yaw rate- and VSA-controlled steering wheel angle, increasing w_1 to receive more of the yaw rate-controlled wheel steering angle than the VSA-controlled wheel steering angle improved the vehicle response. The yaw rate tracking error was significantly reduced as w_1 increased. The vehicle model with improved yaw rate tracking performance also showed significantly improved VSA, even though the VSA standalone controller was deactivated.
- Increasing w_1 improved the yaw rate tracking very efficiently. However, it can cause unrealistically large steering inputs from trying to track the desired yaw rate too closely.
- The ESC homologation process defined by FMVSS 126 and UN/ECE-R 13H was employed to test the nonlinear full vehicle model in CarSim equipped with the IVDC controller in MATLAB/Simulink. The vehicle model equipped with the IVDC controller passes the ESC homologation standards by recovering the yaw rate after COS very quickly. To pass the ESC regulation performance requirement, the ratio between the yaw rate measured 1 second after the COS and the peak yaw rate is 35%. The vehicle model with the IVDC controller achieved 0.0979%. The vehicle model with the IVDC controller also passed the responsiveness test by having a lateral displacement of 2.313 m at 1.07 seconds after COS, which is greater than the minimum value of 1.83 m.
- The steady state VSA value predicted by the linear bicycle model was proven to be more suitable as the target VSA value for the AFS design, as compared to zero VSA. The controlled vehicle with target VSA of zero prevented a vehicle from turning as the driver intended, as the controller attempts to reduce VSA by having as little maneuver as possible. However, different control outcomes can be expected when the DYC is activated with zero VSA as the control target.
- The proposed variable control effort distribution method using the stability index χ in the AFS controller design does not outperform the fixed linear combination of two coefficients for yaw rate- and VSA-controlled steering wheel angles. The proposed method successfully

changed the control objectives during the simulation, depending on the vehicle stability. However, handling performance, measured by the yaw rate tracking error, and stability, measured by the VSA tracking error, were both outperformed by the fixed linear combination method used to compute the resultant corrective steering wheel angle. The addition of a non-linear variable in the controller design and poor performance of the VSA standalone controller in the AFS were found to be main causes of the results. Therefore, better performance can be expected by improving the VSA standalone controller.

- Individual performance and functionality of the AFS controller and DYC controller were confirmed by performing a DLC maneuver test with very aggressive steering amplitude (600°). The handling performance was significantly improved by employing the AFS controller, resulting in very low yaw rate tracking error. The DYC successfully stabilized the vehicle from spinning out by employing the differential braking systems to generate the corrective yaw rate. However, yaw rate tracking error was greater with only the DYC controller in comparison with only the AFS controller. The average vehicle travel speed was reduced when only DYC was employed to stabilize the vehicle. This drawback was solved when both AFS and DYC were activated in the IVDC controller. This maintained the average speed of the vehicle during simulation while tracking the vehicle yaw rate very close to the desired values.

6.3 Recommendations

Some recommendations are made for the current research project in the future:

- The DYC controller can be updated to employ the ABS to prevent the brakes from locking, which can occur in the current controller when generating excessive braking torques to correct the vehicle lateral motion.
- The current IVDC controller as the ESC controller can be more sophisticated for vehicle dynamics control research purpose if both ABS and TCS controllers are implemented.
- The IVDC contrller can predict nonlinear vehicle behaviour by implementing vehicle components with nonlinear behaviour, instead of the linear bicycle model. For example, a look up table for components with nonlinearity, such as an anti-roll bar, can be implemented since it affects the nonlinear steady state slip angle.
- The vehicle model can be improved by adopting the validated vehicle data, such as testing data for the tires, aerodynamics, suspension, and more. Testing data can be obtained and more sophisticated vehicle design can be done in ADAMS Car in the future. Vehicle models are designed in CarSim based on the template with parameter tuning. However, ADAMS Car gives users more flexibility in the vehicle modelling process since the vehicle topology can be chosen completely by the user in ADAMS Car.

- The current tire model in this project does not show any lags during the change of its dynamic behaviour. This can be improved by implementing the transient response, obtained from multiple simulation tests or a physical test. Implementation of this will improve the simulation results to be more realistic by getting rid of the high frequency wheel angle corrections.
- The co-simulation test data can be validated by on-road experiments.
- The idea of varying the control effort between two control objectives in the AFS controller can potentially be improved to be better than the current method of combining two control outputs by using fixed coefficients, but another method must be proposed. An improved VSA standalone controller design can be one of many options.
- Exploring the target VSA that can be adopted in any vehicle stability controller design may be beneficial in improving the controller's stability performance.

6.4 Contributions (Engineering Significance)

This thesis explored the benchmark IVDC controller design. The benchmark IVDC controller was improved by exploring the effect of controller tuning parameters; this is not available in the literature. In addition, the effect of changing the coefficients for each standalone controller's corrective wheel steering angles was explored. It was observed that the yaw rate tracking was improved significantly more than the VSA tracking was improved by changing the coefficients in similar way. The yaw rate threshold filter was added to the original design, which prevented the DYC controller from intervening during undesired situations, such as when the yaw rate error was very low, when minimal corrective outputs are required.

This research project also described which vehicle parameters must be considered to match the benchmark vehicle model provided that a simple vehicle model is re-designed in a sophisticated MBD tool.

The proposed variable control effort distribution method of calculating the resultant corrective steering wheel angle was shown to successfully change its control effort distribution dynamically. However, it did not outperform the traditional method of using fixed coefficients. The drawbacks of this proposed method can be improved by designing an improved VSA standalone controller. This idea can lead to improved control design for vehicle dynamics controllers that have multiple control objectives for a single control output.

References

[1] W. O. Schiehlen, “Simulation based design of automotive systems”, *Concurrent Engineering: Tools and Technologies for Mechanical System Design*, Springer, 1993, pp. 303–337.

[2] N Hampl, “Advanced simulation techniques in vehicle noise and vibration refinement”, *Vehicle Noise and Vibration Refinement*, Elsevier, 2010, pp. 174–188.

[3] M. Blundell and D. Harty, “Multibody systems simulation software”, *The Multibody Systems Approach to Vehicle Dynamics*, M. Blundell and D. Harty, Eds., Oxford: Butterworth-Heinemann, 2004, ch. 3, pp. 75 –130, ISBN: 978-0-7506-5112-7.

[4] M. Software. (2020). Automotive industry, (visited on 05/14/2020).

[5] “Sae international surface vehicle information report "automotive stability enhancement systems", sae standard j2564”, Society of Automotive Engineers (SAE), J2564 Standard, Nov. 2017.

[6] J. H. Park and C. Y. Kim, “Wheel slip control in traction control system for vehicle stability”, *Vehicle system dynamics*, vol. 31, no. 4, pp. 263–278, 1999.

[7] R. Matsumoto, *Vehicle traction control system for preventing vehicle turnover on curves and turns*, US Patent 4,976,330, 1990.

[8] E. Liebemann, K Meder, J Schuh, and G Nenninger, “Safety and performance enhancement: The bosch electronic stability control (esp)”, SAE Technical Paper, Tech. Rep., 2004.

[9] G. Chen, C. Zong, and X. Guo, “Traction control logic based on extended kalman filter for omni-directional electric vehicle”, SAE Technical Paper, Tech. Rep., 2012.

[10] S. Ghosh, A. Deb, M. Mahala, M. Tanbakuchi, and M. Makowski, “Active yaw control of a vehicle using a fuzzy logic algorithm”, SAE Technical Paper, Tech. Rep., 2012.

[11] Z. Jin, L. Zhang, J. Zhang, and A. Khajepour, “Stability and optimised h-infinity control of tripped and untripped vehicle rollover”, *Vehicle System Dynamics*, vol. 54, no. 10, pp. 1405–1427, 2016.

[12] I. E. Mousavinejad, Y. Zhu, and L. Vlacic, “Control strategies for improving ground vehicle stability: State-of-the-art review”, *2015 10th Asian Control Conference (ASCC)*, IEEE, 2015, pp. 1–8.

[13] A. Erke, “Effects of electronic stability control (esc) on accidents: A review of empirical evidence”, *Accident Analysis & Prevention*, vol. 40, no. 1, pp. 167–173, 2008.

[14] A. Lie, C. Tingvall, M. Krafft, and A. Kullgren, “The effectiveness of electronic stability control (esc) in reducing real life crashes and injuries”, *Traffic Injury Prevention*, vol. 7, no. 1, pp. 38–43, 2006.

[15] "Federal motor vehicle safety standard (fmvss) "electronic stability control systems (esc)", fmvss no.126", National Highway Traffic Safety Administration (NHTSA), FMVSS 126, Mar. 2007.

[16] C. Gomes, C. Thule, D. Broman, P. G. Larsen, and H. Vangheluwe, "Co-simulation: State of the art", *arXiv preprint arXiv:1702.00686*, 2017.

[17] T. Eriksson, "Co-simulation of full vehicle model in adams and anti-lock brake system model in simulink", *Unpublished master's thesis. Chalmers University of Technology.*, 2014.

[18] E. Mousavinejad, Q.-L. Han, F. Yang, Y. Zhu, and L. Vlacic, "Integrated control of ground vehicles dynamics via advanced terminal sliding mode control", *Vehicle System Dynamics*, vol. 55, no. 2, pp. 268–294, 2017.

[19] B. Minaker, *Fundamentals of Vehicle Dynamics and Modelling: A Textbook for Engineers With Illustrations and Examples*, ser. Automotive Series. Wiley, 2019, ISBN: 9781118980095.

[20] H. B. Pacejka, "Tire and vehicle dynamics (third edition)", *Tire and Vehicle Dynamics (Third Edition)*, H. B. Pacejka, Ed., Third Edition, Oxford: Butterworth-Heinemann, 2012, p. iv, ISBN: 978-0-08-097016-5.

[21] R. Rajamani, *Vehicle dynamics and control*. Springer Science & Business Media, 2011.

[22] M. Gipser, "Adams/ftire-a tire model for ride & durability simulations", *ADAMS User's Conference Tokyo*, 2000.

[23] M Fitzgerald, "Lane departure warning boots anti-rollover protection", *Strategy Analytics in Automotive DesignLine.*, vol. 405845, 2005.

[24] S. Anwar, "Generalized predictive control of yaw dynamics of a hybrid brake-by-wire equipped vehicle", *Mechatronics*, vol. 15, no. 9, pp. 1089–1108, 2005.

[25] W. Cho, J. Yoon, J. Kim, J. Hur, and K. Yi, "An investigation into unified chassis control scheme for optimised vehicle stability and manoeuvrability", *Vehicle System Dynamics*, vol. 46, no. S1, pp. 87–105, 2008.

[26] I. Mousavinejad and R. Kazemi, "Variable structure controller design for steer-by-wire system of a passenger car", *Journal of Mechanical Science and Technology*, vol. 28, no. 8, pp. 3285–3299, 2014.

[27] R. N. Jazar, *Vehicle dynamics: theory and application*. Springer, 2017.

[28] Y. Håland, "The evolution of the three point seat belt from yesterday to tomorrow", *IRCOBI Conference, Madrid*, 2006.

[29] K. Udugu, V. R. Saddala, and S. Lingan, "Active and passive safety: An overview on establishing safety assessment standards in india", *SAE Technical Paper*, SAE International, Feb. 2016.

[30] A. Jarašūniene and G. Jakubauskas, "Improvement of road safety using passive and active intelligent vehicle safety systems", *Transport*, vol. 22, no. 4, pp. 284–289, 2007.

[31] SAE, *Automotive stability enhancement systems*, J2564, SAE, Nov. 2017.

[32] R. Emig, H Goebels, and H. Schramm, "Antilock braking systems (abs) for commercial vehicles-status 1990 and future prospects", SAE Technical Paper, Tech. Rep., 1990.

[33] M. Schinkel and K. Hunt, "Anti-lock braking control using a sliding mode like approach", *Proceedings of the 2002 American Control Conference (IEEE Cat. No. CH37301)*, IEEE, vol. 3, 2002, pp. 2386–2391.

[34] Y. S. Kueon and J. S. Bedi, "Fuzzy-neural-sliding mode controller and its applications to the vehicle anti-lock braking systems", *Proceedings IEEE Conference on Industrial Automation and Control Emerging Technology Applications*, 1995, pp. 391–398.

[35] S. Rajendran, S. K. Spurgeon, G. Tsampardoukas, and R. Hampson, "Estimation of road frictional force and wheel slip for effective antilock braking system (abs) control", *International Journal of Robust and Nonlinear Control*, vol. 29, no. 3, pp. 736–765, 2019.

[36] M. Velardocchia and A. Sorniotti, "Hardware-in-the-loop to evaluate active braking systems performance", SAE Technical Paper, Tech. Rep., 2005.

[37] C. Zetterqvist, "Powertrain modelling and control algorithms for traction control", 2007.

[38] H. Igata, K. Uchida, T. Nakatomi, and K. Komatsuzaki, "Development of new control methods to improve response of throttle type traction control system", SAE Technical Paper, Tech. Rep., 1992.

[39] D. D. Hoffman, "The corvette acceleration slip regulation (asr) application with preloaded limited slip differential", SAE Technical Paper, Tech. Rep., 1992.

[40] A. T. Van Zanten, R. Erhardt, and G. Pfaff, "Vdc, the vehicle dynamics control system of bosch", *SAE transactions*, pp. 1419–1436, 1995.

[41] H. Leffler, "The brake system of the new 7 series bmw with electronic brake and wheel slip control", SAE Technical Paper, Tech. Rep., 1995.

[42] F. Gustafsson, "Slip-based tire-road friction estimation", *Automatica*, vol. 33, no. 6, pp. 1087–1099, 1997.

[43] A. Eidehall, "Tracking and threat assessment for automotive collision avoidance", PhD thesis, Institutionen för systemteknik, 2007.

[44] P Khatun, C. M. Bingham, N. Schofield, and P. Mellor, "Application of fuzzy control algorithms for electric vehicle antilock braking/traction control systems", *IEEE Transactions on Vehicular Technology*, vol. 52, no. 5, pp. 1356–1364, 2003.

[45] P. M. de Koker, J Gouws, and L Pretorius, "Fuzzy control algorithm for automotive traction control systems", *Proceedings of 8th Mediterranean Electrotechnical Conference on Industrial Applications in Power Systems, Computer Science and Telecommunications (MELECON 96)*, IEEE, vol. 1, 1996, pp. 226–229.

[46] K. Huh, D. Hong, P. Yoon, H.-J. Kang, and I. Hwang, "Robust wheel-slip control for brake-by-wire systems", SAE Technical Paper, Tech. Rep., 2005.

[47] S. Kang, M. Yoon, and M. Sunwoo, "Traction control using a throttle valve based on sliding mode control and load torque estimation", *Proceedings of the Institution of Mechanical Engineers, Part D: Journal of Automobile Engineering*, vol. 219, no. 5, pp. 645–653, 2005.

[48] Y Papelis, T. Brown, G. Watson, D. Holtz, and W. Pan, "Study of esc assisted driver performance using a driving simulator", *Document ID*, no. 04, 2004.

[49] J. He, D. A. Crolla, M. Levesley, and W. Manning, "Coordination of active steering, driveline, and braking for integrated vehicle dynamics control", *Proceedings of the Institution of Mechanical Engineers, Part D: Journal of Automobile Engineering*, vol. 220, no. 10, pp. 1401–1420, 2006.

[50] M Gadola, D Chindamo, M Romano, and F. Padula, "Development and validation of a kalman filter-based model for vehicle slip angle estimation", *Vehicle System Dynamics*, vol. 52, no. 1, pp. 68–84, 2014.

[51] D. Chindamo, B. Lenzo, and M. Gadola, "On the vehicle sideslip angle estimation: A literature review of methods, models, and innovations", *applied sciences*, vol. 8, no. 3, p. 355, 2018.

[52] A. Tuononen, T. Lehtonen, and M. Juhala, "Estimation of tyre cornering stiffness from vehicle measurements", *FISITA 2006 World Automotive Congress*, 2006, p. 9.

[53] Z. Palmer. (). 2021 mercedes-benz s-class gets rear-axle steering and trick new airbag tech. Auto Blog, Ed.

[54] M. Aripin, Y. Md Sam, K. A. Danapalasingam, K. Peng, N Hamzah, and M. Ismail, "A review of active yaw control system for vehicle handling and stability enhancement", *International journal of vehicular technology*, vol. 2014, 2014.

[55] M Abe, "Trends of intelligent vehicle dynamics controls and their future", *NTN Technical Review*, vol. 81, pp. 2–10, 2013.

[56] M Selby, W. Manning, M. Brown, and D. Crolla, "A comparison of the relative benefits of active front steering and active rear steering when coordinated with direct yaw moment control", *Proceedings of ASME Int. Mechanical Engineering Congress and Exposition*, 2001, pp. 1–6.

[57] L. Yang and J. Yang, "Nonsingular fast terminal sliding-mode control for nonlinear dynamical systems", *International Journal of Robust and Nonlinear Control*, vol. 21, no. 16, pp. 1865–1879, 2011.

[58] S Khoo, L Xie, and Z.-h. Man, "Integral terminal sliding mode cooperative control of multi-robot networks", *2009 IEEE/ASME International Conference on Advanced Intelligent Mechatronics*, IEEE, 2009, pp. 969–973.

[59] I. E. Mousavinejad, Y. Zhu, and L. Vlacic, "Nonsingular fast terminal sliding mode control approach to front wheel subsystem of steer-by-wire system", *2015 5th Australian Control Conference (AUCC)*, IEEE, 2015, pp. 164–169.

[60] S. Li and L. He, "Co-simulation study of vehicle esp system based on adams and matlab.", *JSW*, vol. 6, no. 5, pp. 866–872, 2011.

[61] A. T. Van Zanten, "Bosch esp systems: 5 years of experience", *SAE transactions*, pp. 428–436, 2000.

[62] H. T. Smakman, "Functional integration of slip control with active suspension for improved lateral vehicle dynamics", 2000.

[63] S. Inagaki, I. Kushiro, and M. Yamamoto, "Analysis on vehicle stability in critical cornering using phase-plane method", *Jsae Review*, vol. 2, no. 16, p. 216, 1995.

[64] M. A. Selby, "Intelligent vehicle motion control", PhD thesis, University of Leeds, 2003.

[65] "Uniform provisions concerning the approval of passenger cars with regard to electronic stability control (esc) systems.", United Nations (UN), Tech. Rep., Jan. 2017.

[66] A. Lutz, B. Schick, H. Holzmann, M. Kochem, H. Meyer-Tuve, O. Lange, Y. Mao, and G. Tosolin, "Simulation methods supporting homologation of electronic stability control in vehicle variants", *Vehicle system dynamics*, vol. 55, no. 10, pp. 1432–1497, 2017.

Appendix A

MATLAB File for the IVDC Controller

```
%% Input
mu= 0.90;
%% Vehicle Parameters
m_u= 1300;    %m(unladen)[kg]
lf= 1.2247; %a(unladen)[m]
lr= 1.4373; %b(unladen)[m]
d=1.4376;    %Wheel Track Width[m]
Izz_u= 1808.8;%Vehicle yaw moment of inertia[kg.m^2]
Rw=0.285;     %Effective Wheel Rolling Radius[m]
Cf_avg=40000; %N/rad
Cr_avg=40000; %N/rad
ku=m_u*((lr*Cr_avg-lf*Cf_avg)/(2*Cf_avg*Cr_avg*(lf+lr)));
%% UNLADEN & DRY ROAD
m=m_u; Izz=Izz_u;
%% Calculated Variables
kmh_to_ms=1000/3600;
rad_to_deg=180/pi;
deg_to_rad=1/rad_to_deg;
steering_ratio=1/18.4;
%% Controllers Parameters
    chatter_b=100;        % To get rid of chattering: e*bs -1 / e^bs +1
%AFS - Yaw
    alpha_d_yawangle= 2.1;  %
    gamma_yawangle_1=1.305; %
    gamma_yawangle_2=1.285; %
    beta_d_yawangle= 0.009; %
    k_d_yawangle_1=0.001;   %
    k_d_yawangle_2=1.5;     %
%AFS - Sideslip
    alpha_dd_beta= 1.5;     %Original: 50(must be +)
    beta_dd_beta= 0.045;    %
    gamma_dd_beta= 0.6;     % (must  be 0< <1)
    k_dd_beta= 0.05;        %
%DYC - Sideslip
    alpha_d_beta=2.1;       %
    gamma_beta_1=1.305;     %
    gamma_beta_2=1.01;     %original: 1.285
    beta_d_beta=1.2;        %
    k_d_beta_1=1.6;         %
    k_d_beta_2=1;         %   Original: 1.5
```

Figure A.1: IVDC controller setup file in MATLAB. This .m file must be run prior to the co-simulation so that all blocks of the IVDC controller in Simulink can use the corresponding values

Appendix B

Block Diagrams

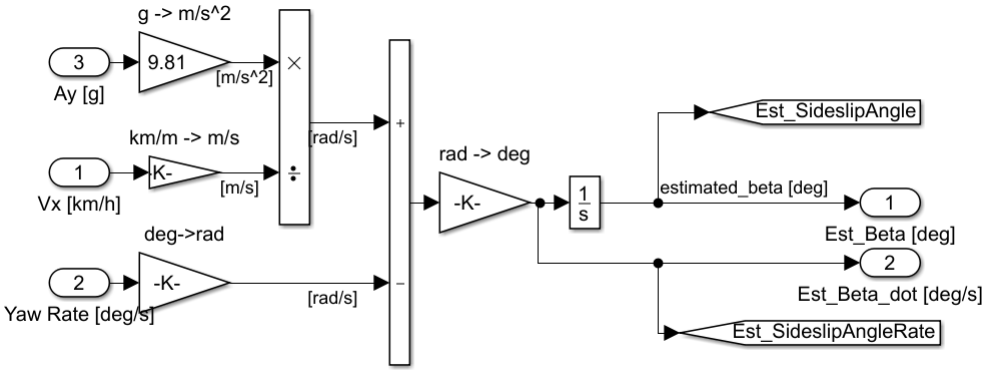

FIGURE B.1: Structure of the VSA and side slip velocity estimator.

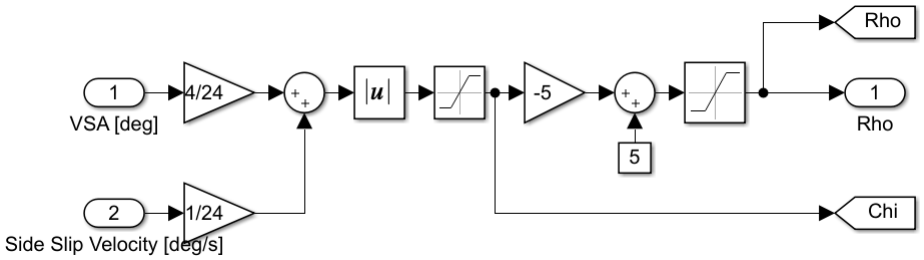

FIGURE B.2: Structure of the phase plane where the stable region and the adaptation gain is calculated

.

As seen in Figure B.3, the differences between the actual and desired values of VSA and vehicle yaw rate are calculated to be used in the standalone controllers.

Differential braking function in MATLAB is used to determine the magnitude of the braking torque and the corresponding wheel to be braked as seen in Figure B.9. The MATLAB function (dfbrk) can be found in Appendix C

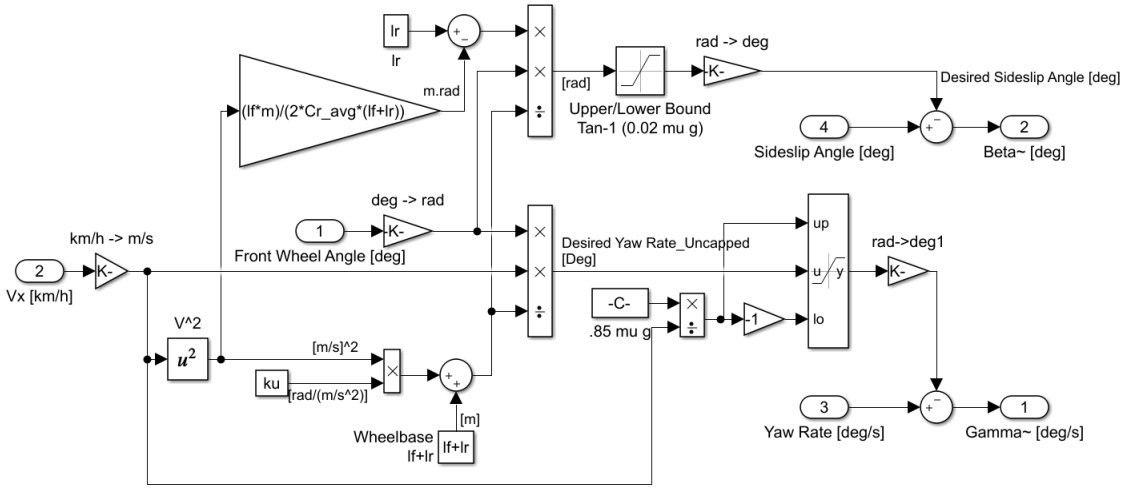

Figure B.3: Structure of the desired yaw rate and desired VSA generator.

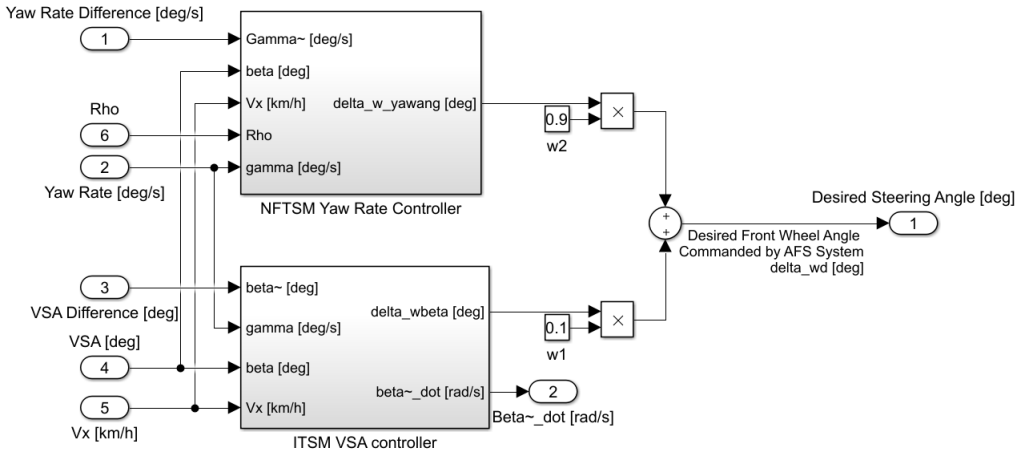

Figure B.4: Structure of the AFS controller.

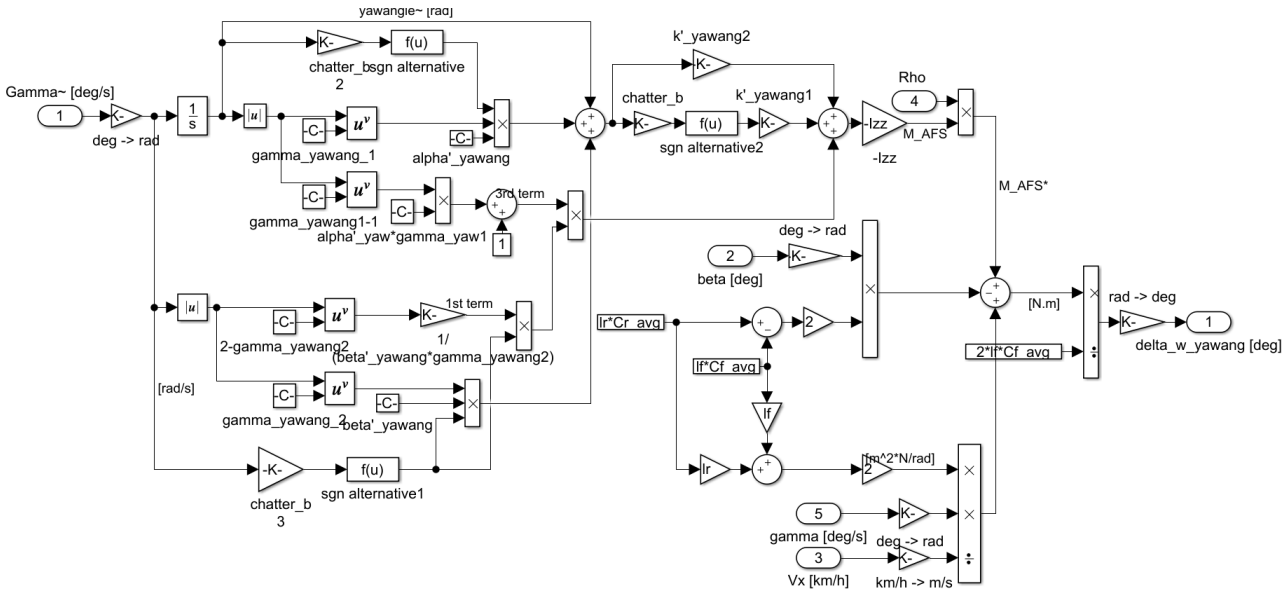

FIGURE B.5: Structure of the yaw rate controller part of the AFS controller using NFTSM control strategy. Adaptation gain is used to replace the M_{AFS}.

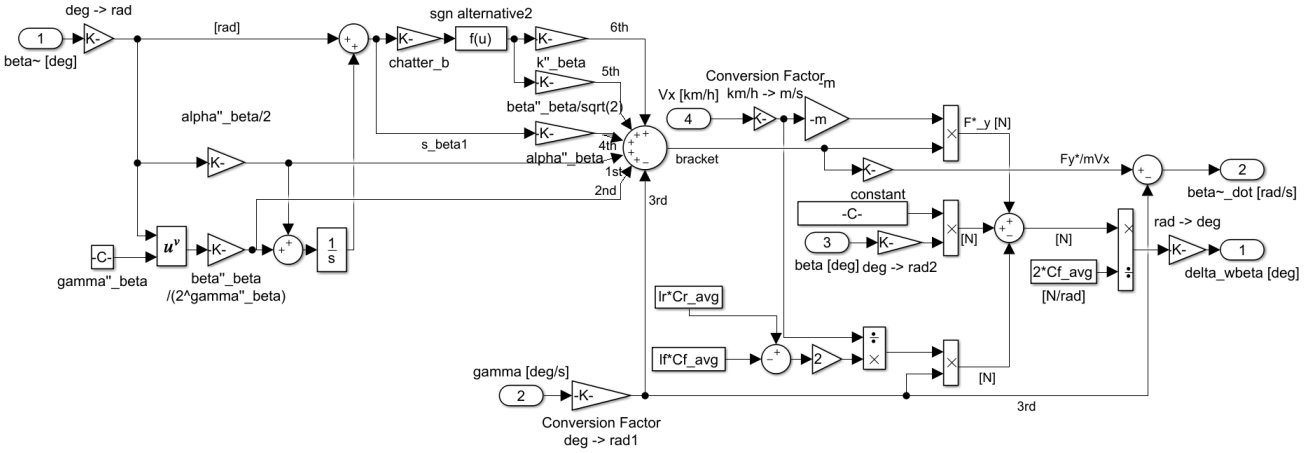

FIGURE B.6: Structure of the VSA controller part of the AFS controller using ITSM control strategy.

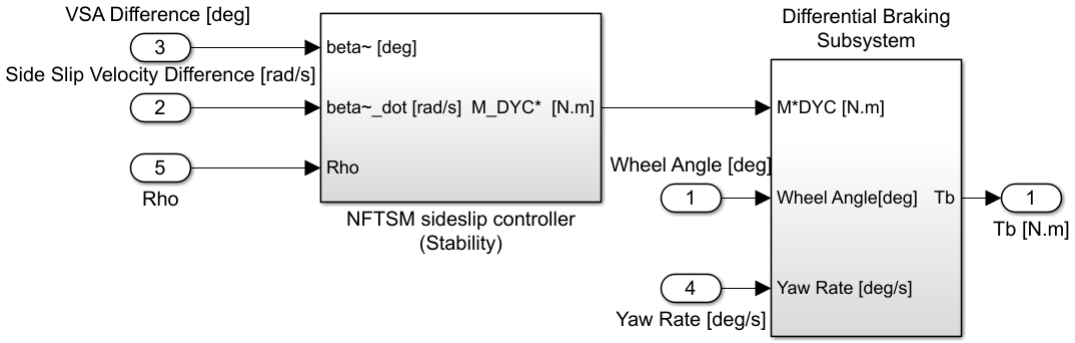

FIGURE B.7: Structure of the DYC controller.

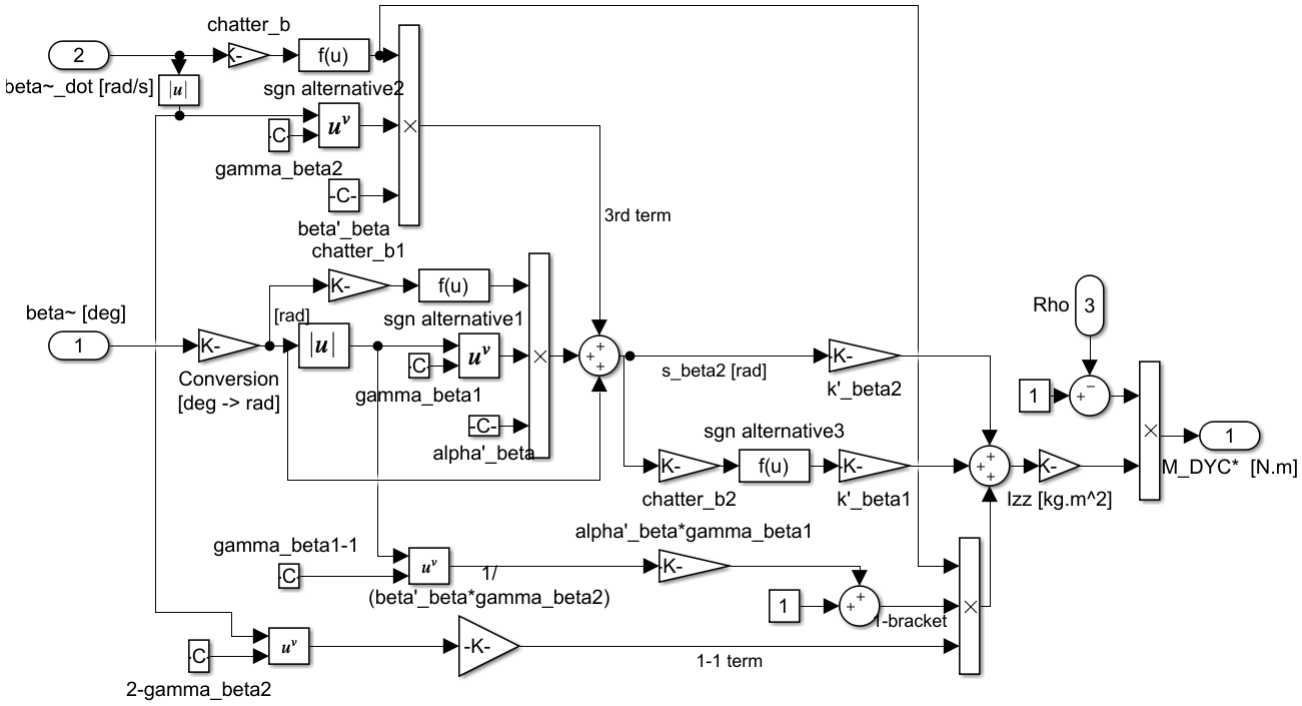

FIGURE B.8: Structure of the VSA controller using NFTSM control strategy. Adaptation gain is used to replace the M_{DYC}.

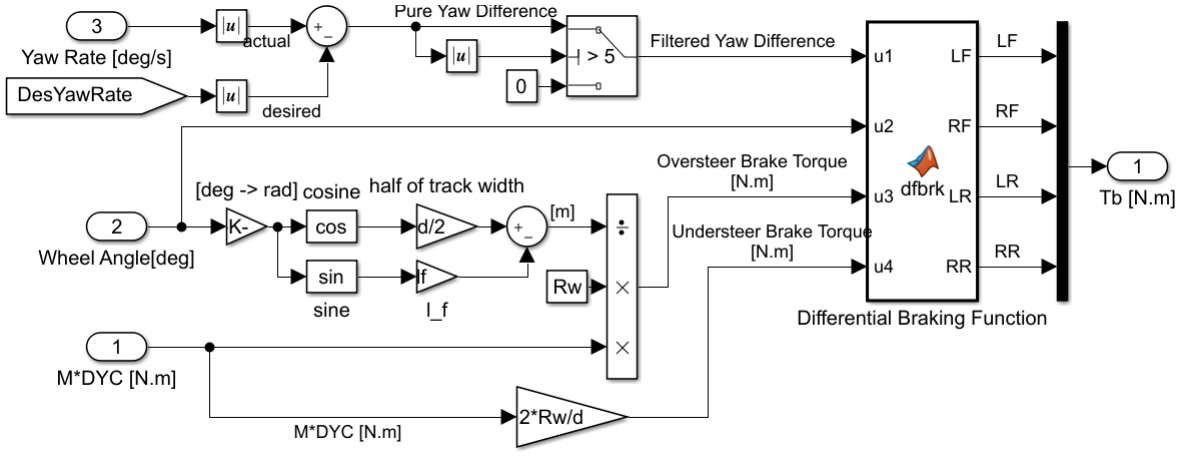

FIGURE B.9: Structure of the differential braking system. Positive steering wheel angle means counter clockwise turning in CarSim. If the yaw rate difference between the actual and the desired values is less than 5°/s, DYC is not activated.

Appendix C

MATLAB Function for the Differential Braking System

```
function [LF,RF,LR,RR]  = dfbrk(u1,u2,u3,u4)
%u1 = OS(+) & US(-) criteria
%u2 = Steering direction (L&R=+&-)
%u3 = OSTb | Desired DYC Torque* [N.m]
%u4 = USTb | Desired DYC Torque* [N.m]
if (u1>0) && (u2>0) %OS & L-turn
    LF=0;
    LR=0;
    RR=0;
    RF=abs(u3); %RF
elseif (u1>0) && (u2<0) %OS & R-turn
    RF=0;
    LR=0;
    RR=0;
    LF=abs(u3); %LF
elseif (u1<0) && (u2>0) %US & L-turn
    LF=0;
    RF=0;
    RR=0;
    LR=abs(u4); %LR
elseif (u1<0) && (u2<0) %US & R-turn
    LF=0;
    RF=0;
    LR=0;
    RR=abs(u4); %RR
elseif u3<0 || u4<0
    LF=0;
    RF=0;
    LR=0;
    RR=0;
else
    LF=0;
    RF=0;
    LR=0;
    RR=0;
end
```

FIGURE C.1: Differential braking system function in MATLAB. This .m file determines how much braking torques are required and which wheel must be activated for braking, based on oversteer/understeer state and the travel direction

Vita Auctoris

Wonjo (Max) Jung was born in Seoul, Republic of Korea. He came to Canada to study in December 2012. He obtained his Ontario high school diploma at the Columbia International College, in Hamilton, Ontario in June 2013. From there he went on to the University of Windsor, in Windsor, Ontario to study Mechanical Engineering, with a specialization in Automotive Engineering, in September 2013.

During his undergraduate degree, he participated in the Society of Automotive Engineers (SAE) Supermileage and Formula SAE design competitions. In addition, he worked for the Schaeffler Group, an automotive and industrial supplier in Herzogenaurach, Germany, and for Fiat Chrysler Automobiles (FCA) Canada at the Automotive Research & Development Center (ARDC) in Windsor, Ontario. He graduated with Distinction from the University of Windsor in 2018 with a BASc in Mechanical Engineering (Automotive Option with Co-op).

He is currently a candidate for a Dual International Master's degree in Automotive Engineering (MASc) at the University of Windsor/Politecnico di Torino, in which highly qualified students spend consecutive years in Canada and Italy participating in a focused automotive research project. His research, supported by a partnership between the universities and FCA, is focused on improving vehicle stability through virtual simulation.